DECLARATION

I, Shanti Krishna A, hereby certify that I had personally carried out the work depicted in the thesis entitled, "**Synthesis and evaluation of novel nanoprobes based on carbon dots for imaging and drug delivery applications**", except where due acknowledgement has been made in the text. No part of the work has been submitted for the award of any other degree or diploma prior to this date.

Date: Signature:

Name of the candidate: SHANTI KRISHNA A

Dr. K. Sreenivasan

Scientist G

Laboratory for polymer analysis

This is to certify that **Shanti Krishna A** in the department/division of **Laboratory for polymer analysis** has fulfilled the requirements of the Ph.D degree of the Sree Chitra Tirunal Institute for Medical Sciences and Technology, Trivandrum. The thesis entitled "**Synthesis and evaluation of novel nanoprobes based on carbon dots for imaging and drug delivery applications"** was carried out under my direct supervision. No part of the thesis was submitted for the award of any degree or diploma prior to this date.

Clearance was obtained from the Institutional Ethics Committee/Institutional Animal Ethics for carrying out the study.

Date: Signature:

The thesis entitled

SYNTHESIS AND EVALUATION OF NOVEL NANO PROBES BASED ON CARBON DOTS FOR IMAGING AND DRUG DELIVERY APPLICATIONS

Submitted by

Shanti Krishna A

for the degree of

Doctor of Philosophy

Of

SREE CHITRA TIRUNAL INSTITUTE

FOR

MEDICAL SCIENCES AND TECHNOLOGY, TRIVANDRUM

Thiruvananthapuram

Is evaluated and approved by

_____ _____

Dr. K. Sreenivasan (Research Guide)

Examiner

ACKNOWLEDGEMENTS

I would like to express my sincere gratitude to my research guide, Dr. K. Sreenivasan for his continuous support and valuable suggestions during the entire course of the work.

I am grateful to Dr. Asha Kishore, Director of our institute, Dr. K. Radhakrishnan, former Director and Mr. Neelakantan Nair, Head, BMT wing, for providing all the facilities during the course of my work. I extend my thanks to The Registrar, Deputy Registrar, Dean, Associate dean and all other staffs in the academic division for their academic assistance.

I am extremely thankful to my doctoral advisory committee members, Dr. Roy Joseph and Dr. Harikrishna Varma for their suggestions and critical comments. I am grateful to the Department of Biotechnology for their financial assistance.

I give my sincere gratitude to Dr. C. Radhakumary for all the support, suggestions and friendly approach throughout the course of my work. I gratefully acknowledge Mr. P.R. Hari and Mr. Rowsen Mosses for their support and friendly behaviour during the entire course of the work.

I sincerely thank Dr. M.R. Rekha and Ms. Priya. S for the cellular uptake studies. I am grateful to Dr. Prabha D. Nair, for her kind permission in using fluorescence spectrometer for my studies. I thank Ms. Rakhi for helping me in getting fluorescence microscopic images. I thank Dr. Annie John, Ms. Susan and Dr. Francis Fernandez for TEM images. I also thank Ms. Lizabona and Ms. Dhanya for zeta potential measurements. I would like to thank Molly Antony for the antibacterial study and for all her help during the course. I thank Dr. T.V. Kumary, Dr. P.R. Anilkumar, Ms. Usha Vasudev, Ms. Deepa and Mr. Vinod for the in vitro cytotoxicity evaluation. I am grateful to Dr. Lissy Krishnan and Dr. Anughya Bhatt for haemolysis assay. I extend my thanks to Dr. Jayasree for allowing me to use the In vivo imaging system and the Laser light facility. I thank Dr. Lakshmi. V. Nair helping me for the same. I am extremely thankful to Dr. Harikrishna Varma, Mr. Nishad and Mr. Vijayan for ESEM and XRD analysis. I thank Dr. Kallyana Krishnan and Mr. Satheesh for zeta

potential measurements. I thank Mr. Willipaul for zeta potential measurements in the initial phase of the studies. My sincere thanks to Dr. P. Ramesh and Dr. M.C. Sunny for their suggestions and help during my project work before PhD registration. I acknowledge NIIST, Trivandrum for proton NMR and HRTEM analysis and RGCB, Trivandrum for confocal microscope facility.

I sincerely thank my former labmates Dr. Gopu, Mr. Karthik, Dr. Soma Dey, Dr Priya A. Nair and Mr. Sreekanth for their support and friendship. I thank Mrs. Nimmy Mohan for her support and company during the course. I am grateful to Mr. Rajan and Mrs. Anitha for their care and I extend my thanks to Mrs. Mayuri, Mrs. Christina, Mrs. Shabeena, Ms. Krishna Priya, Ms. Remya, Mrs Rethikala and Ms. Jincy for their friendship and company while sharing home. I also thank Dr Amrita, Ms Charu and Ms Treesa for their friendship and support.

I owe my deep sense of gratitude to my beloved parents and sister for their prayers, encouragement and affection which helped me to complete my work successfully overcoming all the difficult situations. I would also like to express love to my niece, kunju. I am grateful to my in laws for their unconditional love and support. Heartfelt thanks to my husband, Dr. Sreekanth Radhakrishnan for his encouragement, support and love. I thank Almighty God for showering his blessings and giving me courage to face the difficulties leading to the successful completion of my thesis.

Shanti Krishna

Contents

List of Figures

List of Tables

List of Schemes

Abbreviations

AD	Adipic acid
CDs	Carbon dots
CTAB	Hexadecyltrimethylammoniumbromide
EDC	N-(3-Dimethylaminopropyl)-N'ethylcarbodiimide
ESEM	Environmental scanning electron microscopy
FTIR	Fourier transform infrared spectroscopy
DCC	Dicyclohexylcarbodimide
DG	Digitonin
DLS	Dynamic light scattering
DMAP	4-Dimethylaminopyridine
GA	Glutamic acid
HA	Hyaluronic acid
HRTEM	High resolution transmission electron microscopy
IVIS	*In vivo* imaging system
MDSC	Modulated differential scanning Calorimetry
MTT	3-(4,5-dimethyl thiazol-2-yl)-2,5-diphenyl tetrazolium bromide
MX	Methotrexate
NMR	Nuclear magnetic resonance spectroscopy
PEGD	Poly(ethylene glycol) bis(3-aminopropyl) terminated
PVA	Polyvinyl alcohol
TEM	Transmission electron microscopy
TGA	Thermogravimetric analysis
XRD	X-ray diffraction

SYNOPSIS

Nanotechnology is the brainchild of the new millennium. Its varied applications have paved way for several breakthroughs in the realm of biomedical technology. In this challenging era when illness multiplies, timely and accurate disease diagnosis is very important. Thus, well founded novel approaches matter very much in areas like disease treatment, diagnosis and monitoring. Nanomedicine has tremendous implications in the given context. The biomedical application of nanoscale materials for diagnosis and therapy has gained impetus in recent times. The development of multifunctional nanoparticles as representative nanomedicine is a case in point. They enable target specific delivery of imaging or therapeutic agents for biomedical applications.

The photoluminescence properties and photo stability make fluorescent nanomaterial robust as ideal probes for biomedical applications. Carbon dots (CDs) are zero dimensional carbon based nanomaterial with excellent photoluminescence property. In this study, we designed various fluorescent nanosystems based on a single platform CDs, to address diverse issues. Appropriate modifications were done for each study.

The thesis comprises six chapters including introduction, literature review followed by the materials and methods adopted for different studies, fourth and fifth chapters

include results and discussion respectively. The last chapter comprises summary, conclusion and future perspectives.

The first chapter covers the introduction related to the area of research and the second one describes literature review on the major research published with appropriate citations. Rest of the chapters is divided into five sections. The first section explains the preparation of PEG diamine passivated CDs and its conjugation to glutamic acid (GA), a naturally occurring ligand with affinity towards calcium. The novelty of this work is to map calcium rich sites by utilising the fluorescent property of CDs. The extent of calcification as well as the precise location of calcium deposits has significant implications in clinical diagnosis. During repetitive loading, micro damage accumulates in bone in the form of microcracks and these cracks when undetected in the initial stage can end up in bone fracture. As these cracks are calcium releasing and GA being calcium specific molecule, CDs conjugated with GA can easily target those sites. Hyaluronic acid (HA) was also conjugated to the CDs considering its biocompatibility. Additionally, HA can prevent protein adsorption and opsonisation stemming from its hydrophilic and polyanionic features in physiological environment. HRTEM image of CD confirmed their spherical morphology with an average size of 5 nm. Conjugation of HA and GA onto CDs (HAGACD) were confirmed by FTIR, H^1NMR, TEM, TGA and zeta potential measurements. HAGACD gave an emission maximum at 455 nm when excited at 360 nm reflecting that the conjugation didn’t alter inherent emission features of CD. *In vitro* cytotoxicity test by direct contact and MTT assay confirmed that HAGACD is noncytotoxic. The selectivity of HAGACD was studied with its

response to other cations and the interferences from other coexisting substances were checked directly with human blood serum. No interferences were observed as the fluorescence intensity of the probe remained the same. The ability of HAGACD to locate calcium deposits was assessed using calcium doped polyvinyl alcohol (PVA) films as well as fresh bones collected from slaughter house. The results indicated that the probe has the potential to map calcium rich sites as well as calcium releasing points such bone cracks.

The main objective of the second section is the simultaneous location of bone cracks and delivery of appropriate drugs to facilitate rapid healing and infection control. Hairline cracks when undetected initially later become site for infection leading to several complications. Therefore early detection as well as proper healing of such cracks is imperative. New strategies to address these issues are currently focused on designing nanoparticles capable of docking onto crack. To achieve specificity, nanoparticles are functionalized with bone targeting molecules along with drug/growth factors. By this approach, simultaneous crack visualization and site specific drug delivery could be achieved. We used CDs modified with GA and ciprofloxacin as model drug (having antibacterial activity). CDs and the conjugate (CDGAC) were characterised by FTIR, H^1NMR, HRTEM, UV-Visible spectrometer and fluorescence spectrophotometer. *In vitro* cytotoxicity evaluation by direct contact and MTT assay affirmed that CDGAC is noncytotoxic. They were also found to be non-haemolytic at all chosen concentrations with haemolysis values less than 1%. Microbial inhibition assay using the bacterial strain *E.coli* was carried out. The results proved that CDGAC itself is antibacterial and the drug need not be cleaved

from the probe for hampering bacterial infection. Fresh bone was used to demonstrate the binding of CDGAC and imaged with *in vivo* imaging system to locate the bound CDGAC on the crack of the bone surface. The result apparently suggested the ability of the probe to locate even minor bone cracks. Our results indicated that there is significant scope in negotiating functionalized CDs as theranostic agents.

The third section depicts a simple method to visualize cholesterol deposits using digitonin (DG) conjugated CDs (CDDG). High blood cholesterol is risky as it may result in atherosclerosis which eventually leads to heart attack. Cardiovascular disease remains the No. 1 global cause of death with 17.3 million deaths each year and is expected to rise to more than 23.6 million by 2030. Detection of cholesterol deposits in the initial stage itself is very important. But the usually employed techniques for such plaque detection involve lengthy procedures and expensive instrumentation. An early visualization of cholesterol rich plaques using fluorescent nano probes designed here is a simple method which may aid in diagnosis of atherosclerosis and it seems that our finding may catalyze further developments in this crucial domain. DG, a glycoside obtained from Digitalis purpurea is well known for its affinity towards cholesterol. Conjugation of DG onto CDs was confirmed by FTIR, H^1NMR, TEM and Zeta potential measurements. The conjugation does not affect the fluorescent property of CD and CDDG showed an emission peak maximum of 455 nm on excitation at 360 nm. CDDG was selective to cholesterol and does not interfere with other analytes. Tissue with heavy fat deposit extracted from the blood vessels that surround the human heart was incubated with CDDG and

viewed under UV lamp. The tissue was also imaged using *in vivo* imaging system. They were compared with a fat free tissue under the same conditions. The fat deposited tissue shows fluorescence while fat free tissue is non fluorescent confirming that the probe can recognize and dock onto the cholesterol plaques in real situation.

The fourth section deals with the designing of hybrid system of CDs and gold nanorods (NRs), so that the photothermal property of NRs can be utilised for the possible disruption of cholesterol plaques apart from imaging them via the fluorescent property of CDs. The hybrid system (CDNR) was characterised using FTIR, TEM, UV-Visible and Fluorescence techniques. NRs with aspect ratio less than 5 nm were prepared in this study. The fluorescence property of CDs is retained even after the conjugation of NRs. The hybrid can be used to locate the cholesterol deposits on tissues exploiting the fluorescent nature of CDDG. It is reasoned that the photo thermal property of NRs could be employed to remove the fat deposits by elevating the local temperature. The tissues incubated with the hybrid probes were washed well and then exposed to Laser light (808 nm and 1.5 W) for 5 minutes. The temperature was found to be increased by 10 ^{0}C. Further analysis of the tissues using ESEM indicated remarkable changes in the morphology of the deposit reflecting its disruption. In addition non toxic nature and the cellular internalisation of CDNR make it an efficient system for theranostic applications. The results emerged envisaged that this hybrid nano system offers a novel therapeutic approach for diagnosis and treatment in nanomedicine.

The fifth section describes CDDG as an efficient probe in cancer therapy. DG has traditionally been known as cell membrane permeabilizing agent. Based on this fact, we modified CDs with DG (CDDG) and further conjugated with methotrexate (MX). The nanoprobe (CDMX) was subjected to physico chemical characterizations, cytotoxic evaluation and cellular uptake studies. Nearly 80 % of the drug was found to be retained in the probe at physiological pH. Significantly more amount of drug (>80 %) was released at pH 5.0 which is beneficial considering the lower pH inside cancer cells. Thus CDMX has the potential to carry the drug safely to the predetermined site. Improved cytotoxic response of CDMX due to the cell permeabilizing effect of DG was observed and it can be assigned to the enhanced uptake of CDMX by the cells which in fact facilitates the transport of more drugs into the cells. The confocal images of the cells incubated with CDDG and CDMX confirmed that they are efficiently taken up by the cells. DG can assist in better internalization of drug carriers and thus significantly can increase the therapeutic potential of the drug. Additionally it seems that potential theranostic probes can be created from CDs by less complex chemical approaches.

Last chapter gives the overall summary and conclusion. The whole thesis is focussed on the use of carbon based nontoxic, fluorescent nanoprobes for disease diagnosis, imaging and drug delivery applications. We have been brought home the fact that these types of entities will in course of time achieve a breakthrough on the medical front. The present day diagnostic scenario has inherent flaws. The *in vitro* studies we carried out here are versatile in content and are likely to have a tremendous appeal in the days to come. Future outlook is directed to assess the suitability of the probes for

the *in vivo* applications. To achieve these goals, *in vivo* studies using appropriate animals will be carried out.

1 INTRODUCTION

1.1 An introduction to nanotechnology and nanomaterials

Nanotechnology is a multidisciplinary field involving the efficacy of biological materials along with the basic rules of physics, chemistry and material science. The size of nanomaterials ranges from 1-100 nm. Nanotechnology plays a pivotal role in biomedical applications, mainly in the areas of sensing, imaging, drug delivery and disease diagnosis. These nanotechnological applications in the field of medicine have been referred to as nanomedicine (Mensah et al., 2015). In nanomedicine, nanoplatforms as theranostic agents can offer promising therapeautic paradigms (Xie et al., 2010). Theranostic nano systems offer opportunities for simultaneous diagnosis and therapy via imaging and environmental responsive drug release combined on a single platform (Janib et al., 2010). Multifunctional nanomaterials as diaganostic and therapeautic systems are ideal candidates owing to their features such as large surface area enabling the conjugation or loading of considerable amount of drug/imaging agents, incorporation of targeting moieties for targeting the diseased sites, tuning of size and surface modification resulting in prolonged circulation in blood etc. Commonly used nanomaterials for biomedical applications are quantum dots (QDs), gold nanoparticles (GNPs), magnetic nanoparticles and carbon based nanomaterials. Nanosystems for biomedical applications are designed considering the biocompatibility and toxicity of the nanomaterial along with the desired diaganostic effect.

1.2 Fluorescent nanomaterials for biomedical applications

Fluorescent nanomaterials have received much attention in the biomedical field as diagnostics and for the investigation of molecular interactions as they are sensitive and easy to operate (Jun et al., 2011). A variety of nanomaterials such as QDs, metal nanoclusters, carbon based materials etc have been widely investigated for various applications such as sensing, imaging and drug delivery applications. For these applications fluorescence property can be utilized to follow the distribution of the drug inside the organism and provide information for the optimization of disease treatment. Fluorescent nanomaterials have started replacing traditional organic dyes as they offer superior optical properties such as brighter fluorescence and wider selections of excitation and emission wavelengths. Nano probes have better photostability and targeting ability when compared to the molecular probes. Nanosensors have calibration plots which make them quite different from the molecular probes. Nanomaterials in contrast to molecular probes are inert, less cytotoxic and do not possess the property of non specific binding to cellular biomacromolecules (Zhong, 2009).

For biomedical applications fluorescent nanomaterials should possess water solubility, biocompatibility, chemical and photostability (Li et al., 2014). The two types of photo-luminescence mechanisms for fluorescent materials are down conversion and up conversion. The down conversion is stokes shift emission process whereas up conversion is an anti-stokes process (Shinde et al., 2012). Nano fluorescent probes commonly used for biomedical applications are quantum dots (QDs), carbon based nanomaterials, metal clusters and silicon nanoparticles. They

have potential applications in biomedical field for diagnosis and treatment of diseases. There is a significant scope in negotiating functionalized fluorescent nanoprobes as theranostic agents for early detection and treatment of diseases.

1.3 Carbon dots

Nanosized fluorescent carbon based materials dubbed as carbon dots (CDs) have drawn increasing attention in recent years. Among a wide variety of fluorescent nano materials, QDs are a forerunner for bioimaging applications. Their roles in cellular imaging, drug delivery and diagnosis are undisputed (De et al., 2008). Unfortunately, QDs are toxic to living systems even at low concentrations. CDs are one of the eco-friendly potential candidates for QDs. CDs have size- and surface chemistry different from traditional semiconductor-based quantum dots (Song et al., 2014). These zero-dimensional carbonaceous nanomaterials have evoked much interest as benign probes for optical imaging of living and nonliving components. The notable attractions of these materials are their water solubility, chemical inertness, easiness in functionalization and excitation-wavelength (λ_{ex}) dependent photoluminescence (Wang et al., 2011) (Zhu et al., 2012) (Tao et al., 2012). These features along with non toxicity and biocompatibility make CDs ideal candidates for investigating biological systems (Baker and Baker, 2010). Multistep design approaches can generate CDs with engineered surface features having better biocompatibility and long-term stability, for a wide variety of applications (Ding et al., 2014).

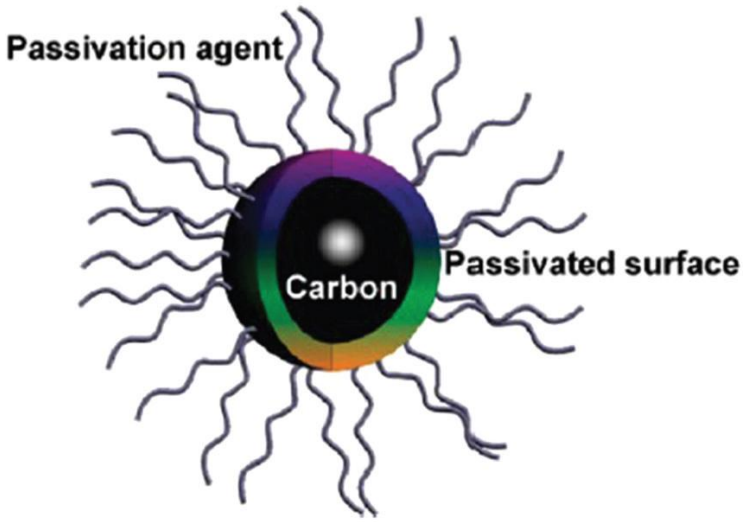

Figure 1: Schematic view of carbon dot (Li et al., 2010)

1.3.1 Optical Properties of CDs

CDs show absorbance in the UV region extending towards the visible region which attributes to the π-π*, n- π* or other transitions. One of the most fascinating properties of CDs is their photoluminescence (PL). They exhibit excitation dependent emission, a unique feature of CDs which may be due to the presence of many varied sized nanoparticles or various emissive traps on the surface of the CDs. The origin of PL may be due to factors such as quantum effect, surface defects or due to the recombination of electron–hole pairs localized within small sp^2 carbon clusters embedded with sp^3 matrix. Their PL properties can be tuned via modification and or electron/energy transfer (Wang and Hu, 2014). Sun et al have claimed that the PL is due to the surface energy traps (Sun et al., 2006). Surface passivation is important for attaining PL, for which the mechanism for luminescence being radiation recombination of excitons. It has been reported that the origin of PL can also be due to the carboxylate groups if present on the surface of the CDs (Hu et

al., 2009) (Li et al., 2011). CD also shows phosphorescence (Deng et al., 2013) and chemiluminescence properties (Lin et al., 2012) (Teng et al., 2014) (Zhao et al., 2013). The dual nature of CDs as electron donors and acceptors enable them for optronics, catalysis and sensing applications. The emission mechanism of CDs is based on the radiative recombinations of the carbon nanoparticle confined electrons and holes due to which they exhibit fluorescence.

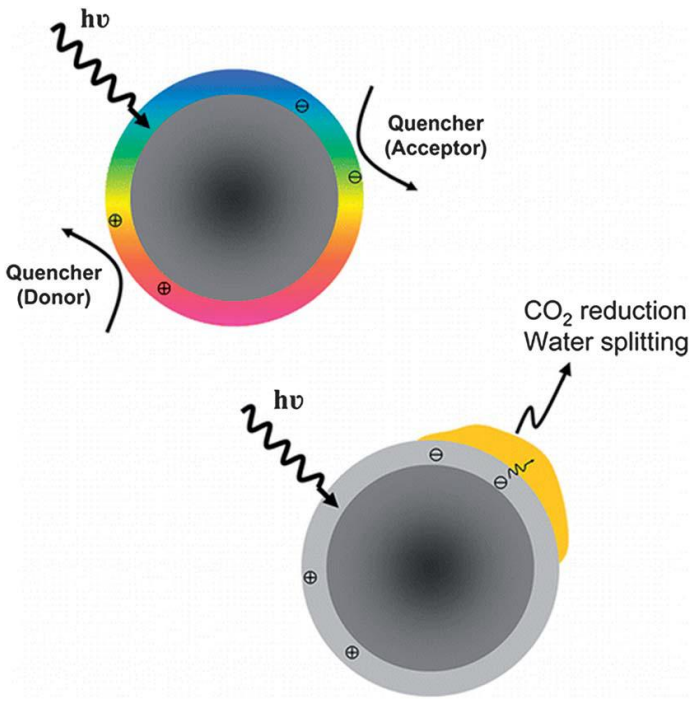

Figure 2: Scheme representing the mechanism of optical property exhibited by CDs (Cao et al., 2013)

1.4 Orthopaedic disorders

Bone disorders are one of the major causes for mortality to human beings especially elderly patients thus affecting the overall health and the quality of life (Wang et al., 2014). Bone diseases comprise a variety of skeletal-related disorders such as arthritis, osteoporosis, osteoarthritis, osteosarcoma, and metastatic bone cancer. Multifunctional 'smart' entities with the ability to sense, diagnose, image and cure

numerous ailments have tremendous possibilities (Anderson et al., 2004). The use of tools of nanotechnology in drug delivery for treating various orthopedic diseases is important when considering bone regeneration using bone implants and replacement strategies (Gindy and Prud'homme, 2009). New targeting approaches are employed to deliver drugs to the bone cracks which include fusion proteins or nanoparticles with targeting functionalities (Luhmann et al., 2012). Bone cracks release calcium (Yadav et al., 2013) which could be detected by incorporating molecules having calcium affinity within the drug delivery vehicle.

Clinical fracture susceptibility, to a large extent, has been implicated to micro damage accumulated in bone in vivo due to mechanical loading and aging. Considering the gravity of this issue, extensive efforts have been expended to design methodologies to locate and visualize such type of damages. Many of these approaches are non-specific and fail to precisely locate the micro cracks. Since these defects are Ca ion releasing, Ca specific molecules have been employed for optically imaging the damage.

1.4.1 Glutamic acid

Glutamic acid (GA) is a naturally occurring amino acid well known for its affinity for calcium and hence used for targeting calcium rich sites such as bone cracks as well as calcified tissues. Fluorochromes such as calcein with carboxylate functional groups could target microdamage via chelation with calcium ions on the exposed surface of the damaged tissue. Similar to those fluorochromes, GA also contains carboxylate groups as the functional entities. Structure of GA is shown in Figure 3. Gold nanoparticles functionalized with GA were investigated for targeting microdamage in bone tissues (Zhang et al., 2010). Gold nanoparticles modified with GA, phosphonate

and bisphosphonate were investigated for their binding affinity to hydroxyapatite (Ross and Roeder, 2011) and targeted labeling of damaged bone tissue in vitro (Ross et al., 2012).

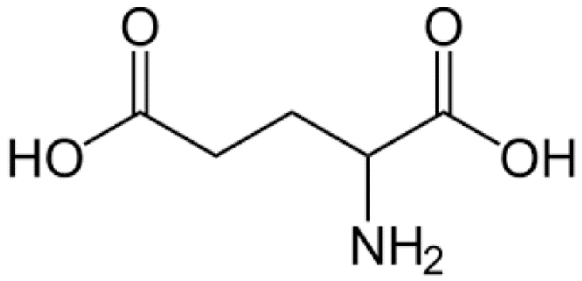

Figure 3: Structure of glutamic acid

1.4.2 Ciprofloxacin

The IUPAC name of ciprofloxacin is 1-cyclopropyl-6-fluoro-4-oxo-7-(piperazin-1-yl)-quinoline-3-carboxylic acid. The structure is shown in Figure 4.

In the study for the simultaneous bone crack detection and drug deposition using CDs, we chose ciprofloxacin as a model drug owing to its antibacterial activity. Ciprofloxacin is commonly used to treat infections in bone, joints, urinary tract, skin and abdomen. It is a second generation fluoroquinolone well known for their broad spectrum of activity. It is a commonly used antibiotic valued for their availability in oral and intravenous formulations.

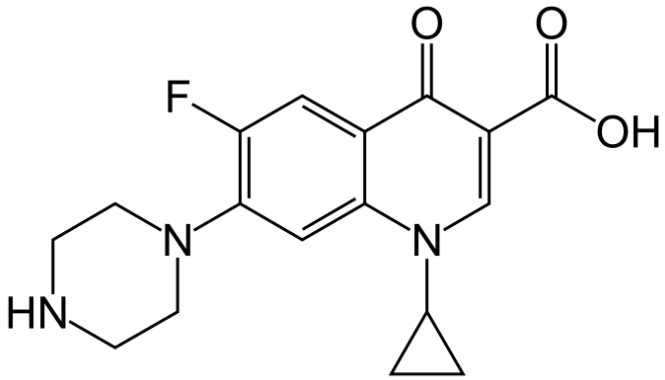

Figure 4: Structure of ciprofloxacin

1.4.3 Importance of nanomaterials and calcium specific molecules in bone crack detection

Nanomaterials can offer many unique features for the potential targeted delivery of treatments for bone diseases which include carrying the drug to the specific site while keeping the drug concentrated, protecting the drug from being degraded by body fluids and increasing the circulation time in the body, loading other targeting molecules to achieve specific delivery via surface modification of NPs (Gu et al., 2013).

With the advantages of nanotechnology it is possible to achieve targeted drug delivery for bone-related disorders. Nanoparticles (NPs) for drug delivery of bone diseases include organic as well as inorganic NPs. Antibiotics and chemotherapeautics are the commonly used drugs for bone diseases. The effect of magnetic NPs on osteoblasts *in vitro* has been studied by Pareta et al (Pareta et al., 2008). These NPs can be localized in bone sites in presence of magnetic field. Currently, bisphosphonates and GA are used for the targeted delivery of bone diseases. It has been reported that gold nanoparticles (AuNPs) functionalized with

GA has been used for targeting damaged bone tissue (Ross and Roeder, 2011). Their objective was to investigate the binding affinity of functionalized AuNPs for targeted delivery to bone mineral, using hydroxyapatite crystals as a synthetic analog *in vitro*. AuNPs were surface functionalized with either L-glutamic acid, 2-aminoethylphosphonic acid, or alendronate for targeting calcium. Surface functionalized AuNPs were shown to exhibit targeted labeling of damaged bone tissue in vitro (Ross et al., 2012).

1.5 Cardiovascular diseases

Cardiovascular disease, a class of diseases involving heart or blood vessels include coronoray artery disease, stroke, hypertensive heart disease, peripheral artery disease, venous thrombosis etc. Among these coronoray artery disease, stroke, hypertensive heart disease and peripheral artery disease involve atherosclerosis which is due to high blood pressure, high blood cholesterol, diabetes, smoking etc. According to the report from the American Heart Association, on the basis of Heart Disease and Stroke Statistics — 2015 update cardiovascular disease remains the No. 1 global cause of death with 17.3 million deaths each year, and is expected to rise to more than 23.6 million by 2030. As per the guidelines of National Cholesterol Education Program (NCEP), elevated individual plasma cholesterol levels exceeding 6.2 mM (240 mg/dL) are indications of poor cardiovascular conditions (Nauck et al., 2000). High blood cholesterol can result in atherosclerosis by forming fatty plaques on arteries and resulting in the hardening of arteries. Hence early detection of blood cholesterol level is very important in such cases and hence blood cholesterol estimation is one of the widely performed assays in biochemistry labs. A study on cholesterol crystals in

atherosclerotic plaques has been reported (Suhalim et al., 2012). High level cholesterol can damage the endothelium causing the cholesterol to enter the artery walls followed by cholesterol invasion, i.e bad cholesterol (LDL) accumulate in the arteries. The streaming of white blood cells to digest the LDL cholesterol takes place and the accumulation of cells together with cholesterol for years becomes cholesterol plaque in the artery walls. The growth of cholesterol plaques in the arteries blocks the blood flow. Cholesterol plaques can immediately rupture and the abrupt blood clot formed over the rupture results in serious health issues. Early and appropriate medical diagnosis is of supreme importance for controlling these life threatening issues.

1.5.1 Cholesterol

Cholesterol is an important lipid for human body and a major structural component of all animal cell membranes. The integrity of biological membranes and fluidity is maintained by cholesterol. Cholesterol also acts as a precursor for the production of vitamin D, bile acids and steroid hormones. Structure of cholesterol is given in Figure 5.

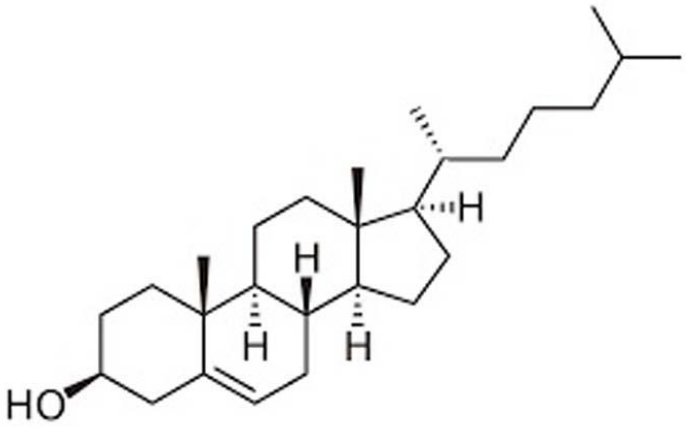

Figure 5: Structure of cholesterol

An elevated cholesterol concentration in blood is risky and is associated with cardiovascular diseases. A build up of cholesterol result in the narrowing of arteries causing atherosclerosis. Over decades, atherosclerotic disease may result in myocardial infarction or stroke. Desirable cholesterol level corresponding to lower risk for heart disease is less than 5.2 mM (200 mg/dL) and its life threatening when the level exceeds 6.2 mM (240 mg/dL).

1.5.2 Nanomaterials for cholesterol detection

In laboratories for the estimation of cholesterol in blood, enzymatic methods using auto analyzers are adopted since 1980. Enzymatic methods have their own limitations such as intrinsic instability and loss of activity. To overcome these defects nano systems for cholesterol detection have been widely employed. A non enzymatic cholesterol sensor based on porous tubular silver nanoparticles was reported. The biosensor showed good stability and low interferences thus confirming the system to be a promising platform for cholesterol detection (Li et al., 2010). Electrochemically based cholesterol biosensor has been reported by Lee et al. They used macroporous gold electrode with platinium nanoparticles for non enzymatic free-cholesterol sensing (Lee and Park, 2010). Gold nanoparticles conjugated with digitonin for cholesterol detection has been reported. The system was found to have the potential as an enzyme free cholesterol sensor as the digitonin could specifically bind to cholesterol (Raj et al., 2011). Enzyme free assay for cholesterol detection with tomatine conjugated gold nanoparticles has also been reported. The binding of tomatine to cholesterol was proved and the feasibility of the system for practical applications was studied by estimating cholesterol in human serum samples (Raj et

al., 2014). β-cyclodextrin-graphene based hybrid system for the optical detection of cholesterol has recently been reported. Fluorescence of β-cyclodextrin incorporated with rhodamine gets quenched in presence of graphene and recovery of fluorescence occurs on adding cholesterol (Mondal and Jana, 2012). Non-enzymatic cholesterol sensing exploiting the electrochemical approach, based on host guest interaction between β-cyclodextrin/poly(N-acetylaniline)/graphene modified electrode with methylene blue and cholesterol has also been reported (Yang et al., 2015). Another system based on β-cyclodextrin-graphene with methylene blue was also developed. Cholesterol being replaced by methylene blue resulted in an inclusion complex within the hydrophobic core of the hybrid system and the matrix was found to be sensitive and selective for cholesterol sensing (Agnihotri et al., 2015).

1.5.3 Digitonin

Digitonin (DG) is a glycoside obtained from digitalis purpurea and is well known for its affinity towards cholesterol. It is also used for solubilizing membrane proteins and permeabilizing cell membranes.

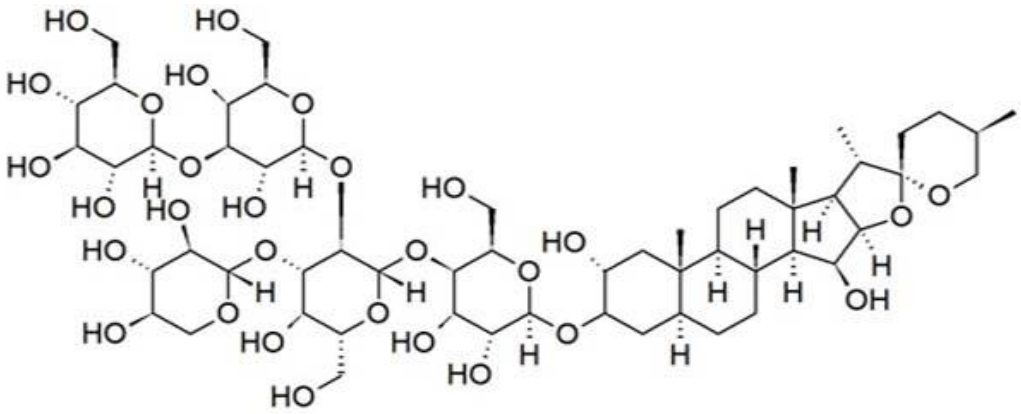

Figure 6: Structure of digitonin

Digitonin conjugated gold nanoparticles for cholesterol detection has been reported. Selectivity of the method ensures the system to be an ideal enzyme free cholesterol sensor and is an attractive alternative for enzyme based sensing platforms.

1.6 Gold Nanorods

Gold nanorods (NRs) have emerged as potential candidates for sensing, imaging and drug delivery due to their absorption and scattering properties. NRs have been widely exploited for various applications due to their unique plasmonic property, i.e their longitudinal surface Plasmon resonance (LSPR) can be tuned by altering their aspect ratio (Xu et al., 2014). Optical control and sensitivity to changes in local environment are other important traits of NRs as a result of which they have been explored for broad spectrum of biomedical applications (Stone et al., 2011). It has been reported that NRs when compared with gold nanoparticles have better interaction and hemodynamics as drug carriers for cancer treatments (Barua et al., 2013). Unique blend of CDs and AuNRs to carry chemotherapeutic agent has been reported by Pandey et al. Biocompatibility and imaging property of CDs together with the photothermal property of NRs are the advantages of such hybrid systems (Pandey et al., 2013). Since it is a blend, the chance of reaching at the indented site through circulatory system may be remote.

1.7 Carbon dots for drug delivery and cell imaging

World Health Organization Report (2011) indicates that Cancer causes more deaths than coronary heart disease or stroke. Worldwide, 14.1 million new cases of cancer and 8.2 million deaths due to cancer were estimated in 2012 (Ferlay et al., 2015) and

is expected to rise over 20 million new cancer cases in low and middle income countries by 2025. In United States in 2015, new cases and deaths due to cancer were estimated to be 658,370 and 589,430 respectively and cancer is considered as the second leading health threat (Siegel et al., 2015). The development of nanomedicine is a promising approach for improved therapeutic potential in cancer treatment. Nanotechnologies to a great extent result in improved distribution and targeting of anticancer medication (Wicki et al., 2015).

Drug delivery systems based on nanomaterials are widely reported. Gold nanoparticles (AuNps) are one of the most widely investigated nanocarriers for drug delivery. However, their drawbacks such as toxicity, limitation of drug choice, quenching of fluorophores etc limit the applications of AuNps in nanomedicine. CDs can overcome these limitations because of non toxicity, ease of functionalization and tracking ability due to strong fluorescent properties. They serve as ideal drug carriers and fluorescent tracers. There are several reports on CDs based drug delivery systems which are reviewed in detail under section 2.2.

Traditional QDs have been widely used for in vitro and in vivo optical imaging experiments, but the issues of toxicity limits their use in cell imaging applications. CDs are well suited for cellular imaging owing to their high photostability and non toxic nature.

1.7.1 Methotrexate

The IUPAC name of methotrexate (MX) is (2s)-2-[{4-{[(2,4-Diaminopteridin-6-yl)methyl](methyl)amino}benzoyl)amino]pentanedioic acid. MX is an antifolate

drug widely used in the treatment of cancer. Its action is by inhibiting the metabolism of folic acid. The structure of MX is given in Figure 7.

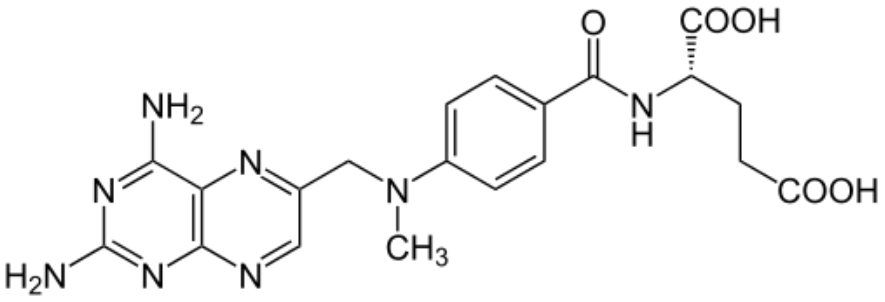

Figure 7: Structure of methotrexate

1.8 Hypothesis

Functionalized carbon dots, non toxic and biocompatible in nature, can open up new paradigms in imaging and drug delivery applications. A single nanosystem with diagnostics and therapeutic capabilities can offer better prognosis. Theranostic probes shaped from carbon dots can possibly be employed in the early detection and treatment of diseases.

1.9 Objectives of the study

Nano sized CDs have been widely used as benign probes in drug delivery and imaging applications owing to their high fluorescence along with the most required nontoxicity and biocompatibility. In this study we planned to design CD based nanoprobes for imaging and drug delivery applications. CDs were modified with appropriate moeities for diverse applications. The objectives are as follows,

- To modify PEG diamine passivated CDs with GA, a naturally occurring amino acid with proven affinity to calcium ions, for *in vitro* detection of cracks in bone

- To design multifunctional CDs for simultaneous bone crack detection and drug deposition.

- Preparation of DG conjugated CDs for detection and visualization of cholesterol deposits in tissues.

- Synthesis of gold nano rods and its conjugation to CDs for the simultaneous imaging and possible disruption of cholesterol plaques by exploring photothermal properties of gold nanorods.

- DG conjugated CDs amended with methotrexate (anticancer drug) for cellular imaging and drug delivery.

The following chapters are summarized below. Chapter 2, Literature review illustrates the significance of each system with proper citations. Chapter 3, Materials and Methods, explains the reagents used for the experiments, synthetic routes and physicochemical characterization methods involved in each study. Chapter 4 details the results and observations of the *in vitro* studies using CD based nanoprobes for visualizing bone cracks, cholesterol deposits and cellular uptake studies thereby raising a scope in negotiating functionalized CDs as theranostic agents. Chapter 5, Discussion, critically evaluates the results obtained in this study. Chapter 6, Summary and Conclusion summarizes the study in terms

of the most important results emerged and concludes by highlighting the most important findings from the study.

2 LITERATURE REVIEW

2.1 Synthesis of Carbon dots

CDs were accidently discovered by arc discharge approach during the purification of single walled carbon nanotubes in 2004 (Xu et al., 2004). Original report on CDs were the non fluorescent ones generated by Sun et al in 2006 via laser ablation using graphitic target, which were then modified with poly ethylene glycol (PEG) to obtain fluorescent CDs (Sun et al., 2006). Since 2006, several physical and chemical methods have been adopted for the production of CDs.

Synthetic methods for the preparation of CDs can be classified into two, top down and bottom up. In top down method CDs are obtained from macroscopic carbonaceous matrices. Electrochemical, oxidation and laser ablation are the three important methods under top down category. Carbon nanotubes and graphite are the commonly used materials for electrochemical synthesis. The advantages include low cost and easy manipulation. Deng et al used low molecular weight alcohols for electrochemical carbonization (Deng et al., 2014). Carbon dots were prepared from multiwalled cabon nano tubes by Zhou et al (Zhou et al., 2007). Electro-oxidation of graphite electrode against saturated calomel electrode was reported by (Zhao et al., 2008). Synthesis of CDs by laser irradiation has the advantages of high pressure and high heat of laser. Hu et al developed a single step protocol for the production of CDs via the laser irradiation of graphite powders. CDs were obtained by laser irradiation of carbon material suspension in organic solvent (Hu et al., 2009). Li et al reported an easier method using nano carbon material (Li et al., 2011). Chemical oxidation is an effective method widely employed for the large scale production of

CDs. Dehydration of carbohydrates in presence of H_2SO_4 followed by the formation of CDs in presence of HNO_3 and passivation using amine terminated compounds was reported by Peng et al (Peng and Travas-Sejdic, 2009). Qiao et al have reported the formation of CDs via direct chemical oxidation route (Qiao et al., 2010)

Organic precursors are used for the preparation of CDs in bottom up method. Microwave, pyrolysis and ultrasonic are the various approaches in bottom up category. Microwave assisted synthesis is cheap and easy. Diethylene glycol stabilized CDs were obtained via microwave irradiation, sucrose being the carbon precursor (Zhai et al., 2012). Wang et al have reported CDs from egg shell membrane via microwave assistance (Wang et al., 2012). CDs were synthesized by microwave assisted pyrolysis of citric acid with various amine molecules (Liu et al., 2014). Studies have proved that external heat causes carbonization resulting in the formation of CDs (Yang et al., 2009). Amino functionalised CDs were synthesized with citric acid as the carbon precursoor, surface passivated with PEG diamine by Wang et al (Wang et al., 2010). Thermal carbonisation of ammonium citrate salts to obtain CDs has been reported by Bourlinos et al (Bourlinos et al., 2008). Hydrothermal treatments were more efficient than electrochemical oxidation. Precursors include Chitosan, sucrose, bovine serum albumin, orange juice, honey, grass and plant leaves. Sahu et al have synthesized CDs by hydrothermal treatment of orange juice (Sahu et al., 2012). Amorphous CDs were obtained by heating jaggery, bread, cornflakes or biscuits as reported by Chattopadhyay‘s group (Sk et al., 2012). Ultra sound synthetic routes have also been opted for the production of CDs (Li et al., 2011) (Park et al., 2014).

CDs passivated with functional groups are more fluorescent when compared with the naked CDs (Luo et al., 2013). Naked CDs without surface functionalization exhibit fluorescence with low quantum yield. Surface passivation is usually carried out using molecules with amino moieties such as PEG diamine, PEI, ethylene diamine etc.

2.2 Properties of Carbon dots

Photostability is a key property which makes CDs ideal candidates for biomedical applications (Liu et al., 2012) (Qiao et al., 2010) (Yang et al., 2011). Drawback of organic dyes is photo bleaching as a result of which they are being replaced by CDs. Most of the synthesized CDs have size less than 10 nm due to which they can easily pass through the cell membrane and enter cytoplasm. Quantum yield (QY) is another characteristic feature of CDs. QY can be increased via passivation, doping, purification processes etc (Miao et al., 2015). CDs functionalised with diamine-terminated oligomeric or poly (propionylethyleneimine-co-ethyleneimine) gave QYof 4-10% (Sun et al., 2006). A reductive pathway was adopted by Zheng et al to increase the QY of CDs. QY was increased from 2 % to 24 % when CDs were treated with sodium borohydride (Zheng et al., 2011).

Non toxicity of CDs has been reported by several groups. MTT and Trypan blue assays for determining the cell viability of CDs has been reported by Ray et al (Ray et al., 2009). Non toxic effect of CDs on cells and sprouted green grams was studied by Song et al and CDs were found to be most biocompatible when compared with QDs and gold nanoparticles (Song et al., 2013).

2.2.1 Fluorescence properties of CDs

Two classes of mechanisms have been proposed for the fluorescence emission of CDs (Lim et al., 2015). One of the mechanisms is due to the band gap transitions originating from the conjugated π-domains, isolated with electron rich sp^2 hybridized islands. π-connections should not be present between those islands as it might result in the quenching of the fluorescence involving strong absorption in the UV region and weak fluorescence emission (Cao et al., 2013) (Eda et al., 2010) (Hummers and Offeman, 1958). Another mechanism is associated with surface defects. Strong visible emission attribute to the electronic transitions due to the recombination of electron hole pairs in the localised **π** and **π*** levels of sp^2 sites lying between the bandgap of **σ** and **σ*** states of sp^3 matrix (Chen and Robertson, 1998). The surface defects get stabilized due to functionalization leading to effective radiative recombination electrons and holes resulting in better fluorescence emission (Cao et al., 2013).

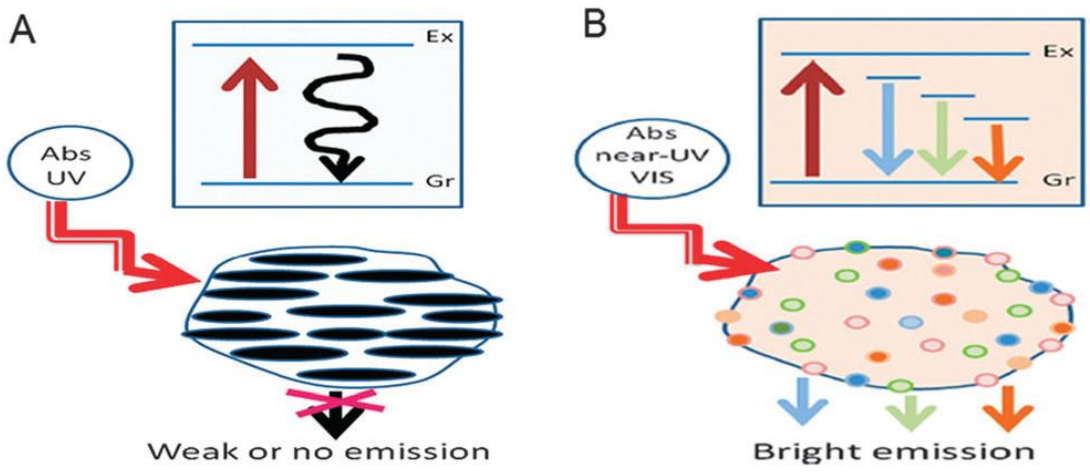

Figure 8: Scheme representing mechanisms for weak and bright fluorescence (Demchenko and Dekaliuk, 2013)

2.3 Applications of Carbon dots

In recent years, biomedical applications of CDs have set an increasing trend due to their biocompatibility, non toxic nature and excellent photoluminescent properties as already discussed before. QDs can be hazardous to health as they contain heavy metals which are toxic and hence they are being replaced by CDs for various applications like sensing, imaging and drug delivery. CDs having size lesser than 10 nm can be easily taken up, excreted and have longer blood circulation times when compared to the large sized particles.

The traits such as low cytotoxicity and excellent biocompatibility make CDs ideal platform for sensing and imaging applications (Wen et al., 2015). CDs have been used for biosensing of biomolecules as well as small analytes including DNA (Bai et al., 2011), dopamine (Li et al., 2014) (Qu et al., 2013), ascorbic acid (Gong et al., 2015) etc. Blood glucose sensing based on CDs from phenylboronic acid has been reported by Shen et al (Shen and Xia, 2014). Hg^{2+} detection using sensor based on amine coated CDs has also been reported (Yuan et al., 2014). A chemosensor based on CDs synthesized from starch has been reported by Basu et al for the selective detection of fluoride ions in aqueous solution which can be used for detecting environmental pollutants (Basu et al., 2015). Aptamer functionalised CDs for sensitive and selective detection of thrombin has been reported by Xu et al (Xu et al 2012).

CDs are attractive candidates for bioimaging due to their biocompatibility and photoluminescent properties. Hydrophilic CDs are preferred to hydrophobic ones for imaging applications (Esteves da Silva and Gonçalves, 2011). The expediency of

CDs as fluorescence contrast agents in mice were first analyzed by Yang et al (Yang et al., 2009). The same method was later followed in nude mice by Tao et al (Tao et al., 2012). Hyaluronic acid conjugated CDs were used for the targeted delivery of liver diseases. The study includes in vitro bioimaging along with the in vivo real time bioimaging ensuring the bioimaging property of CDs (Goh et al., 2012). Li et al have reported cellular imaging using CDs obtained by the carbonization of sucrose with oleic acid. CDs prepared with lithium intercalated graphite as the carbon source, were used as cell imaging agents without any modification (Chen et al., 2013) (Zhu et al., 2014). Recently, Zheng et al have prepared CDs from D-glucose and L-aspartic for the diagnosis of brain cancer cells without the aid of any other targeting moieties (Zheng et al., 2015). CDs for the fluorescence imaging of Zebra fish have also been reported and their distribution revealed the absorption, distribution, metabolism and the excretion route (Kang et al., 2015). Depending on the passivating agents and the mode of passivation the internalization of CDs varies (Lim et al., 2015). Several studies have reported on the localization of CDs in cytoplasm alone (Wang et al., 2011) (Hu et al., 2014) or both cytoplasm and cell membrane (Cao et al., 2007) (Hsu et al., 2013) (Qiao et al., 2010).

CDs can serve as ideal drug delivery systems due to their ease of functionalization followed by conjugation of drug molecules and targeting moieties (Lim et al., 2015). Lai et al have synthesized CDs via pyrolysis of glycerol and confined their growth within mesoporous silica for improved size distribution followed by capping of polyethylene glycol (Lai et al., 2012). The system was then loaded with anticancer drug, doxorubicin, thus forming a versatile platform for drug release and cell imaging. Mewada and coworkers designed a system of sorbitol derived CDs for the

targeted delivery of doxorubicin in presence of folic acid. The drug loading capacity of doxorubicin was found to be 86% thus confirming CDs as ideal drug delivery vehicle. The system was found to be less toxic to cells and showed high killing rate of cancer cells when compared to free doxorubicin (Mewada et al., 2014). CDs derived from phenylalanine were used for the delivery of the drug haloperidol in presence of cysteamine as the linker (Pandey et al., 2013). Zheng et al have conjugated an anticancer drug, oxaliplatin on the surface of CDs to form a multifunctional theranostic agent with combining chemotherapy and bioimaging properties (Zheng et al., 2014). Doxorubicin loaded hyaluronic acid and CDs based nanocomplex as theranostic carrier have been recently reported (Yang et al., 2015). Wang et al have reported CDs from commercial beer for image guided cancer therapy (Wang et al., 2015).

Pandey et al have reported hybrid tri-functionalized probe comprising CDs, gold nanorods and doxorubicin for drug delivery, bioimaging and photothermal therapy (Pandey et al., 2013). Kim et al formed an assembly by coupling CDs with gold nanoparticles and thereafter conjugated with polyethylenimine-plasmid DNA for the delivery of DNA to the cells (Kim et al., 2013). Wang et al have introduced multifunctional hybrid system including Fe_3O_4 nanocrystals and CDs thereby providing NIR controlled drug release profile as well as combined photothermal treatment (Wang et al., 2014).

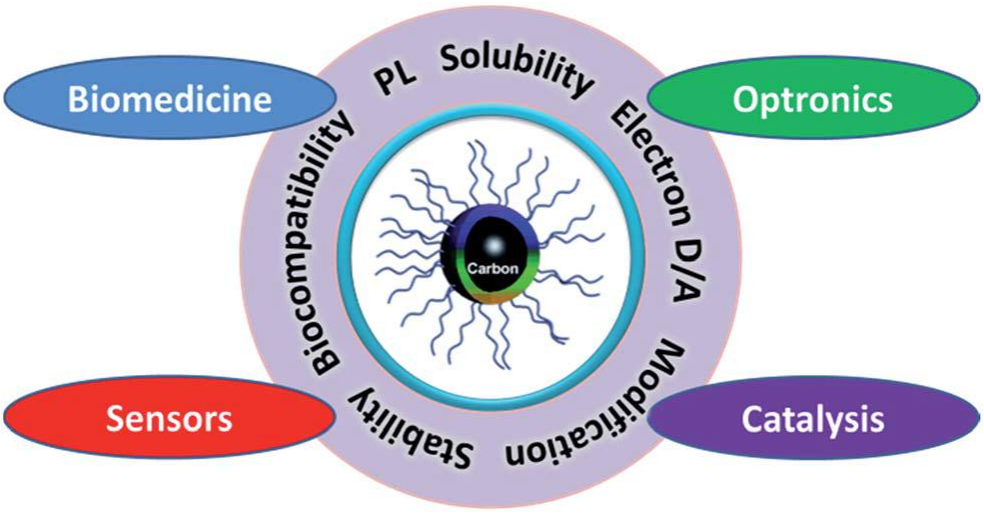

Figure 9: Scheme representing the use of CDs for various applications due to their unique features (Wang and Hu, 2014)

3 MATERIALS AND METHODS

3.1 In Vitro detection of calcium in bone by modified carbon dots

3.1.1 Materials

Hyaluronic acid (HA) was purchased from Fluka Analytical, Bangalore, India. Citric acid anhydrate, Poly(ethylene glycol) bis(3-aminopropyl) terminated (PEGD, MW 1500), L-glutamic acid (GA), glycerine, N-(3-Dimethylaminopropyl)-N' ethyl carbodiimide (EDC) were obtained from sigma Aldrich, Bangalore, India.

L-929 cells (mouse fibroblast cells) were obtained from ATCC (Bangalore, India) and 3-(4,5-dimethylthiazol-2-yl)-2,5-diphenyltetrazolium bromide (MTT reagent) was obtained from Sigma Aldrich, Bangalore, India.

3.1.2 Synthesis of amino functionalized Carbon dots (CDs)

CDs were synthesized according to the method reported earlier (Wang et al. 2010). Briefly, 9 ml of glycerin and 600 mg of PEGD were taken in a 100 mL three-neck flask degassed with nitrogen. When the temperature was raised to 250 °C, 600 mg of citric acid was added and allowed to react at this temperature for 3 h. The resulting product was cooled to room temperature and dialyzed against distilled water using a cellulose ester dialysis membrane [molecular weight cut off (MWCO) = 3500] for 2 days in order to remove any unreacted components.

3.1.3 Conjugation of HA and GA onto CD

The conjugation of HA and GA onto CDs was done on the basis of the EDC chemistry via the formation of an amide linkage between the carboxyl groups of HA and GA and the amine groups of the CD. 0.5 wt% HA and 0.1 wt% GA were mixed

with CD (5 mL, 1mg/ mL) in presence of 5 wt% EDC. pH of the solution was maintained at ~ 4.2 and the reaction mixture kept overnight at 4 °C. The resulting solution was dialyzed against distilled water in a dialysis membrane of MWCO = 3500 for 2 days and stored in refrigerator until used.

3.1.4 Physico chemical characterization

3.1.4.1 Fourier Transform Infra Red (FTIR)

FTIR spectra were recorded in the range 600-4000 cm^{-1} on a Nicolet 5700 FTIR Spectrometer, Nicolet Inc, Madison, USA using a Diamond ATR accessory.

3.1.4.2 Proton Nuclear Magnetic Resonance (H^1NMR)

H^1NMR spectrum of HAGACD was recorded using Bruker AV 500 NMR (500 MHz) spectrometer (Switzerland).

3.1.4.3 High Resolution Transmission electron microscopy (HRTEM)

HRTEM was performed in an FEI, TECNAI S Twin microscopy with an accelerating voltage of 100 KV. The sample solutions (CD) were prepared by dispersion under an ultrasonic vibrator. They were then deposited on a formvar coated copper grid and dried in a vacuum at room temperature before observation.

3.1.4.4 Transmission Electron Microscopic (TEM)

TEM images were obtained on a Hitachi, H 7650 microscope, Hitachi, Tokyo, Japan. The colloidal solution (HAGACD) was deposited onto a 200 mesh copper grid coated with a formvar film and dried overnight.

3.1.4.5 Determination of particle size and zeta potential

The technique of Dynamic Light Scattering (DLS), Malvern Instruments Ltd, UK was used for the determination of size and the zeta potential of the nano particles.

3.1.4.6 Thermo gravimetric analysis (TGA)

TGA was done on a SDT Q600, simultaneous DTA-TGA system (TA Instruments Inc., USA). 5mg of the sample was taken in a platinum cup and heated under nitrogen atmosphere at a heating rate of 10 °C from room temperature to 500 °C.

3.1.4.7 UV-Visible spectrophotometer

The UV-Visible absorption spectra of the CD and HAGACD were recorded using a UV-Visible spectrophotometer, Varian, Cary 100 Bio, Melbourne, Australia.

3.1.4.8 Spectrofluorimeter

The fluorescence spectra were measured using a Spectrofluorimeter, Varian, Cary Eclipse model EL 0507, Melbourne, Australia.

3.1.4.9 Fluorescence microscope

The fluorescent images were taken using a Fluorescent microscope, Leica DM IL Generic, Switzerland.

3.1.5 Cytotoxicity studies

The *in vitro* cytotoxicity of HAGACD was carried out by direct contact assay as per ISO 10993-5 and by MTT [3-(4,5-dimethylthiazol-2yl)-2,5-diphenyltetrazoliumbriomide] assay as per reported protocol (Ciapetti et al.1993).

3.1.5.1 Direct contact method

HAGACD was filtered through 0.22 µ pore size syringe filter. 40 µL of it was soaked on a filter paper and placed on confluent monolayer of L929 mouse fibroblast cells in triplicate. The negative controls (high density polyethylene) and the positive controls (Stabilized PVC disc) in triplicate were also placed on cells. After incubation at 37±1 ºC for 24±2 h, cell monolayer was examined microscopically for the response around the test samples. The cytotoxic reactivity of test and control samples was evaluated microscopically (Leica Inverted Fluorecsence Microscope, DMI 6000; Leica microsystem, Wetzlro, Germany).

3.1.5.2 MTT assay

MTT assay was performed to measure the metabolic activity of cells to reduce yellow coloured tetrazolium salt (MTT) to purple colored formazan. 1 mg of HAGACD was dissolved in 2 mL culture medium containing serum and then diluted to get 100 µg, 50 µg, 25 µg and 12.5 µg per 100 µL and was filtered using 0.22 µ membrane filter.100 µL of various concentrations of the probe, extract of negative control, UHMWPE (Ultra high Molecular Weight Poly Ethylene), cell control and positive control [phenol stock solution diluted (1.3 mg/mL) with culture medium containing serum] were placed on subconfluent monolayer of L-929 cells. After incubation of cells with the samples and controls at 37±1 ºC for 24 ± 2 h, extract and control medium was replaced with MTT solution (1mg/ml in medium without supplements), wrapped with aluminium foil and incubated at 37±2 ºC for 2 h. After discarding the MTT solution, 100 µL of isopropanol was added to all wells and

swayed the plates. The color developed was quantified by measuring absorbance at 570 nm using a spectrophotometer (Model UVM 340, ASYS, Austria).

3.1.6 Haemolysis assay

Blood from human volunteer was collected into the anticoagulant ACD. Each sample was transferred to polystyrene petri dishes and 2 mL blood was added, 1 mL blood was taken immediately for initial analysis and remaining 1 mL blood was incubated with samples for 30 min under agitation at 70 ± 5 rpm using an Environ shaker thermo stated at 35 ± 2 ºC. Four empty polystyrene culture dishes were exposed with blood as reference. The total hemoglobin in the whole blood samples were measured using automatic Hematology Analyzer (Sysmex-K 4500). The free hemoglobin liberated into the plasma after exposure to samples were measured using diode array spectrophotometer and the percentage hemolysis was calculated using the formula, (Free Hb/Total Hb/1000) x 100.

3.1.7 Preparation of Poly Vinyl Alcohol (PVA) films containing Ca

PVA, hot water soluble films were cast without Ca^{2+} and with varying concentrations of Ca^{2+} (0.02M, 0.25M, 0.5M, 1M, 2M and 3M). Equal weight of the films were cut and immersed in 2 ml of HA conjugated with GA and CD (HAGACD) for 30 min. Films were washed, dried and observed through a fluorescent microscope at 20x using a blue filter.

3.1.8 Interaction of the probe with cations other than calcium and coexisting substances in blood

Solutions of appropriate concentrations of sodium, potassium, magnesium and iron were prepared and 100 µL of the same were added separately to 2 mL HAGACD in order to have their final concentrations similar to their respective contents in blood serum (eg: Sodium- 145 mM/L, Potassium- 5.0 mM/L Magnesium- 2.5mg/dL and Iron (Fe^{3+}) - 60 ng/mL). The fluorescence intensity of these solutions was measured by spectrofluorimeter.

To investigate the interferences from other coexisting substances, the experiment was done in presence of human blood serum.

3.1.9 Interaction of the probes with bone

Freshly cut bones collected from slaughter house were cleaned and removed skin. Bone pieces were incubated with HACD (probe without GA) and HAGACD solutions for 30 min rinsed in distilled water and illuminated using a UV source (365 nm) and photographed.

3.2 Simultaneous bone crack detection and drug deposition using modified carbon dots

3.2.1 Materials

Citric acid anhydrate, Poly(ethylene glycol) bis(3-aminopropyl) terminated (MW 1500), glycerine, L-glutamic acid (GA), EDC, ninhydrin and ciprofloxacin were obtained from sigma Aldrich, Bangalore, India

L-929 cells (mouse fibroblast cells) were obtained from American Type Culture Collection (ATCC, Bangalore, India) and 3-(4,5-dimethylthiazol-2-yl)-2,5-diphenyltetrazolium bromide (MTT reagent) was obtained from Sigma Aldrich, Bangalore, India.

3.2.2 Conjugation of GA and ciprofloxacin onto CD

CDs were synthesized as reported earlier (Wang et al. 2010), which is detailed in the section 3.1.2. 10 mL amino functionalised CDs (1.5 mg/ mL) were reacted with aqueous solutions of 6.0 mM each of ciprofloxacin and GA in presence of 0.26 M EDC at pH ~ 4.2. The reaction mixture was kept overnight at 4 °C. The solution was purified by dialyzing against distilled water using a cellulose ester dialysis membrane [MWCO = 3500] for 2 days in order to remove any unreacted reactants and the resulting solution (CDGAC) was used for further studies. The amount of GA conjugated onto CD was calculated by ninhydrin method (Meyer, 1957). Unreacted GA obtained after the dialysis of CDGAC was estimated by this method. This quantity was subtracted from the initial amount of GA to get quantity of GA in the conjugate. The amount of ciprofloxacin conjugated onto CD was calculated from the antibacterial study by Minimum Inhibitory Concentration (MIC) method using tube dilution.

3.2.3 Physico chemical characterization

FTIR, H^1NMR, HRTEM, UV-Visible spectrophotometer and Spectrofluorimeter were done as described in the section physiochemical characterization, 3.1.4.1, 3.1.4.2, 3.1.4.3, 3.1.4.8 and 3.1.4.9 respectively.

3.2.3.1 Thermo gravimetric analysis (TGA)

TGA was carried out using an SDT Q600, simultaneous DTA–TGA system (TA Instruments Inc., USA). Approximately 3 mg sample was taken in a platinum cup and heated under nitrogen atmosphere at a rate of 10 ºC min^{-1} from room temperature to 900 ºC.

3.2.3.3 Differential scanning calorimeter (DSC)

Thermal analysis was carried out with DSC, (TA Instruments, USA) DSC Q100, using MDSC (Modulated DSC) mode under nitrogen atmosphere at a heating rate of 3 ºC min^{-1} and at a modulation amplitude of 1 ºC for a period of 60 s.

3.2.3.4 X-ray diffraction studies (XRD)

The XRD analysis of the materials was carried out using an X-ray diffractometer (Bruker, Model-D8 advance, Switzerland).

3.2.4 Cytotoxicity studies

The *in vitro* cytotoxicity of CDGAC was carried out by direct contact assay and MTT assay.

3.2.4.1 Direct contact method

Cytotoxicity evaluation by direct contact was carried out as explained in section 3.1.5.1

3.2.4.2 MTT assay

MTT assay of CDGAC was performed as detailed in section 3.1.5.2

3.2.5 Haemolysis assay

The assay was based on earlier report (Rekha et al. 2009). Blood was drawn from a healthy volunteer and the collected blood (anticoagulated with sodium citrate) was centrifuged at 1000 rpm for 10 min (Sigma, Refrigerated centrifuge, 3K300), plasma removed and washed with normal saline and again centrifuged. Supernatant was discarded and the pellet was diluted 1:10 with saline. 100 µL of this was added to 100 µL of the sample (triplicate) and incubated for 45 minutes under agitation (70±5 rpm) using an orbital shaker (Orbitek, Scigenics, Biotech, Chennai) thermostated at 37±1 ^{o}C. The samples were again centrifuged and supernatant made up to 1 mL with saline and absorbance was measured at 540 nm. Saline was used as the negative control and 1 % Triton-X was used as the positive control. The absorbance for Triton X with maximum haemolysis was taken as 100 % and the extent of haemolysis for the samples were calculated from the respective absorbance.

3.2.6Antibacterial study

Antibacterial activity was studied using the bacterial strain *E.coli* (ATCC25922) by Minimum Inhibitory Concentration (MIC) method using tube dilution followed by sub culturing on Muller Hinton Agar.

3.2.7 Detection of bone cracks using *in vivo* imaging system *(IVIS)*

Freshly collected bone from slaughter house was cleaned and incubated with CDGAC overnight. Thereafter washed, dried and imaged with the Xenogen (Caliper Life Sciences) IVIS Spectrum *in vivo* imaging system (USA) in which quantitative

monitoring is possible to visualize the bone cracks selectively targeted by the fluorescent probes.

3.3 Detection and imaging of fatty plaques on blood vessels using functionalized carbon dots

3.3.1 Materials

Citric acid anhydrate, Poly(ethylene glycol) bis(3-aminopropyl) terminated (MW 1500),Glycerin, Adipic acid (AD), EDC, Digitonin, Dicyclohexylcarbodiimide (DCC), Dimethylamino pyridine (DMAP), Cholesterol, Valine, Cystine, Glycine, Lysine, Tryptophan, Methionine, ascorbic acid, dopamine, glutathione and uric acid were obtained from sigma Aldrich, Bangalore. All other chemicals used were of analytical grade and obtained from Merck India Ltd, Mumbai, India.

3.3.2 Conjugation of DG onto CDs

CDs were synthesized as explained in the section 3.1.2. PEG diamine passivated CDs were modified with adipic acid (AD) via EDC chemistry to get carboxyl terminated CDs. CDs (5 mL, 1mg/ mL) were mixed with 2 mL of AD (0.013 M, H_2O) and 2 mL of EDC (0.26 M, H_2O) after adjusting the pH to ~ 4.2. The reaction mixture was kept overnight at 4 °C and the resulting solution was purified by dialyzing against distilled water using a cellulose ester dialysis membrane [MWCO = 3500] for 2 days in order to remove any unreacted reactants. Further, DG was conjugated onto CDAD by DCC/DMAP reaction. CDAD (10 mL, 0.5 mg/mL) was stirred with 1 mL of DCC (0.015 M, DMSO) and 500 µL of DMAP (0.001 M, DMSO), for the activation of –COOH groups on CDAD. 1 mL of DG (0.013 M,

DMSO/H_2O) was then added to the reaction mixture and stirred overnight at room temperature. The solution was dialyzed against DMSO/H_2O mixture using a cellulose ester dialysis membrane [MWCO = 3500] for 2 days and the resulting solution (CDDG) was used for further studies.

3.3.3 Physico chemical characterization

FTIR, H^1NMR HRTEM, TEM, Zeta potential, UV-Visible spectrophotometer, Spectrofluorimeter, fluorescence microscope and DSC using MDSC mode were used as described in the section physiochemical characterization, 3.1.4.1, 3.1.4.2, 3.1.4.3, 3.1.4.4, 3.1.4.5, 3.1.4.7, 3.1.4.8, 3.1.4.9, and 3.2.3.3 respectively.

3.3.4 Haemolysis assay of CDDG

The experimental procedure for determining percentage haemolysis is detailed under section 3.1.6

3.3.5 Interaction of cholesterol with CDDG

The variation in fluorescence intensity of the probe, CDDG in presence of various concentrations of cholesterol (2 mM - 20 mM) was checked. To 2 mL of CDDG 100 µL of cholesterol solutions were added. All the measurements were made in triplicate and the average was taken.

3.3.6 Interference studies with some non specific steroids (Testosterone, Hydrocortisone and corticosterone) and potential coexisting substances in serum

The interference of CDDG was checked in presence of 20 mM of testosterone, hydrocortisone and corticosterone, 200 µL each . The response of CDDG to potential coexisting substances in serum including some amino acids [valine (val), Cystine

(cys), Glycine (gly), Lysine (lys), Tryptophan (trypt) and Methionine (meth)], ascorbic acid (aa), dopamine (dop), glutathione (gt) and uric acid (ua) was also studied.

3.3.7 Binding of cholesterol to the probe, CDDG

To prove that CDDG has high affinity towards cholesterol, cholesterol solution was sprayed on a glass cover slip, air dried and incubated with aqueous CDDG for an hour, washed and viewed under fluorescence microscope at 20X using various filters. Further, the same experiment was carried out with Poly Vinyl Alcohol (PVA) films doped with cholesterol.

3.3.8 Binding of CDDG to the tissues

Fat tissue (with atherosclerotic deposit) and tissue without deposit were extracted from blood vessels surrounding the human heart tissue collected during autopsy. Consent was taken for collecting heart valve for homograft banking as per the ethical guidelines of our Institute. Fat deposited tissues and the muscle portion of the tissues (with no fat deposit) were incubated with CDDG solution for various time intervals i.e. 5 min, 30 min, 1 h, 2 h and 24 h. They were then washed with water and viewed under UV lamp at 365 nm. To mimic the actual *in vivo* condition, the fat deposited tissue and the tissue with no fat deposit were incubated with blood serum containing 230 mg/dL cholesterol mixed with CDDG and kept at 37 ºC under shaking for 1 h. The tissues were also imaged with Xenogen (Caliper Life Sciences) IVIS Spectrum (USA) *in vivo* imaging system at an excitation wavelength of 430 nm.

3.4 Gold nano rod-carbon dot hybrid system for simultaneous imaging and possible disruption of cholesterol plaques

3.4.1 Materials

Hydrogentetrachloroaurate(III)trihydrate($HAuCl_4.3H2O$),Hexadecyltrimethylammoniumbromide (CTAB), Sodium borohydride (99%), L-ascorbic acid, silver nitrate, Mercaptosuccinic acid, Citric acid anhydrate, Poly(ethylene glycol) bis(3-aminopropyl) terminated (MW 1500), Glycerin, Adipic acid(AD), EDC, Digitonin, DCC and DMAP were purchased from Sigma-Aldrich, Bangalore.

Glioma cells (C6 cells from rat brain tumor) were obtained from the National Centre for Cell Sciences (NCCS), Pune, India. 3-(4,5-dimethylthiazol-2-yl)-2,5-diphenyltetrazolium bromide (MTT reagent), Fetal bovine serum (FBS) were purchased from Sigma-Aldrich (Bangalore, India). Trypsin/EDTA and Nutrient F-12 Ham were purchased from Invitrogen (Bangalore, India).

3.4.2 Synthesis of gold nanorods (NR)

NRs were prepared using seed mediated growth method, growth of NRs with plasmon band less than 850 nm as reported by (Nikoobakht and El-Sayed, 2003). In brief, seed solution was prepared by adding 5 ml, 0.2 M CTAB solution to 5 ml, 0.5 mM $HAucl_4$ and stirred well. To this mixture 0.6 ml of 0.01 M ice cold $NaBH_4$ was added, a brownish yellow solution was obtained, vigorously stirred for 2 minutes and the seed solution was kept at 25 °C. CTAB solution (5 ml, 0.2 M) was added to 0.25 ml of 0.004 M $AgNO_3$ solution at 25 °C followed by the addition of 1 mM $HAucl_4$ solution, mixed well and 70 µl of 0.0788 M ascorbic acid was added. Dark yellow growth solution turns colorless to which 12 µl of the seed solution was

added at 27-30 °C. Colour changes to purple within 10 minutes. The solution was centrifuged twice at 10000 rpm for 10 minutes and the pellet formed was redissolved in distilled water for further conjugation.

3.4.3 Conjugation of NRs to CDDG

CDs were synthesized as explained in the section 3.1.2. CDs were modified with DG as detailed in the section 3.3.2.

To the centrifuged 2 mL of NRs (2 mg/ mL) solution, a drop of tween 20 was added, allowed to stand for 20 minutes and incubated with 1 mL of 30 mM mercaptosuccinic acid (MSA) for 3 h. Excess tween 20 and MSA were removed by centrifugation at 10000 rpm for 10 minutes. Thus NRs modified with MSA i.e NRMSA was then conjugated to CDDG using carbodiimide chemistry. 3 mL of NRMSA (1 mg/ mL) was added to 3 mL of CDDG (0.5 mg/ mL) in presence of 1 mL of EDC (0.26 M) at pH ~ 4.2. The reaction mixture was kept overnight at 4 °C. The solution was purified by dialyzing against distilled water using a cellulose ester dialysis membrane [MWCO = 3500] for 2 days in order to remove any unreacted reactants and the resulting solution (CDNR) was used for further studies. The COOH groups of NRMSA react with the available amino groups of CD in CDDG.

3.4.4 Physico chemical characterization

FTIR, TEM, Zeta potential, UV-Visible spectrophotometer and Spectrofluorimeter were used as described in the section physiochemical characterization 3.1.4.1, 3.1.4.4, 3.1.4.5, 3.1.4.7 and 3.1.4.8 respectively.

3.4.4.1 Laser light exposure to the fat deposited tissues

Tissues with fat deposit incubated with CD and CDNR were exposed to Laser (808 nm, 1.5 W) (MDL-111, China) and the temperature changes were measured using a multimeter (Multiravi).

3.4.4.2 Environmental Scanning Electron Microscope (ESEM)

The surface morphology of the tissues after Laser exposure was analyzed using ESEM, Model FEI Quanta 200, Netherlands. The samples were directly placed on the stub, voltage of 20 kV was applied and images were recorded at 500 X magnification, using LFD detector in low vacuum mode.

3.4.5 *In vitro* cytotoxicity study by MTT assay

The *in vitro* cytotoxicity of NR and CDNR were evaluated using a standard 3-(4,5-dimethyl thiazol-2-yl)-2,5-diphenyl tetrazolium bromide (MTT) assay. The C6 glioma cells were trypsinized and seeded into 96 well plates and incubated for 24 h at 37 ^{0}C in 5% CO_2. Cells were then incubated with each sample (1 mg/mL) along with 1% TritonX-100 as the positive control and medium as the negative control in triplicates at 37 ^{o}C for 24 h in 5% CO_2. After 24 h incubation, samples were removed, MTT reagent was added to each well and cells were further incubated for 3 h. The reagent was then removed and dimethyl sulfoxide (DMSO) was added to dissolve the formazan crystals formed by the reduction of MTT and the absorbance was measured at 570 nm using an automated microplate reader (Infinite M200, TECAN). Cell viability was expressed as mean percentage sample absorbance relative to the absorbance of control.

$$Cell\ viability\ = (absorbance\ of\ sample \div\ absorbance\ of\ control)\ \times 100$$

3.4.6 Cellular uptake studies

For cellular uptake studies, C6 glioma cells were trypsinized and seeded into four well plates at a concentration of 1 x 10^5 cells per well and incubated for 24 h at 37 ^oC in 5% CO_2. CDNR was prepared at a concentration of 1 mg/mL of which 100 µL was added to the cell and incubated for 3 hrs in the F12HAM medium containing 10 % FBS at 37 ^oC. After incubation, cells were washed with phosphate buffer saline (PBS), pH 7.4 and fixed in 1 % formaldehyde in PBS. The uptake of nanoparticles was visualized and photographed using laser scanning confocal microscopy, NIKON A1R.

3.5 Methotrexate anchored carbon dots as theranostic probes: Digitonin conjugation enhances cellular uptake and cytotoxicity

3.5.1 Materials

Citric acid anhydrate, Poly(ethylene glycol) bis(3-aminopropyl) terminated (MW 1500),Glycerin, Adipic acid (AD),EDC, Digitonin, DCC, DMAP and Methotrexate (MX) were obtained from sigma Aldrich, Bangalore. All other chemicals used were of analytical grade and obtained from Merck India Ltd, Mumbai, India.

Glioma cells (C6 cells from rat brain tumor) were obtained from the National Centre for Cell Sciences (NCCS), Pune, India. 3-(4,5-dimethylthiazol-2-yl)-2,5-diphenyltetrazolium bromide (MTT reagent), Fetal bovine serum (FBS) were purchased from Sigma-Aldrich (Bangalore, India). Trypsin/EDTA and Nutrient F-12 Ham were purchased from Invitrogen (Bangalore, India).

3.5.2 Conjugation of MX with CDDG

CDs were synthesized as given in the section 3.1.2. CDs were then conjugated with DG via DCC/DMAP as detailed in section 3.3.2

1 mL of methotrexate solution (5 mg/mL, DMSO) was added to CDDG (10 mL, 1mg/ mL) was stirred with 1 mL of DCC (0.015 M, DMSO) and 500 µL of DMAP (0.001 M, DMSO) for 3 h at room temperature and the solution was dialyzed against DMSO alone followed by DMSO/H_2O mixture and distilled water alone using cellulose ester dialysis membrane [MWCO = 3500] the resulting solution (CDMX) was used for further studies.

3.5.3 Physico chemical characterization

FTIR, H^1NMR, Zeta potential, UV-Visible spectrophotometer and Spectrofluorimeter were used as described in the section physiochemical characterization, 3.1.4.1, 3.1.4.2, 3.1.4.5, 3.1.4.7 and 3.1.4.8 respectively.

3.5.4 Drug loading efficiency

The concentration of the unbound drug was measured spectrophotometrically at 303 nm and the calculation was made using the standard caliberation curve of methotrexate. Drug loading efficiency (DLE) was calculated as per the equation,

$$DLE = \frac{(Amount\ of\ drug\ taken - Amount\ of\ unbound\ drug)}{Amount\ of\ drug\ taken} X100$$

3.5.5 *In vitro* drug release study

Release study was carried out using dialysis bag of molecular weight cut off 3500. An aliquot of sample (CDMX, 5 mL) was placed in the bag and suspended in 10 mL

of PBS solution (pH 5.0) at 37 ℃ under mild stirring. Periodically, 2 mL of the release medium was withdrawn and replaced with the same amount of fresh solution. The release was determined by analyzing the sample using UV-visible absorption spectroscopy. The same method was repeated by suspending the dialysis bag containing the sample (CDMX) in PBS at pH 7.4 to evaluate the release profile under physiological conditions.

3.5.6 *In vitro* cytotoxicity study by MTT assay

The *in vitro* cytotoxicity of CM (carbon dots alone conjugated to MX, without DG), CDDG, CDMX and the free drug were evaluated by MTT assay. The methodology for MTT assay using C6 glioma cells is as detailed in the section 3.4.5

3.5.7 Cellular uptake studies

Cellular uptake studies of CM, CDDG and CDMX were carried out using C6 glioma cells and the uptake of nanoparticles was visualized using confocal laser microscope detailed in the section 3.4.6.

4 RESULTS

4.1 In Vitro detection of calcium in bone by modified carbon dots

4.1.1 Synthesis and characterization of modified carbon dots

CDs, surface functionalized with PEGD were synthesized and then conjugated with HA and GA via EDC chemistry as described in materials and method section 3.1.3. FTIR spectra depicted in Figure 10 clearly confirm the formation of HA amended with CD and GA (HAGACD). Typical bands associated with –CONH– can be seen around 1699 cm^{-1}, 1634 cm^{-1} and 1560 cm^{-1} reflecting the conjugation of CD and GA onto HA. Additionally, characteristic peaks of CD can also be seen in the conjugate around 2888 cm^{-1}.

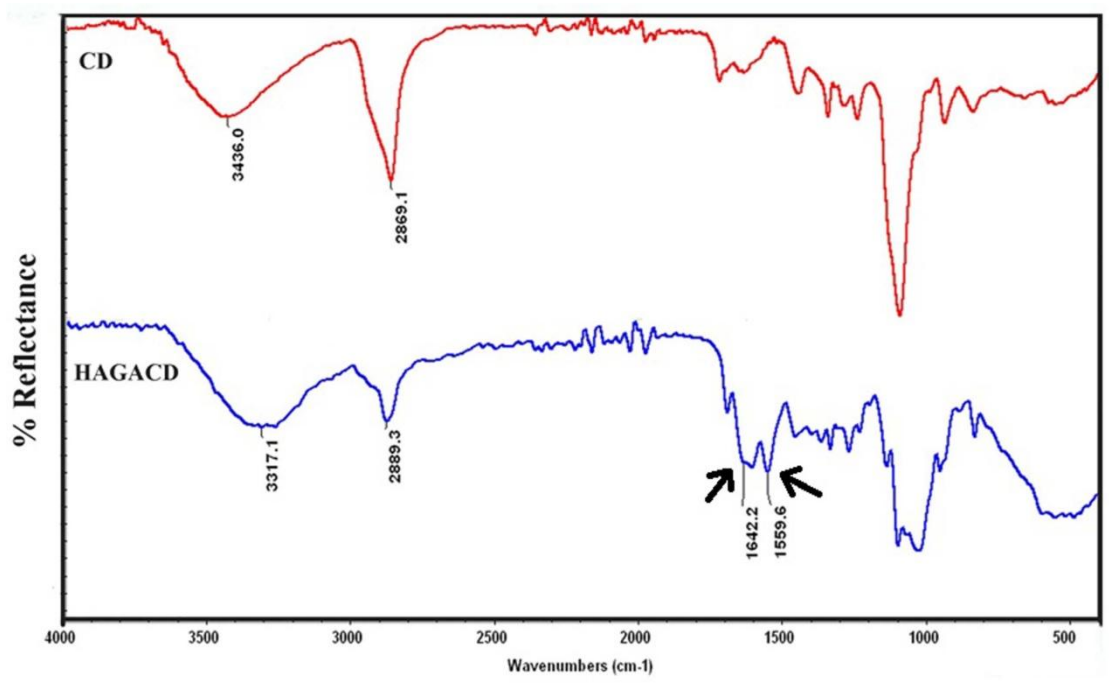

Figure 10: FTIR spectra of CD and HAGACD

H^1NMR spectra of CD and HAGACD are given in Figure 11A and 11B respectively. The peak at δ= 3.6 ppm is attributed to the methylene group of PEGD

(used for the synthesis of CD). The additional signals at 2.8 ppm, 1.8 ppm and 1.1 ppm in HAGACD (Figure 11B) correspond to the methylene group of GA, methyl protons in HA and the aliphatic hydrogen atoms in GA respectively.

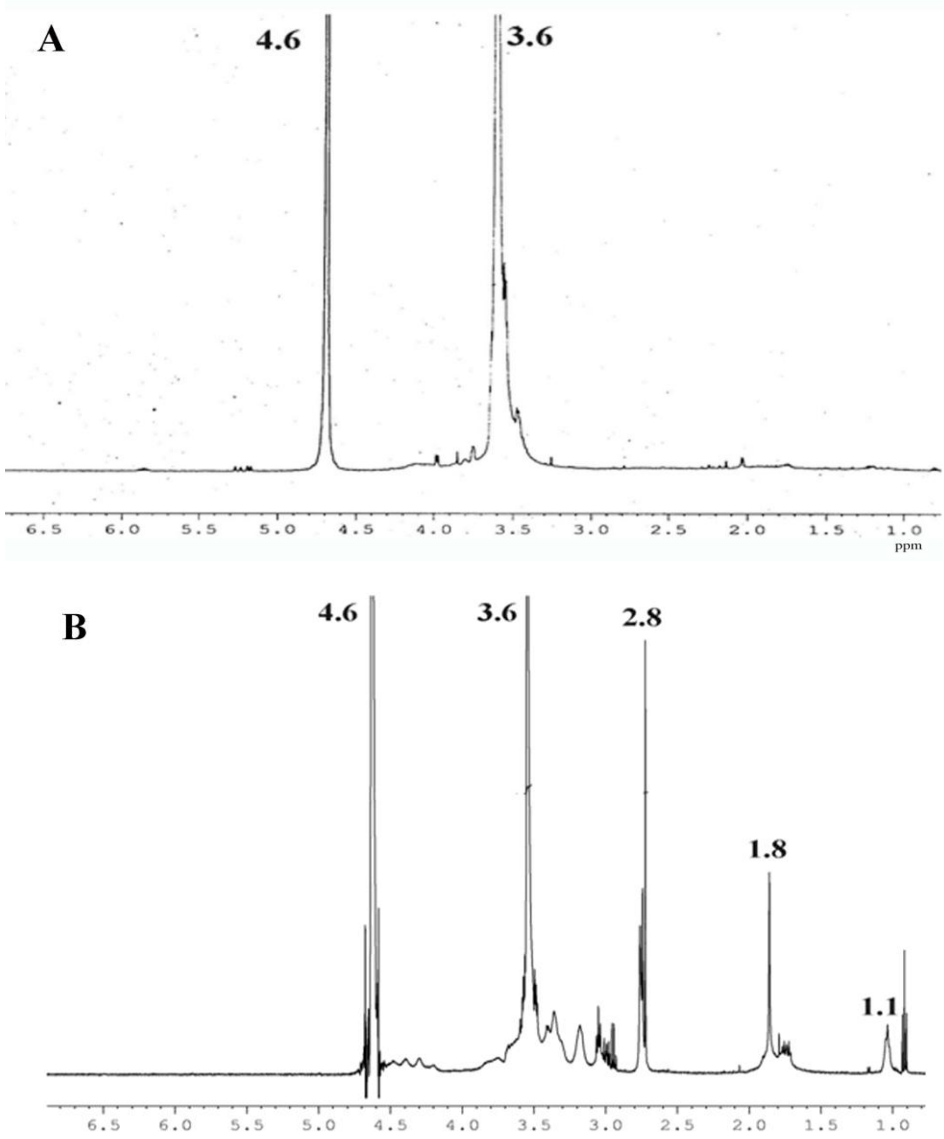

Figure 11: H^1NMR spectra of A) CD and B) HAGACD

HRTEM micrographs given in Figure 12 indicate that CD has an average size 3-5 nm and they possess spherical morphology. The size of HAGACD is significantly higher (95 nm-139 nm) as shown in the TEM images (Figure 12, C and D). The size of HAGACD is also determined by Dynamic Light Scattering analysis (DLS) to

support the increase in size due to conjugation. DLS however, showed higher values (i.e. ~ 500 nm) as evident from Figure 13.

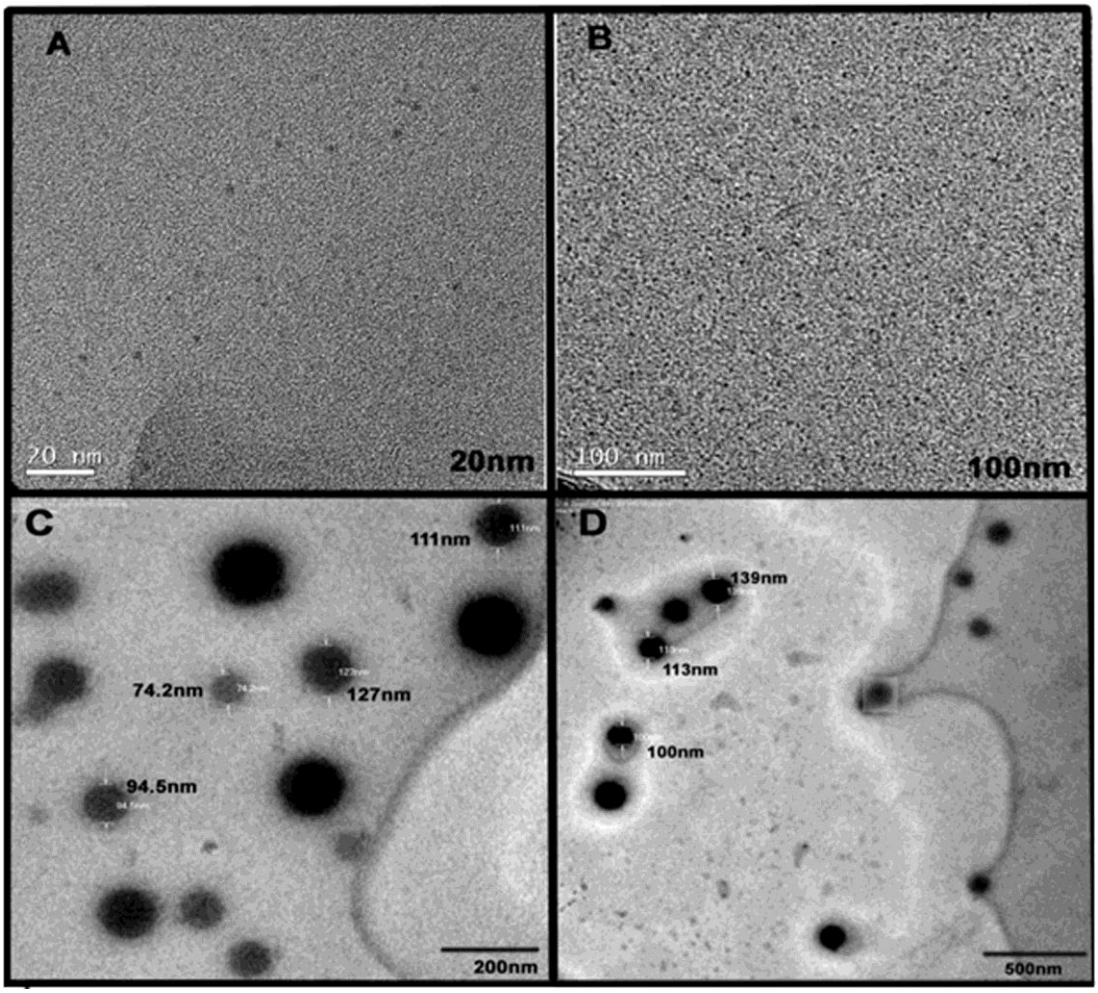

Figure 12: HRTEM micrographs of CD (A and B) and TEM micrographs of HAGACD (C and D)

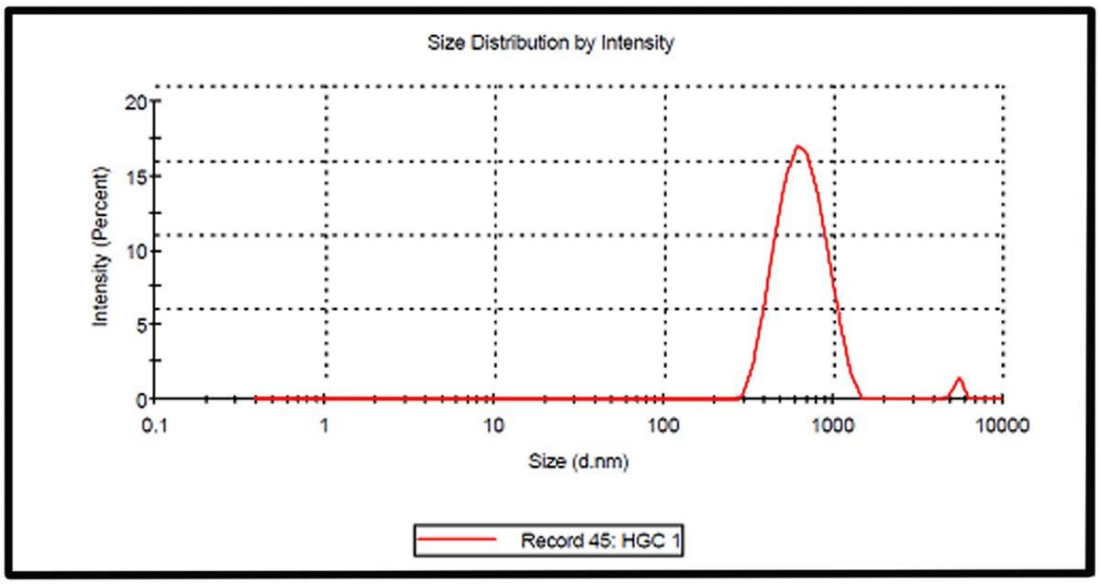

Figure 13: DLS profile of HAGACD

The thermograms of HAGACD and HA are given in Figure 14. The profile of HAGACD is differed from that of HA clearly reflecting the modification of HA to form HAGACD. The zeta potential values of the materials are given in Table 1. The decrease in zeta potential of CD from -20.9 mV to -0.58mV on conjugation further indicates the formation of HAGACD.

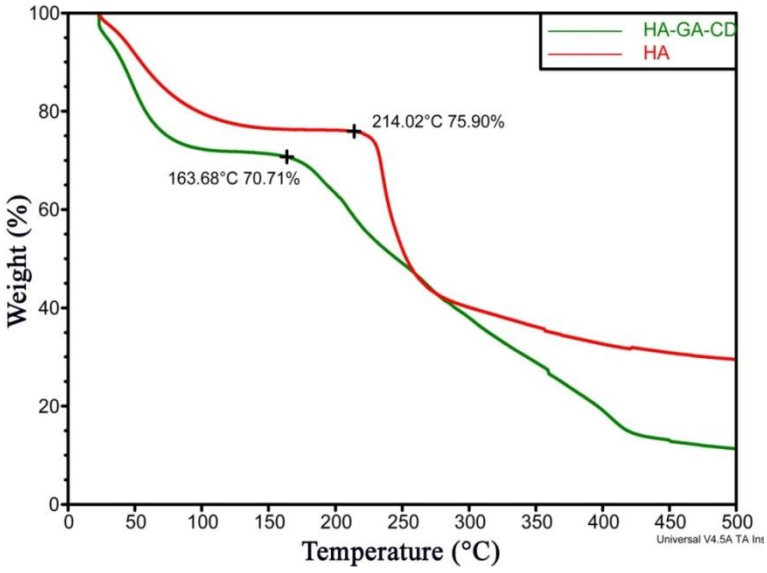

Figure 14: Thermograms of HA and HAGACD

Table 1: Zeta Potential by Dynamic Light Scattering

Sample	**Zeta Potential (mV)**
CD	-20.9
HAGACD	-0.579

UV-Visible absorption spectra of CD and HAGACD in Figure 15A show the absorbance maximum at 350 nm. The corresponding fluorescence excitation spectra (Figure 15B) confirm their excitation at the same wavelength range.

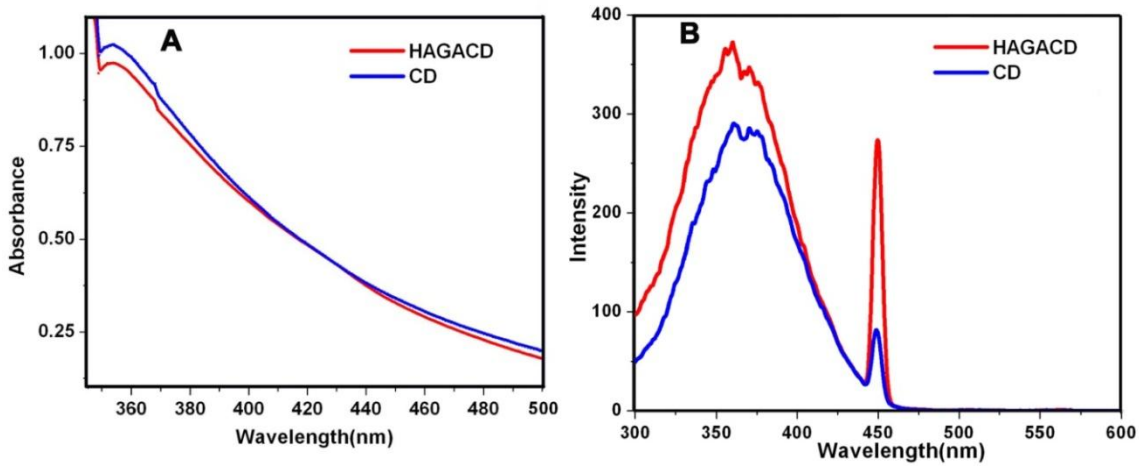

Figure 15: A) UV-Visible absorption and B) Fluorescence excitation spectra of CD and HAGACD

The fluorescence emission spectra of CD and HAGACD are shown in Figure 16. Both CD and HAGACD showed emission peak maximum around 450 nm when

excited at a wavelength of 360 nm. The photographic images of the solutions of CD and HAGACD are shown in the inset of Figure 16.

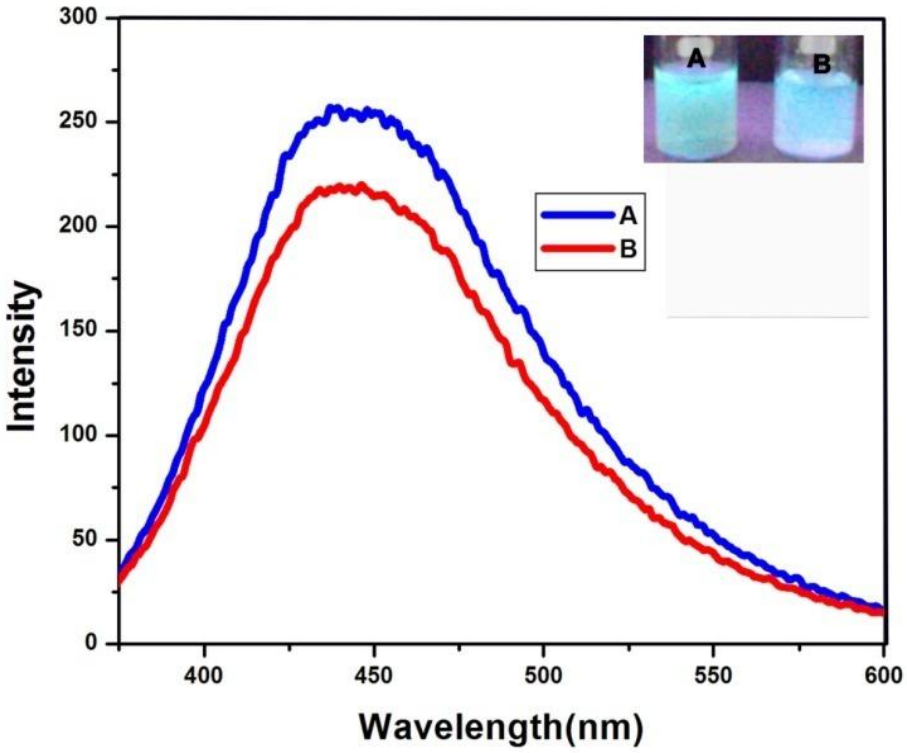

Figure 16: Fluorescence emission spectrum of (A) CD and (B) HAGACD (Inset the corresponding photographic images)

Excitation dependent emission spectrum of HAGACD is depicted in Figure 17. As the excitation wavelength increases the emission wavelength shifts slightly to longer wavelength region with decrease in fluorescence intensity. Emission maximum is observed when HAGACD is excited at 360 nm.

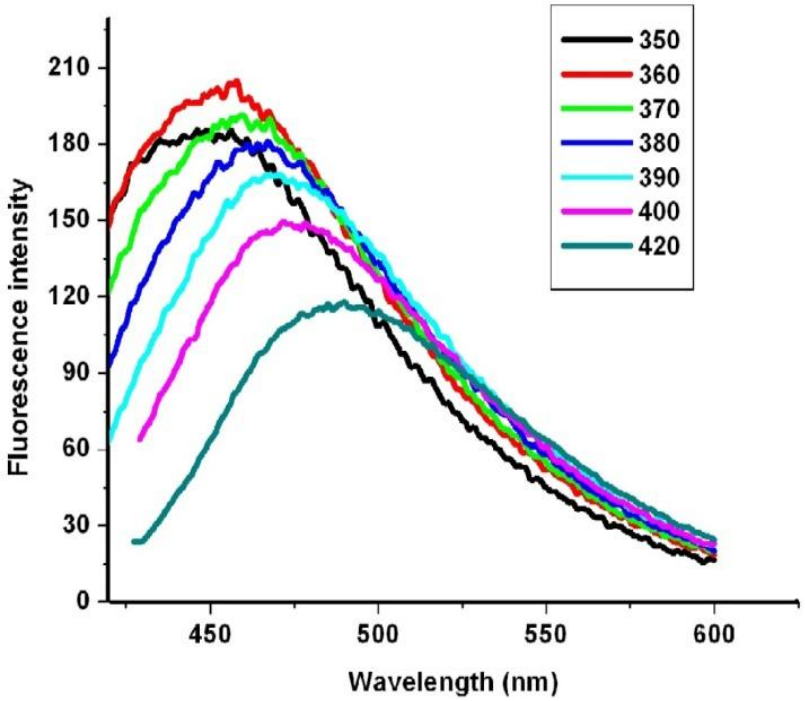

Figure 17: Excitation dependent emission spectra of HAGACD

4.1.2 *In vitro* cytotoxicity study

4.1.2.1 Direct contact method

Figures 18A, 18B and 18C depict optical micrographs of L929 cells in direct contact with HAGACD, PVC (positive control) and HDPE (negative control). Cells morphology is comparable to that of control cells indicating the non cytotoxic nature of HAGACD.

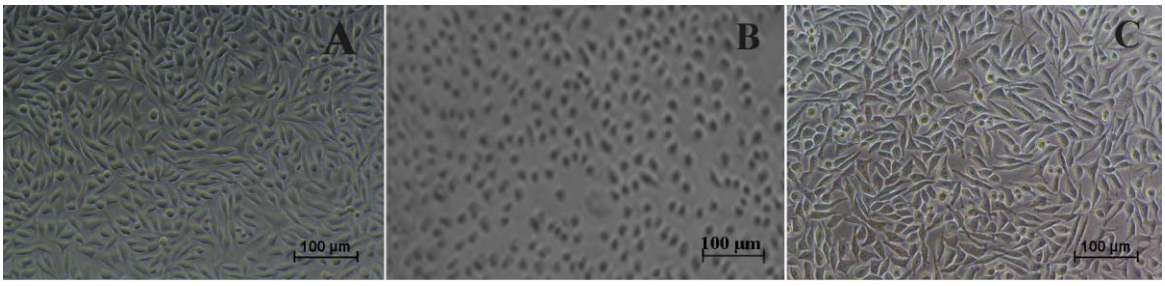

Figure 18: Optical micrographs of L929 cells on direct contact with A) HAGACD B) PVC (positive control) and C) HDPE (negative control)

4.1.2.2 MTT assay

The MTT assay of L929 cells after contact with 100 µg, 50 µg, 25µg and 12.5µg of HAGACD showed 100.79%, 102.6%, 103.13% and 104.68% metabolic activity respectively as shown in Figure 19, further confirming the non cytotoxicity of the conjugate. The results are the average of three replicate experiments.

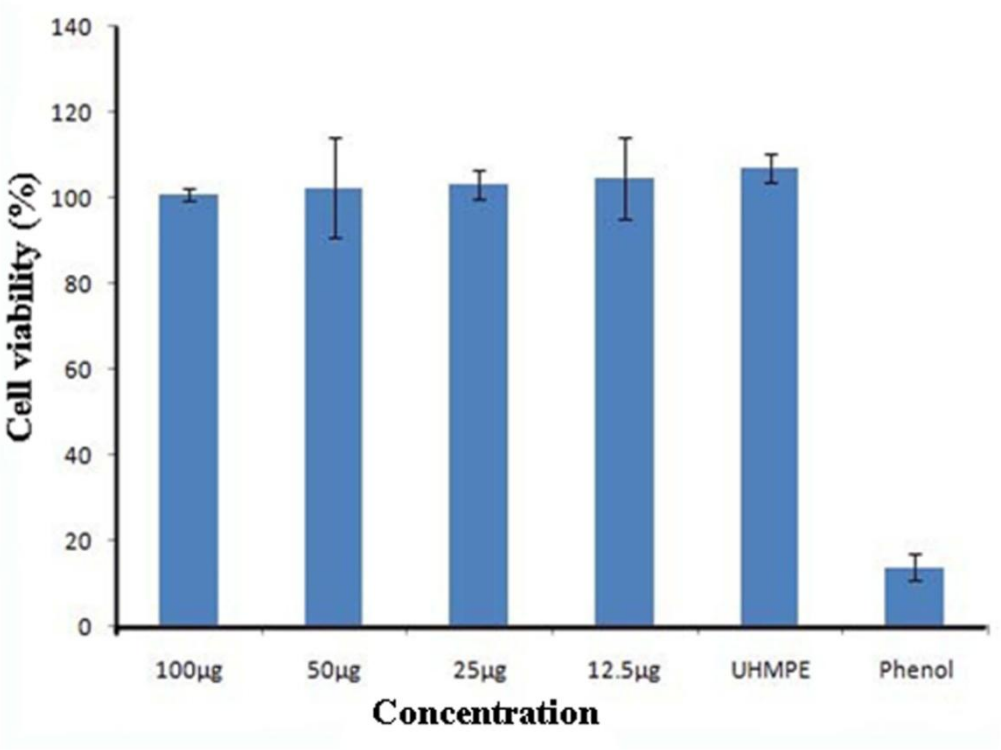

Figure 19: Concentration dependant cell viability by MTT assay

4.1.3 Haemolysis assay

The percentage haemolysis for HAGACD at two different concentrations, 0.5 mg/mL and 1.0 mg/mL were found to be 0.3 % and 0.62 % ensuring that the material is non-haemolytic.

Table 2: Haemolysis assay of HAGACD

Concentration of HAGACD (mg/mL)	Haemolysis %
0.5	0.30
1.0	0.62

4.1.4 Binding of HAGACD to the Polymer films (PVA) doped with calcium

Calcium (Ca^{2+}) incorporated PVA films were used as analogue to bone tissue to study the calcium induced targeting and subsequent mapping. PVA film after 30 min was taken out, rinsed in water, dried over a stream of air and viewed under a fluorescence microscope. As given in Figure 20B, fluorescence was observed from the polymer strip doped with Ca^{2+}. There was no fluorescence from polymer which didn't contain any Ca^{2+} (Figure 20A). We varied the exposure duration of the probes with polymer from 5 min to 60 min to assess the rapidity of interaction of the probes with Ca substrates. Noticeable variation in fluorescence was not observed reflecting that probes bind onto the substrates relatively faster.

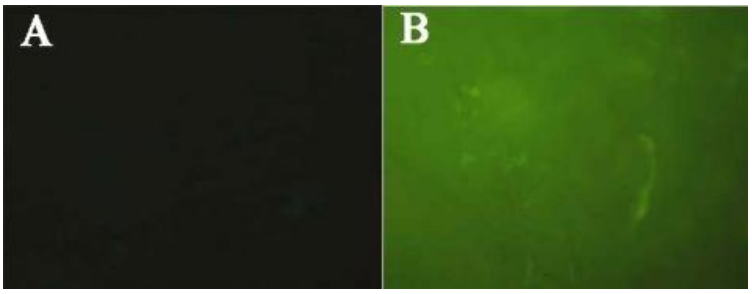

Figure 20: PVA films A) Control B) doped with 1M Ca^{2+}, viewed under fluorescence microscope

PVA films incorporated with 1M, 2M and 3M Ca^{2+} were casted and incubated in HAGACD solution. The fluorescence intensity of the solution after removing the polymer strips was measured in order to estimate the unbound HAGACD. The

intensity of fluorescence decreased with the increase in concentration of Ca^{2+} ascertaining that more probes bind onto polymer containing more Ca^{2+} as seen in Figure 21.

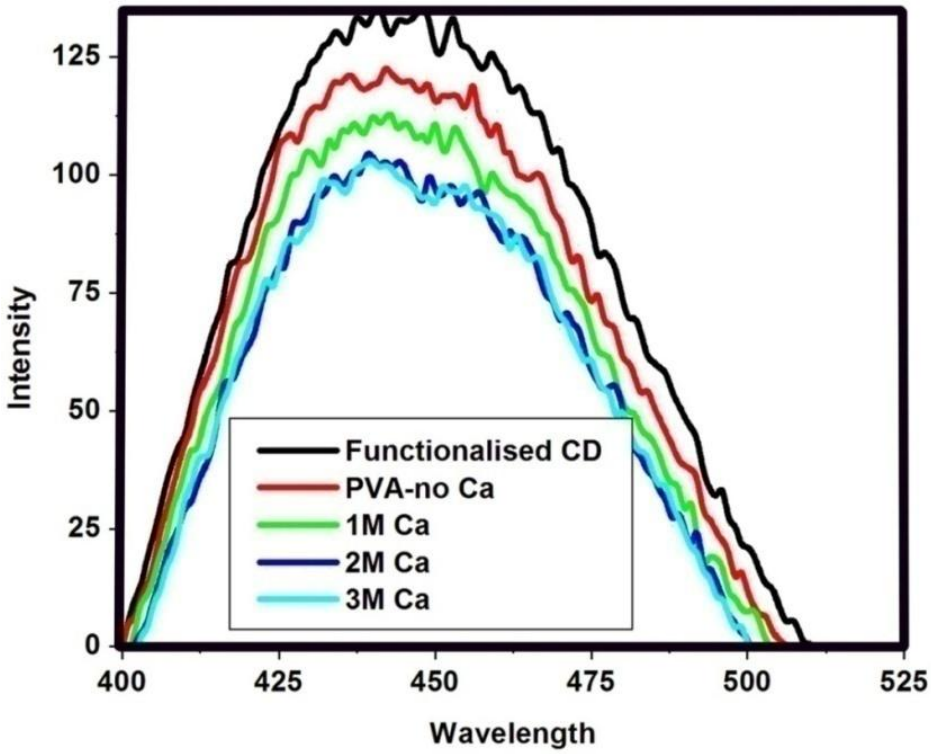

Figure 21: Fluorescence emission of HAGACD solutions after removing the incubated polymer strips. Intensity remains the same of solutions treated with polymer strips containing 2 M and 3 M reflecting saturation in binding

4.1.5 Selectivity of the method

To prove the specificity of HAGACD, its response to other cations was studied. Negligible interference was observed as evident from Figure 22.

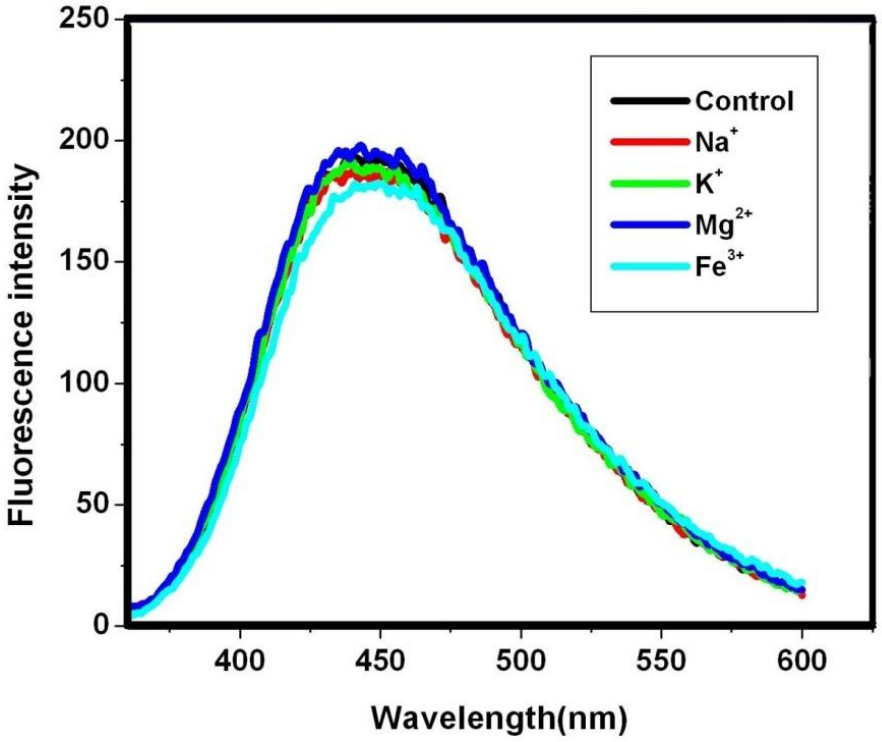

Figure 22: Fluorescence emission of HAGACD solutions in presence of different cations

To check the interferences from other coexisting substances, the experiment was repeated with human blood serum and it was observed that the fluorescence intensity of the probe remained unaffected as shown in Figure 23.

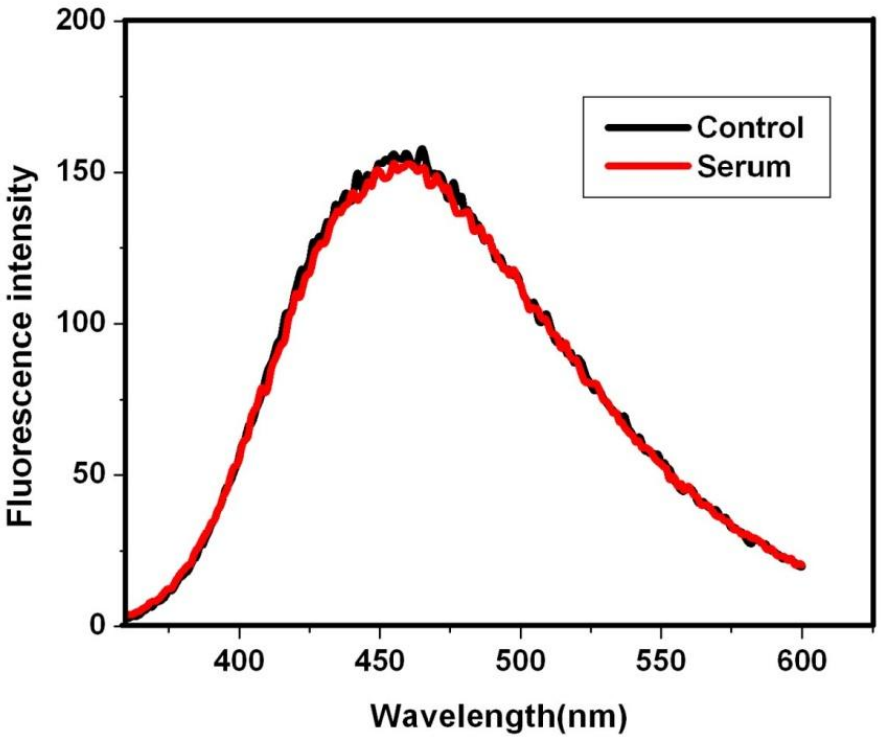

Figure 23: Fluorescence spectra of aqueous HAGACD (control) and aqueous HAGACD solution containing blood serum

The fluorescence intensity of the probe is not quenched on binding with Ca^{2+} as seen in Figure 24 rather it strongly binds on the calcium rich sites which is demonstrated using freshly collected bones.

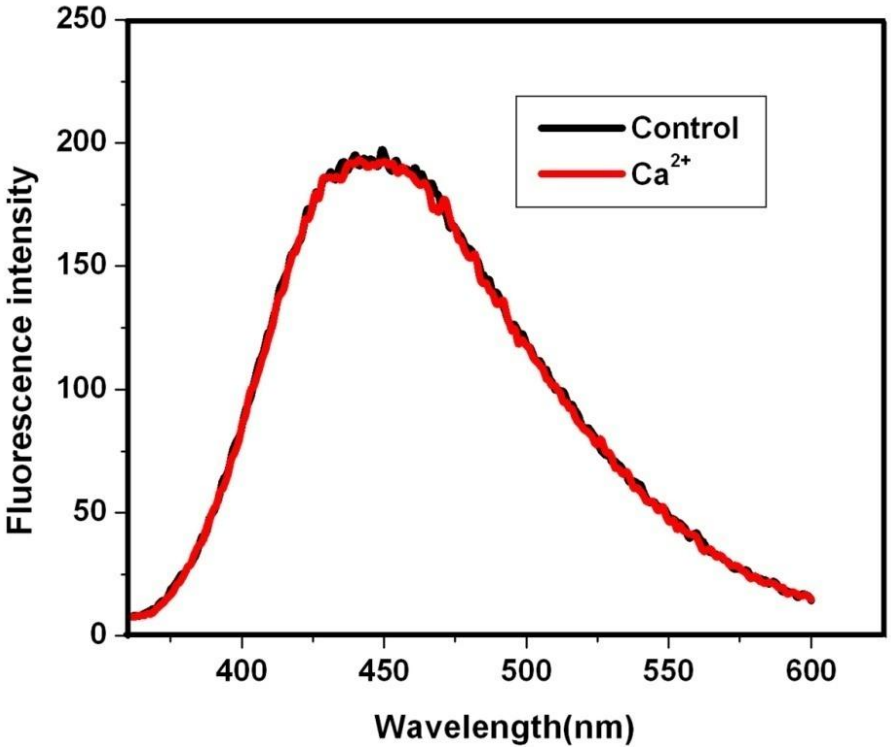

Figure 24: Fluorescence emission of HAGACD in presence of Ca

4.1.6 Binding of HAGACD onto the Ca specific sites in bones

Fresh bones were incubated with HACD (CD conjugated with HA, GA not present) and HAGACD. The images of the bones under UV light are shown in Figure 25 (A-C). Figure 25A is the image of bone as such while 25B is that of exposed to HACD solution (without the Ca^{+2} ligand, GA). It can be seen that very low quantity of HACD is bound onto the bone compared to HAGACD. On the other hand, Figure 25C, the image of bone exposed to HAGACD is highly fluorescent confirming the strong binding of the probe onto the bone surface.

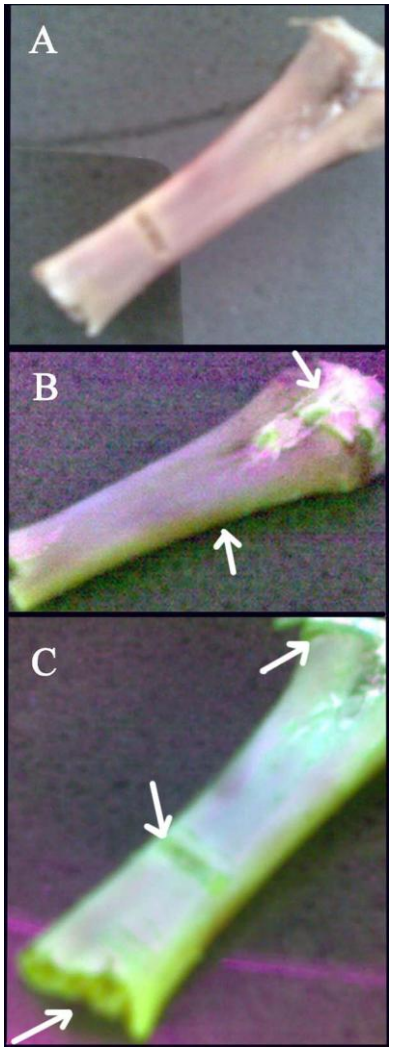

Figure 25: Photographic images of A) control bone B) Incubated with HACD C) Incubated with HAGACD, under UV lamp at 365 nm

4.2 Simultaneous bone crack detection and drug deposition using modified carbon dots

4.2.1 Preparation and characterization of modified carbon dots

Amino functionalized CDs were conjugated with ciprofloxacin and GA via EDC reaction at pH 4.2 (Scheme 1).

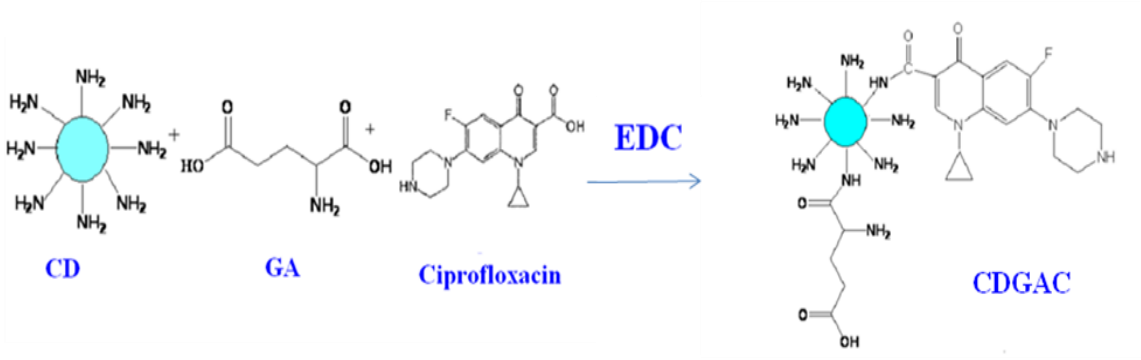

Scheme 1: Schematic representation for the formation of CDGAC

FTIR spectra (Figure 26) reflect the conjugation of GA and ciprofloxacin onto CDs. Bands associated with amide bonds can be seen at 1638 cm^{-1} (-CO- stretching) and 1560 cm^{-1} (-N-H bending) for CDGAC. Characterstic peak of CDs seen at 2870 cm^{-1} is shifted to 2970 cm^{-1} due to conjugation.

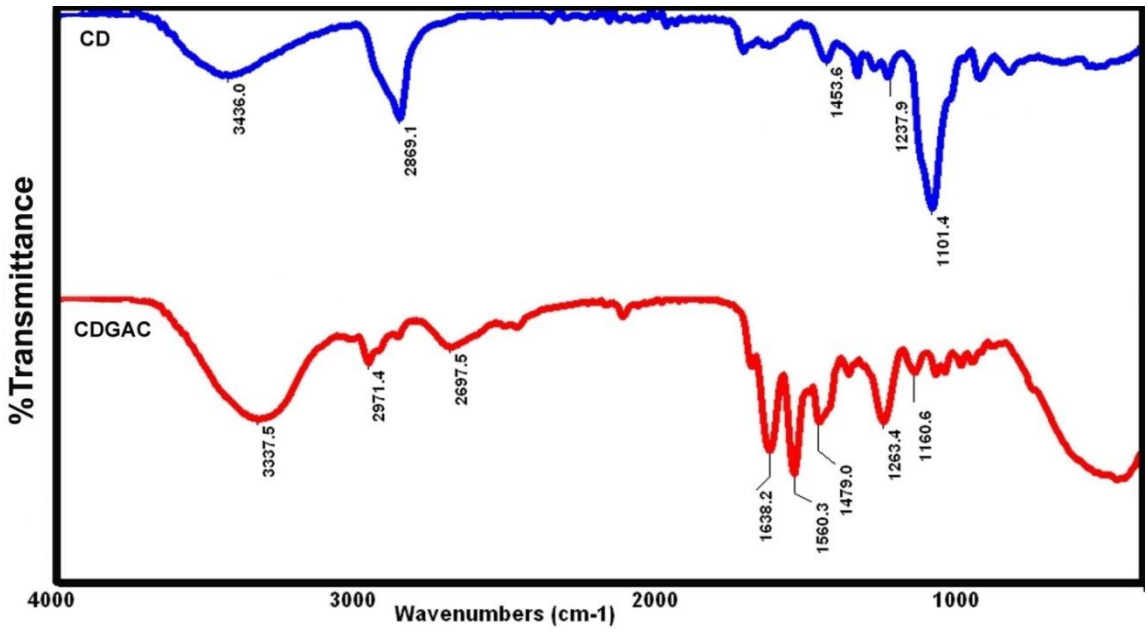

Figure 26: FTIR spectra of CD and CDGAC

H^1NMR spectrum (Figure 27) further confirms the formation of CDGAC. The peak at δ= 3.6 ppm is due to the methylene group of PEG diamine used for the synthesis

of CD. The additional peaks at 3.3, 1.0 and 2.8 ppm in CDGAC ascertain the conjugation of ciprofloxacin and GA onto CD. The signals observed at 3.3 ppm and 1.0 ppm was assigned to the aliphatic hydrogen atoms in ciprofloxacin. The peak at 2.8 ppm corresponds to the methylene group of GA.

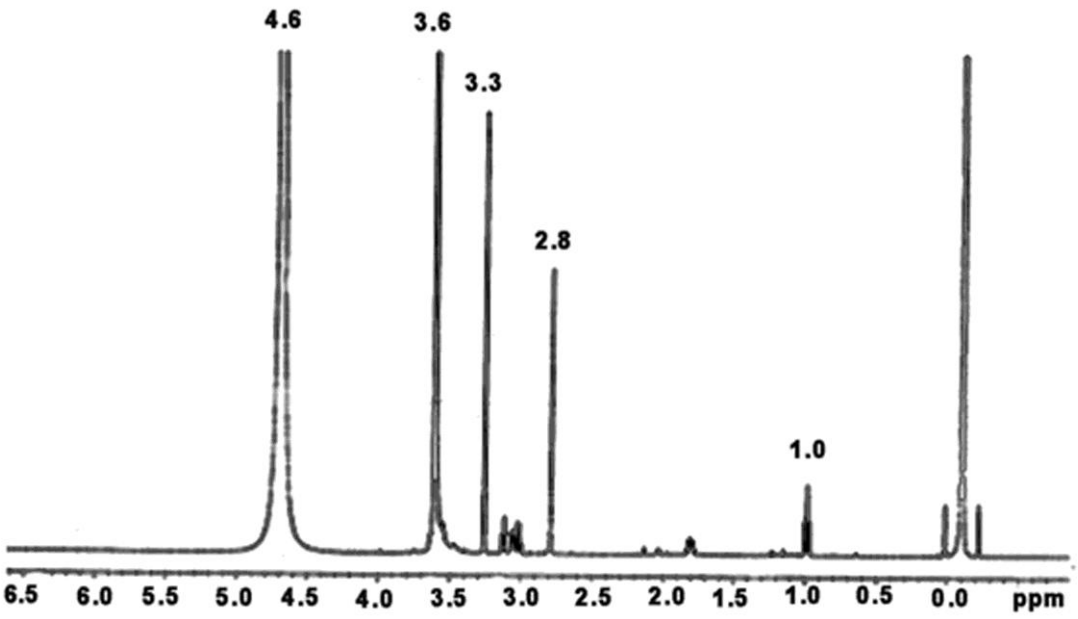

Figure 27: H^1NMR spectrum of CDGAC

HRTEM micrograph (Figure 28A) indicates that CDs have an average size of 4-7. From Figure 28B it is clear that the size of CDGAC increased to 55-60 nm due to conjugation.

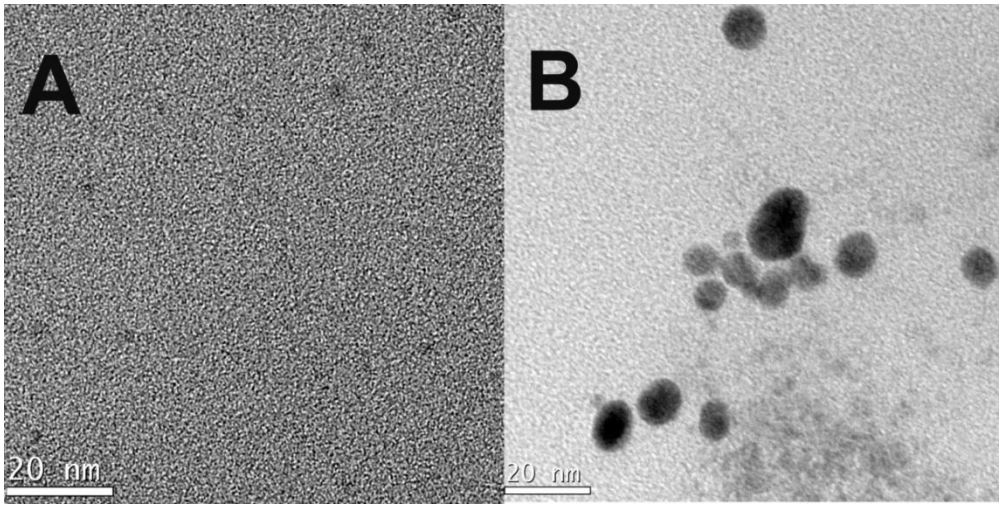

Figure 28: HRTEM micrograph of A) CD and B) CDGAC

TGA of CD and CDGAC are shown in Figure 29. Around 650 ºC the residual weight of CD is 9.5 % whereas for CDGAC it is 6.9 %.

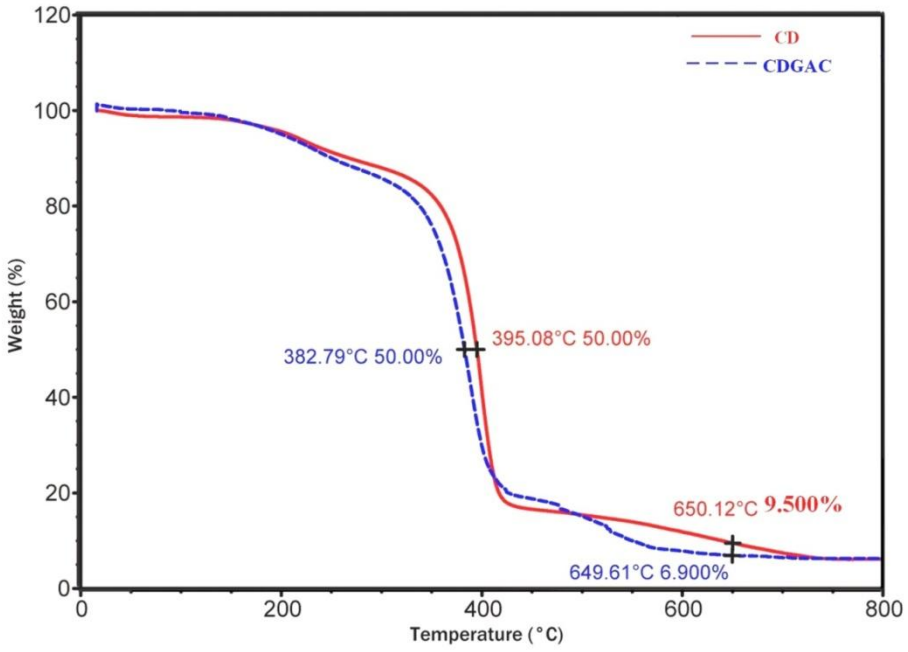

Figure 29: Thermograms of CD and CDGAC

XRD pattern of CD (Figure 30) shows a strong peak at 2θ=19.24º with interlayer spacing (d value) 4.6 Aº and a weak peak is also observed at 2θ=23.14º with d value 3.8 Aº. The sharp peak around 19.24º is assigned to PEG chains by conducting XRD analysis of PEG diamine (PEGD) used for the synthesis of CDs. This was confirmed by MDSC scan. MDSC trace showed a melting peak around 29 ºC (Figure 31) which was assigned to the melting of PEGD associated with CDs by running a separate MDSC analysis on PEGD though pure PEGD melted at higher temperature (51 ºC). CDs after modification with drug and GA also showed more or less similar thermal behavior.

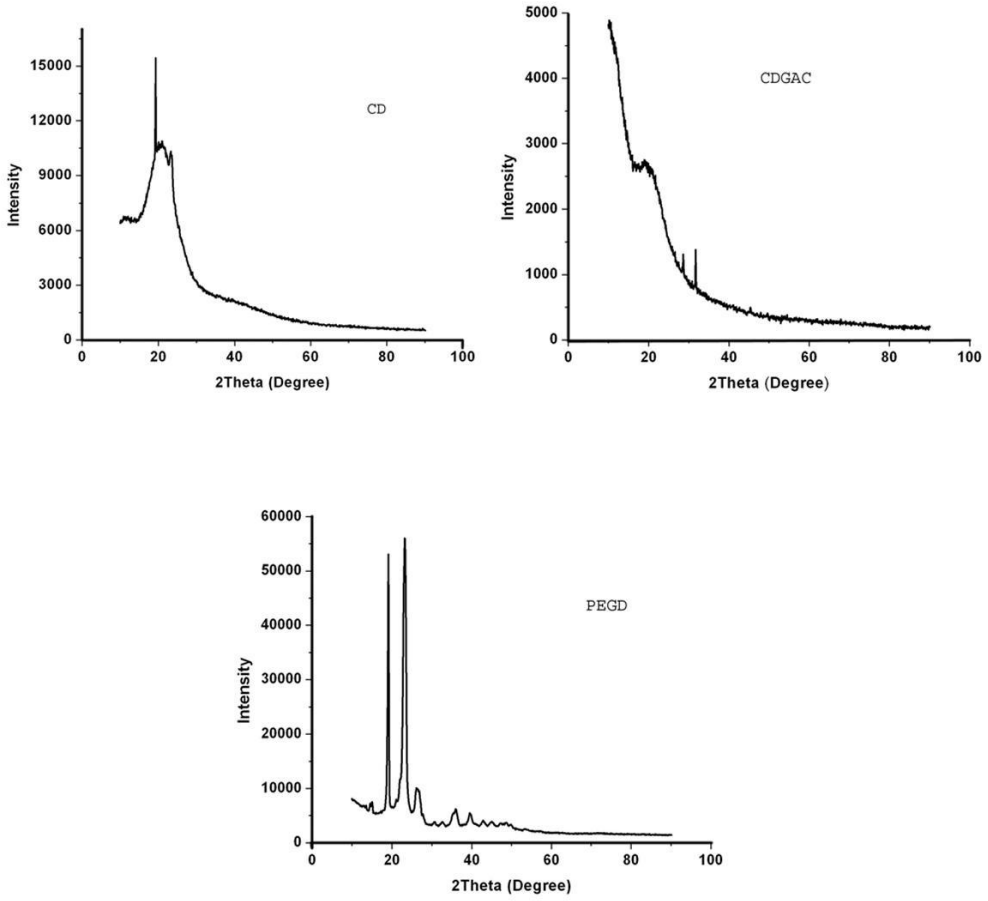

Figure 30: XRD pattern of CD, CDGAC and PEGD

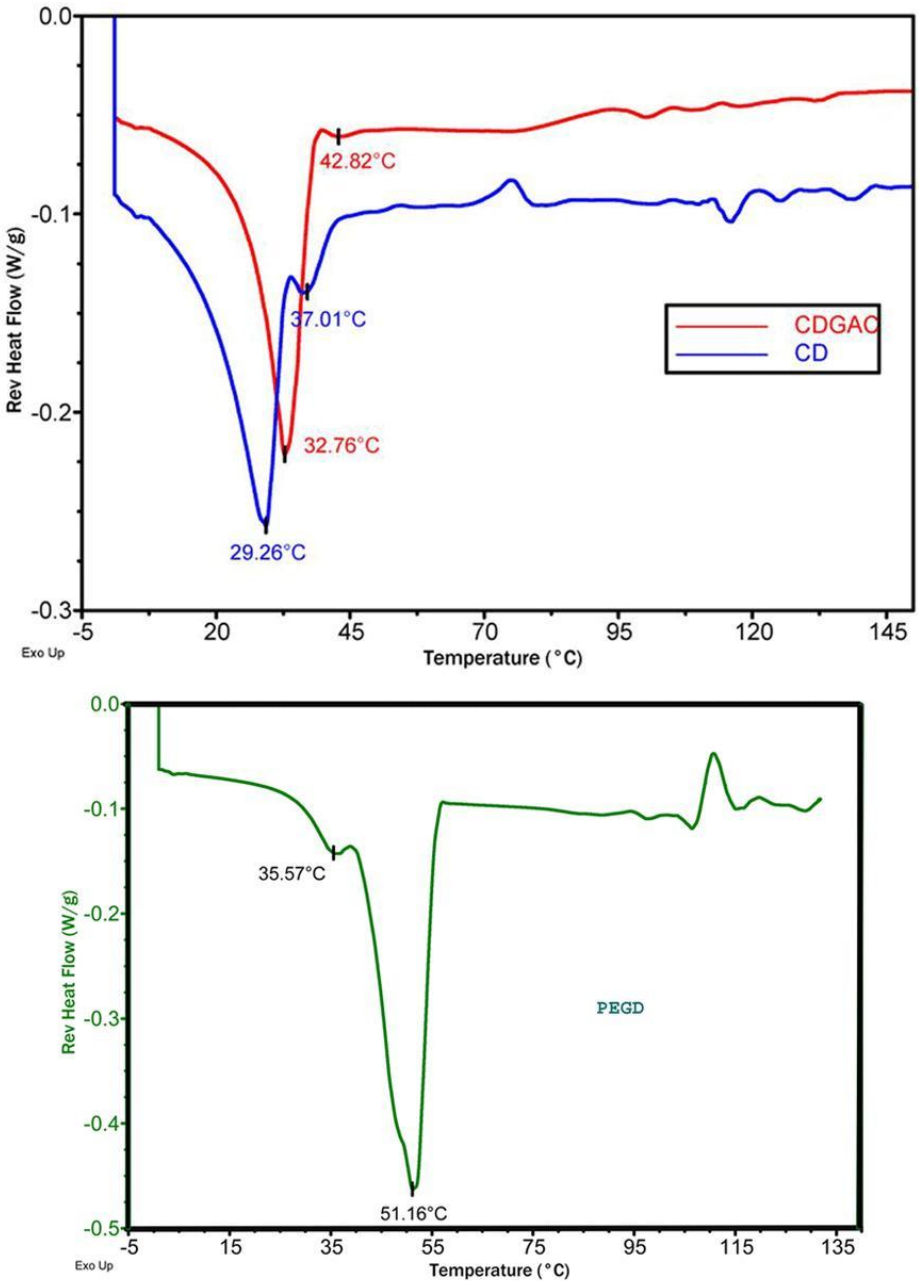

Figure 31: MDSC curve for CD, CDGAC and PEGD

UV-Visible absorption spectra of CD and modified CD are depicted in Figure 32. In addition to the characteristic absorption peak of CD around 360 nm, CDGAC showed peak at 272 nm associated with ciprofloxacin. The results emerged from the above mentioned techniques suggest the formation of CDGAC.

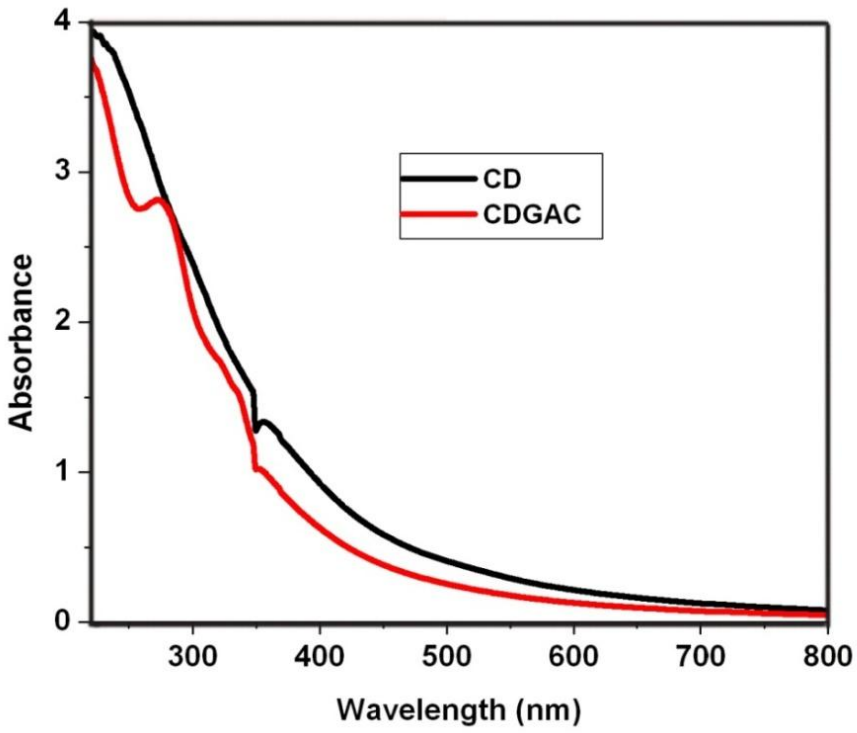

Figure 32: UV-visible absorbance spectra of CD and CDGAC

The fluorescence emission spectra of CD and CDGAC are shown in Figure 33. The photographic images of aqueous CD (A) and CDGAC (B) in day light (A and B) and under UV light (A_1 and B_1) are shown in the inset.

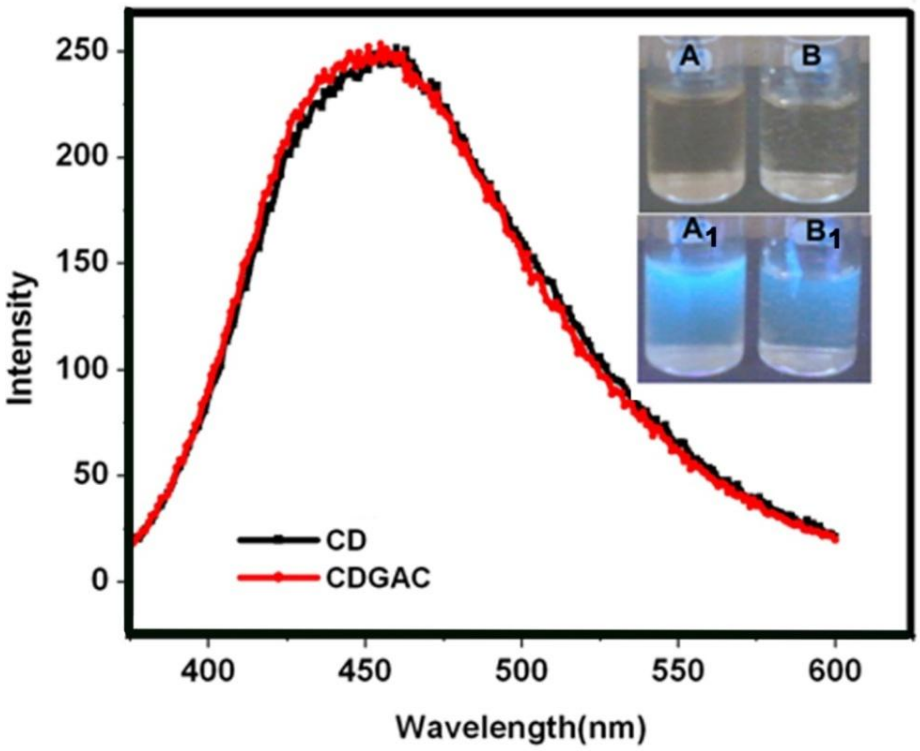

Figure 33: Fluorescence emission spectra of CD and CDGAC [Inset shows photograhic images of CD and CDGAC in day light (A and B) and under UV light (A_1 and B_1)]

Emission spectra of CDGAC at various excitations are given in Figure 34. The maximum emission intensity is observed at an excitation wavelength of 360 nm and this wavelength is fixed for further studies.

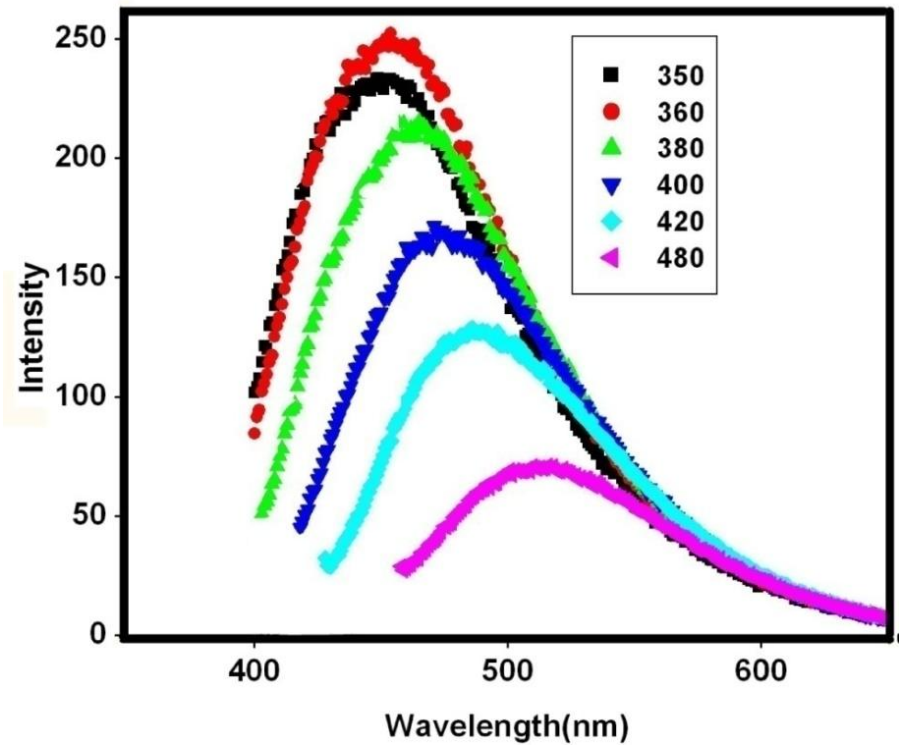

Figure 34: Emission spectra of CDGAC at various excitations

4.2.2 *In vitro* Cytotoxicity studies

4.2.2.1 Direct contact method

Figure 35A depicts that direct deposition of CDGAC onto L929 fibroblast and apparently cells didn't show any reactivity after 24h of contact reflecting the non cytotoxic nature of CDGAC. Figure 35B and 35C are the images for positive control and negative control respectively on contact with L929 cells.

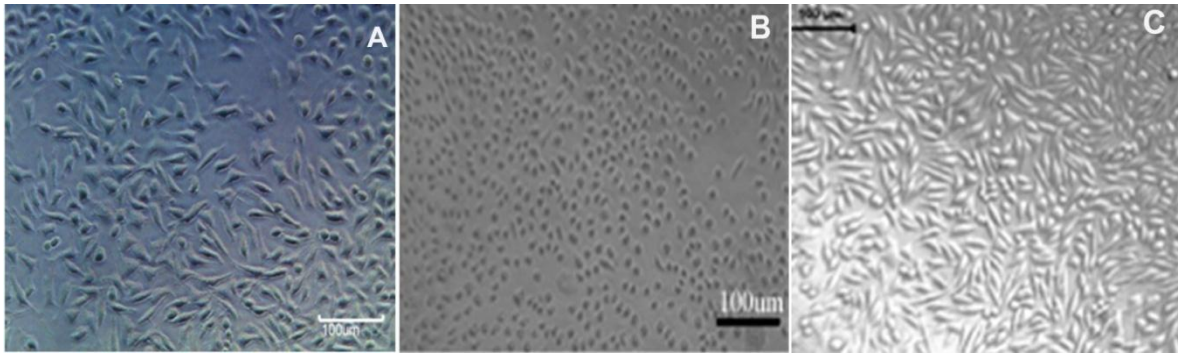

Figure 35: *In vitro* cytotoxicity study- Direct contact method

A) CDGAC B) PVC (positive control) and C) HDPE (negative control)

4.2.2.2 MTT assay

Quantitative assessment of the cytotoxicity of cells on contact with 25µg, 12.5µg and 6.25µg of CDGAC showed 108%, 120% and 109% metabolic activity respectively as shown in Figure 36, confirming the non cytotoxicity of the conjugate. The results are the average of three replicate experiments.

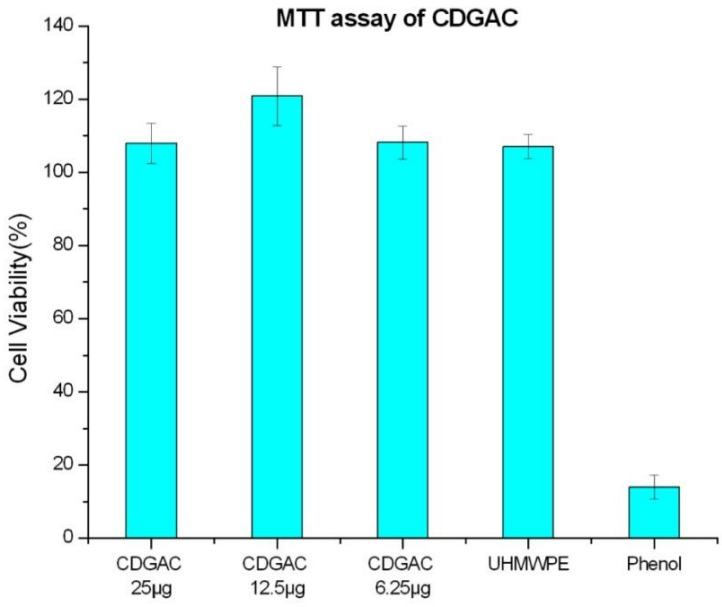

Figure 36: Cytotoxicity assessed by MTT assay.

4.2.3 Haemolysis assay

Percentage haemolysis for different concentrations of CD and CDGAC are given in Figure 37. Samples 1 to 5 correspond to CD 1 mg/mL, CD 0.5 mg/mL, CD 0.25 mg/mL, CDGAC 1 mg/mL and CDGAC 0.5 mg/mL respectively. Photographic images are shown in the inset of Figure 37 and it is clear that the samples are non–haemolytic with values below 1 %.

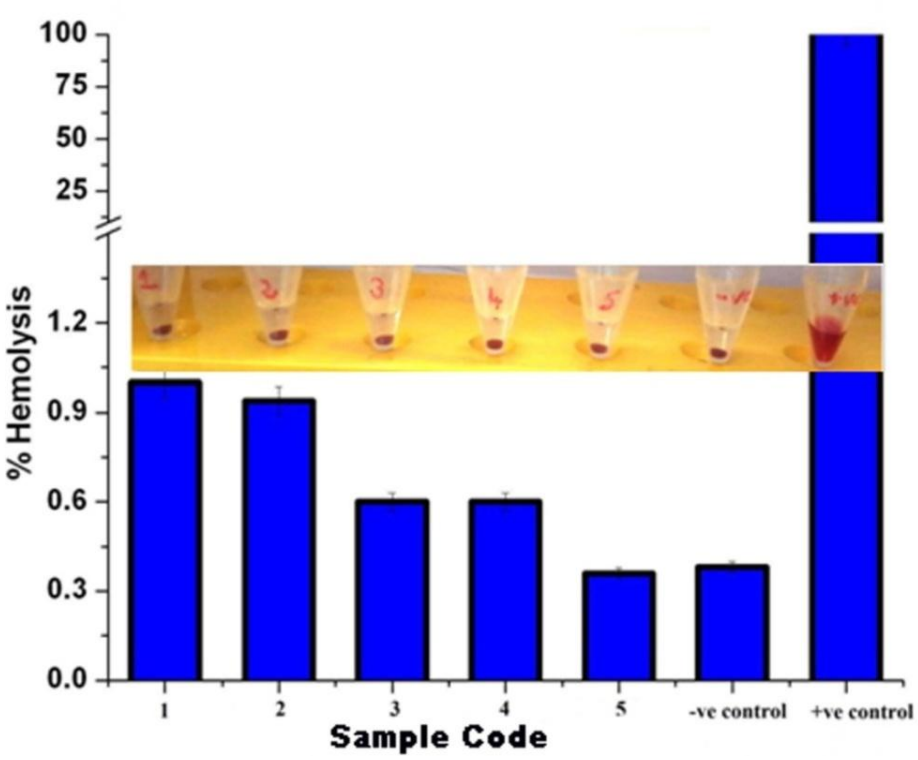

Figure 37 : Haemolysis assay for CD and CDGAC (Sample code 1,2,3,4 and 5 are CD 1mg/mL, CD 0.5mg/mL, CD 0.25mg/mL, CDGAC 1mg/mL and CDGAC 0.5mg/mL respectively)

4.2.4 Antibacterial study

Microbial inhibition assay of CDGAC was carried out. Ciprofloxacin(C), CD and CDGAC were taken in the same Petri dish (using double dilutions in Petri dishes

with serial numbers 1, 2,3,4,5 and 6 respectively) as shown in Figure 38. The bacterial growth (bacterial strain *E.coli*) is inhibited by the probe (CDGAC) at varying concentrations, starting from 0.5 mg/mL (as given in the table 3), upto 1:32 dilutions. The study revealed that the MIC of the standard ciprofloxacin for the bacteria ATCC 25922 E coli determined using tube dilution method is 1.5 µg/mL and the amount of ciprofloxacin conjugated on 1 mg CDGAC is quantified as 96 µg.

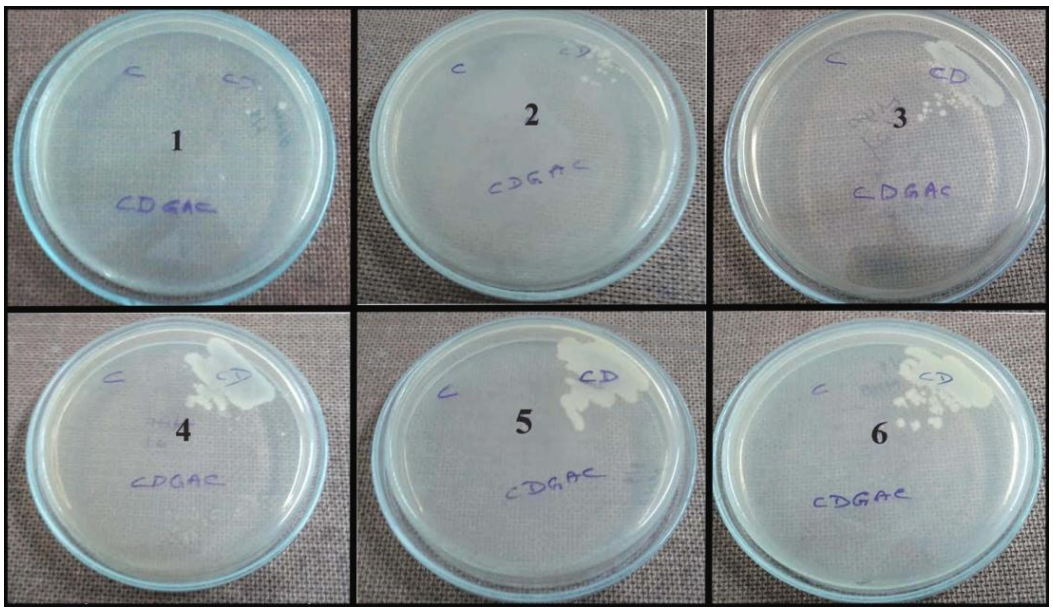

Figure 38: Antibacterial study with CD, CDGAC and C (Ciprofloxacin, Sigma). Sl. Nos 1-6 shows doubling dilutions starting from 0.5 mg/mL for CD & CDGAC and 50 mg/mL for C

Table 3: Antibacterial study by MIC method

Sl No	**Concentration** µg/Ml	**C**	**CD**	**CDGAC**
1.	50000	-	Scanty growth	-
2.	25000	-	Scanty growth	-
3.	12500	-	Moderate growth	-
4.	6250	-	Heavy growth	-
5.	3125	-	Heavy	-
6.	1560	-	Heavy	-
7.	781	-	Heavy	Moderate growth
8.	390	-	Heavy	Heavy
9.	195	-	Heavy	Heavy
10.	97	-	Heavy	Heavy
11.	48	-	Heavy	Heavy
12.	24	-	Heavy	Heavy
13.	12	-	Heavy	Heavy
14.	6	-	Heavy	Heavy
15.	3	-	Heavy	Heavy
16.	1.5	-	Heavy	Heavy

4.2.5 Detection of bone cracks using *in vivo* imaging system

The bones were cleaned and incubated with CDGAC for 24 h. Thereafter washed, dried and imaged with the Xenogen (Caliper Life Sciences) IVIS Spectrum in vivo imaging system to locate the bound CDGAC on the crack of the bone surface. The image was taken at an excitation wavelength of 430 nm since the in vivo imaging system doesn't have shorter excitation wavelength. The color bar indicates that the fluorescence intensity is more for the red region. The bone crack region (marked) is red in color confirming the maximum binding of the probe at the cracked site.

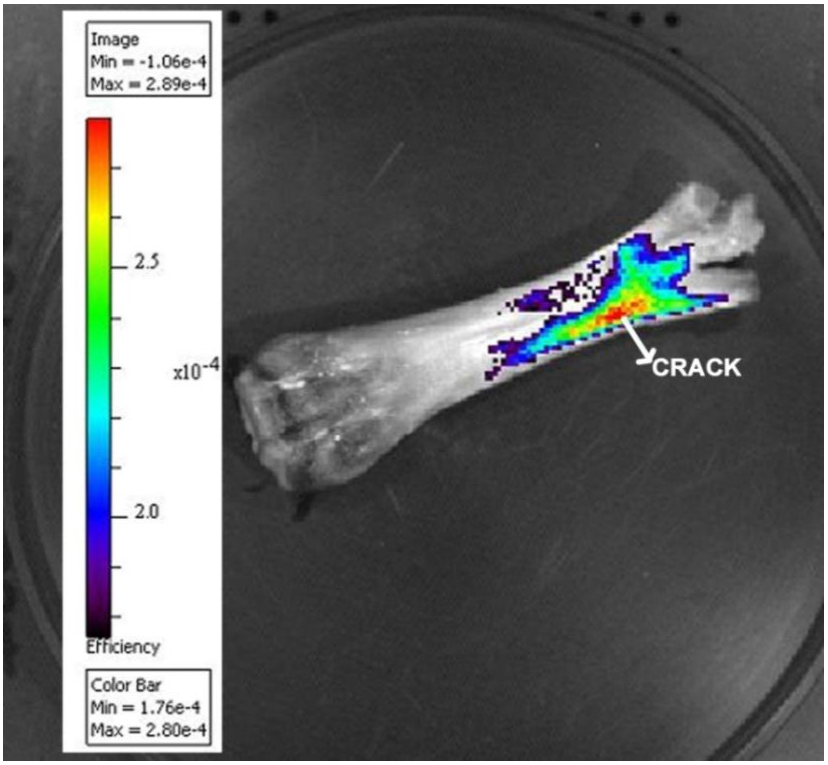

Figure 39: Bone crack detection (marked) by CDGAC imaged with IVIS system.

4.3 Detection and imaging of fatty plaques on blood vessels using functionalized carbon dots

4.3.1 Preparation and characterization of digitonin conjugated carbon dots

Amine capped CDs were modified with DG as detailed in the section 3.3.2. In the first step adipic acid (AD) was conjugated onto CDs via EDC chemistry to form CDAD. DG was then conjugated to the available carboxylic groups of CDAD using DCC/DMAP via esterification reaction.

The formation of CDAD and CDDG are evident from FTIR spectra shown in Figure 40. The peaks at 1637 cm^{-1} and 1558 cm^{-1} corresponding to –CO- stretching and –NH- bending vibrations respectively confirm the formation of CD amended with adipic acid (CDAD). A strong peak at 1650 cm^{-1} is observed substantiating the ester

bond formation between CDAD and DG to form CDDG. The peak at 1011 cm^{-1}, characteristic of C-O-C group due to DG is also present. The shift in the frequency (1650 cm^{-1}) towards low energy region may be due to the steric effect of DG groups conjugated to CDAD.

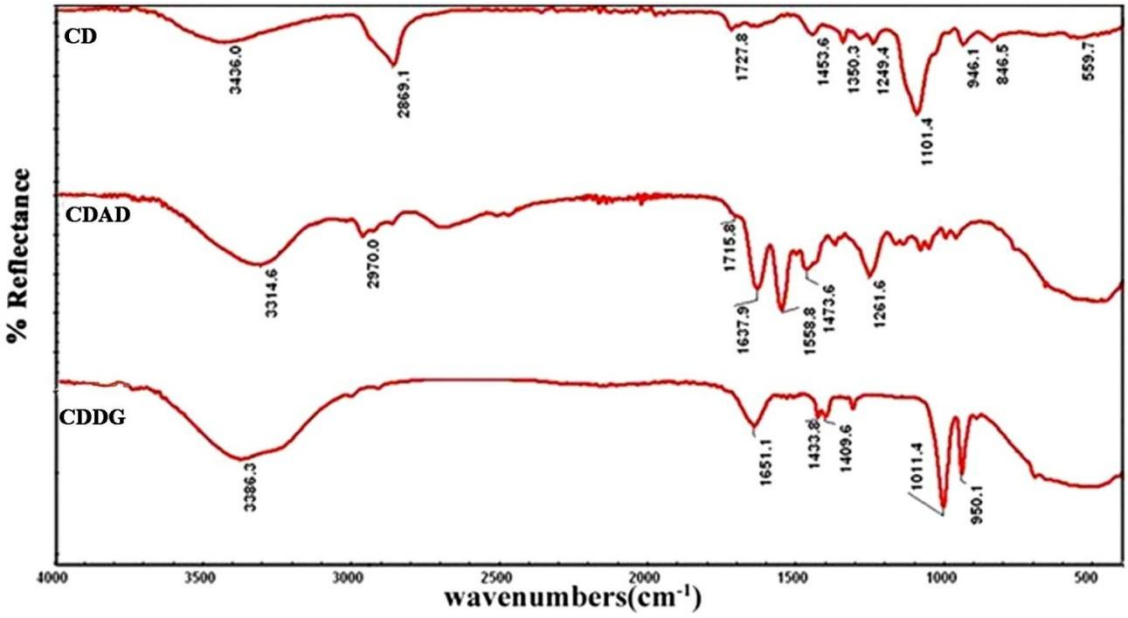

Figure 40: FTIR spectra of CD, CDAD and CDDG

Formation of CDDG was further confirmed by H^1NMR spectra which are shown in Figure 41. The peak at 3.6 ppm for CDDG associated with the methylene group of PEG diamine used for the synthesis of CD, which is evident from the Figure 41A. Those peaks at 2.6 ppm and 1.2 ppm correspond to the methylene groups and aliphatic hydrogen atoms respectively of the DG moiety. These peaks assignment are ascertained by comparing the spectrum of DG alone given in Figure 41B.

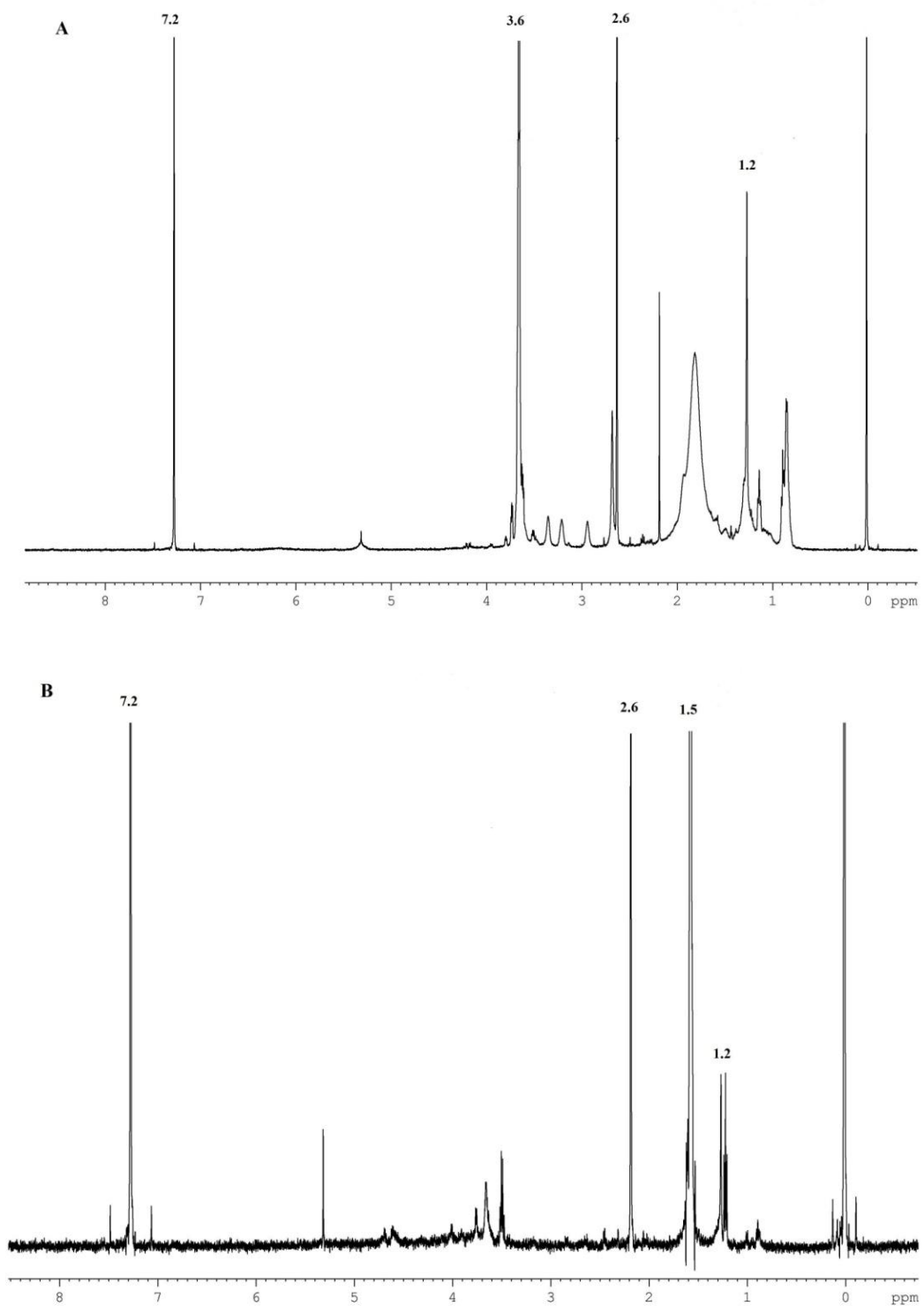

Figure 41: H^1NMR Spectra of A) CDDG B) DG

HRTEM image of CD is shown in Figure 42A and their diameter was around 4±2 nm. TEM image showed spherical shaped CDDG with size 10±2 nm (Figure 42B).

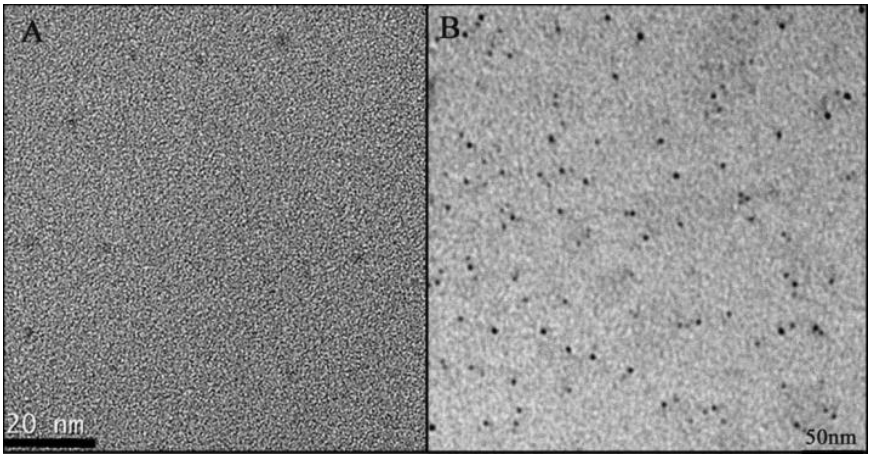

Figure 42: A) HRTEM micrograph of CDs B) TEM micrograph of CDDG

Zeta potential value denotes that the negative charge on CD (-20.90 mV) is reduced to -6.78 mV and -4.99 mV on formation of CDAD and CDDG respectively as shown in Table 4.

Table 4. Zeta Potential values from DLS

S.No	Sample Code	Zeta Potential (mV)
1	CD	-20.90
2	CDAD	-6.78
3	CDDG	-4.99

The absorption maximum of CDDG was observed around 360 nm as evident from the UV-Visible absorption spectrum of CDDG (Figure 43A). Fluorescence excitation and emission spectra of CDDG show an emission peak maximum of 455 nm when excited at 360 nm as given in Figure 43B.

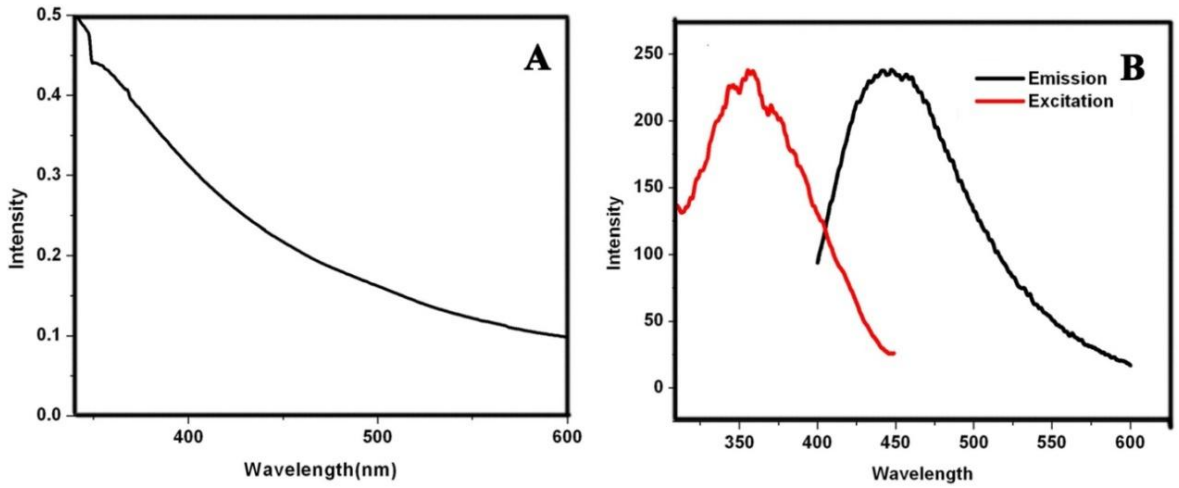

Figure 43: A) UV-Visible absorption spectrum of CDDG

B) Fluorescence excitation and emission spectra of CDDG

Fluorescence emission spectra of CD, CDAD and CDDG are given in Figure 44. The photographic images of CD (A), CDAD (B) and CDDG (C) in day light and UV light are given in the inset of Figure 44. The blue fluorescence under UV lamp at 365 nm for CDAD and CDDG ensure that the conjugation does not affect the fluorescent property of CD.

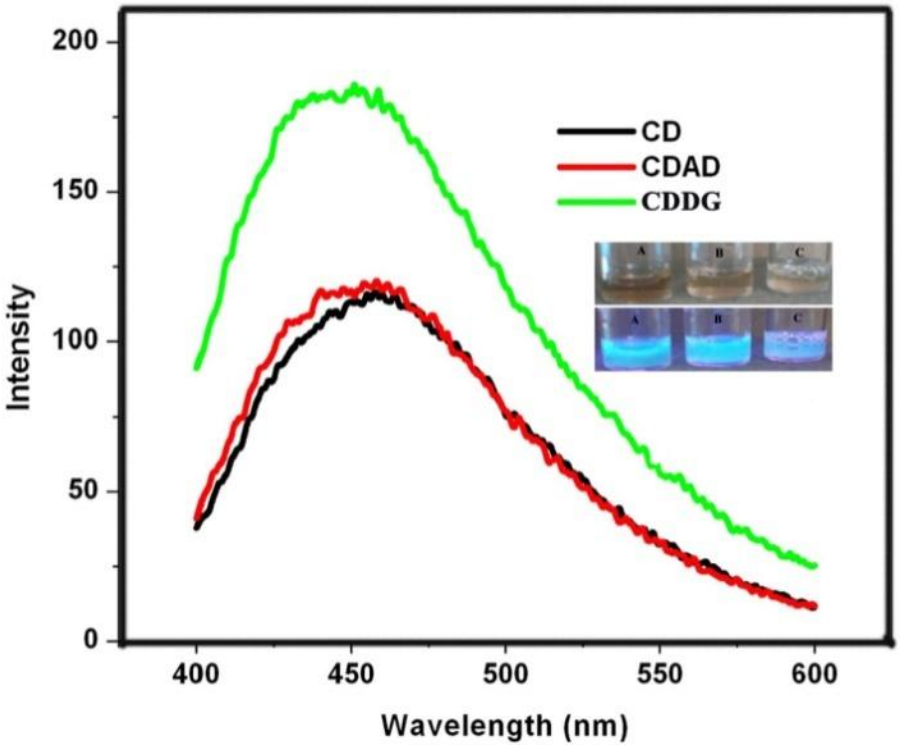

Figure 44: Fluorescence emission spectra of A) CD, B) CDAD and C) CDDG. Inset shows the photograpic images of corresponding solutions in day light and under UV (365 nm)

Excitation dependent emission exhibited by CDDG is given in Figure 45 and it can be seen that the maximum emission intensity is observed at an excitation wavelength of 360 nm.

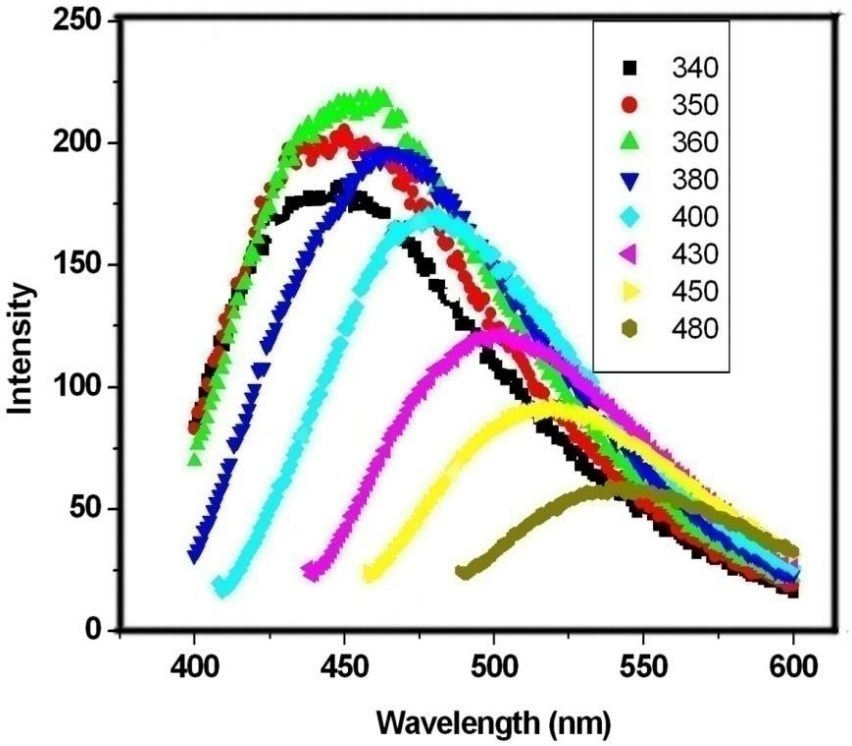

Figure 45: Excitation dependent emission of CDDG

4.3.2 Interaction of CDDG with cholesterol

The change in fluorescence intensity of the probe, CDDG in presence of various concentrations of cholesterol (2 mM - 20 mM) was assessed. A decrease in fluorescence intensity was observed with increasing concentrations of cholesterol as given in Figure 46. Linear relationship between the relative fluorescence intensities of CDDG and various cholesterol concentrations with correlation coefficient of 0.987 was obtained as shown in Figure 47. Effective fluorescence quenching was observed for lower concentrations of cholesterol i.e 2 mM (77 mg/dL) and 4 mM (155 mg/dL) which is far below the cholesterol level (> 6.2 mM) responsible for cardiovascular diseases.

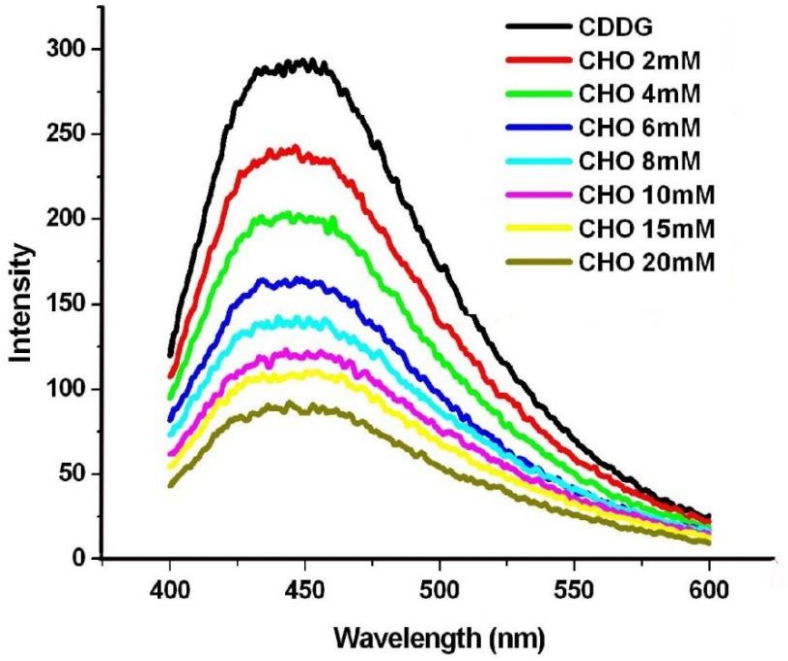

Figure 46: Fluorescence spectra of CDDG in presence of different concentrations of cholesterol

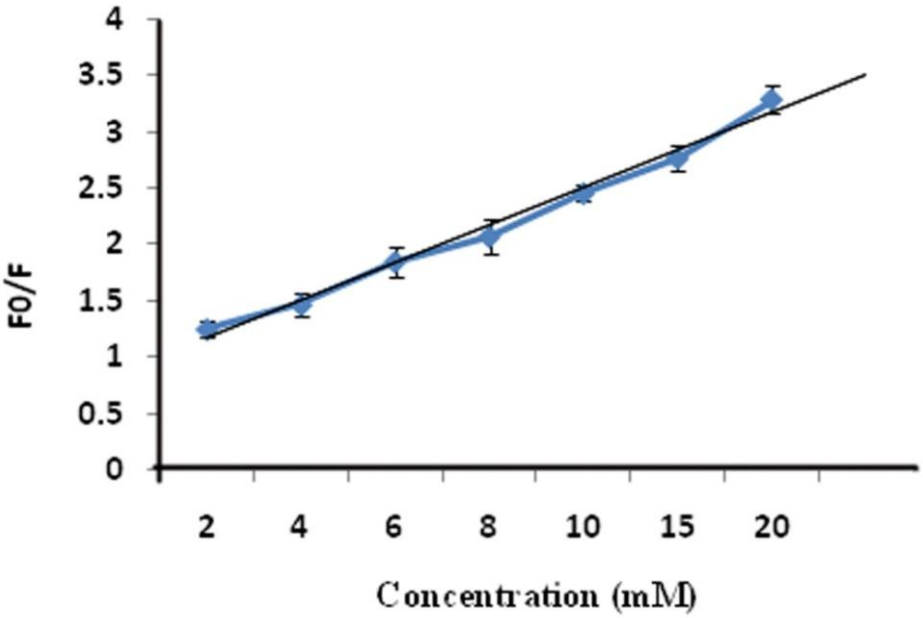

Figure 47: Linear relationship between the relative fluorescence intensities of CDDG and various cholesterol concentrations. F0 and F are the fluorescence intensities of CDDG in the absence and presence of cholesterol respectively

4.3.3 Selectivity of the method

Selectivity of the probe for binding cholesterol was confirmed by studying the interaction with testosterone, hydrocortisone and corticosterone. The interference of CDDG in presence of 20 mM of testosterone, hydrocortisone and corticosterone was checked. The fluorescence intensity of CDDG in presence of other steroids remained unaffected as shown in Figure 48.

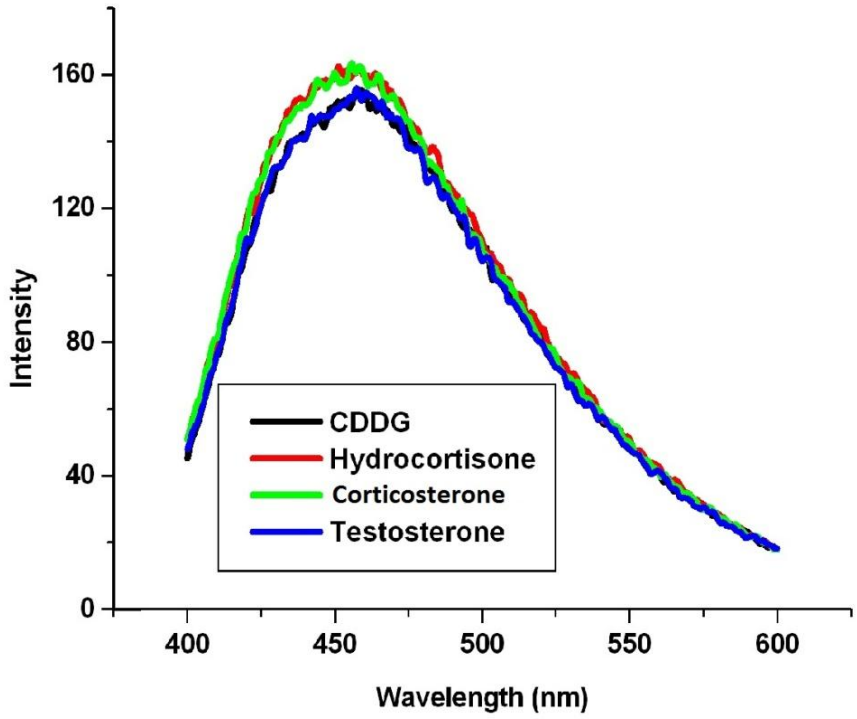

Figure 48: Fluorescence spectra of CDDG in presence of other steroids

The response of CDDG to potential coexisting substances in serum, including some amino acids [valine (val), Cystine (cys), Glycine (gly), Lysine (lys), Tryptophan (trypt) and Methionine (meth)] ascorbic acid (aa), dopamine (dop), glutathione (gt) and uric acid (ua) was also studied. 100 µM concentrations of all these biomolecules were prepared and incubated with CDDG. It was observed that these molecules did

not quench the fluorescence intensity of CDDG significantly when compared with CDDG incubated with 15 mM of cholesterol as given in the Figure 49.

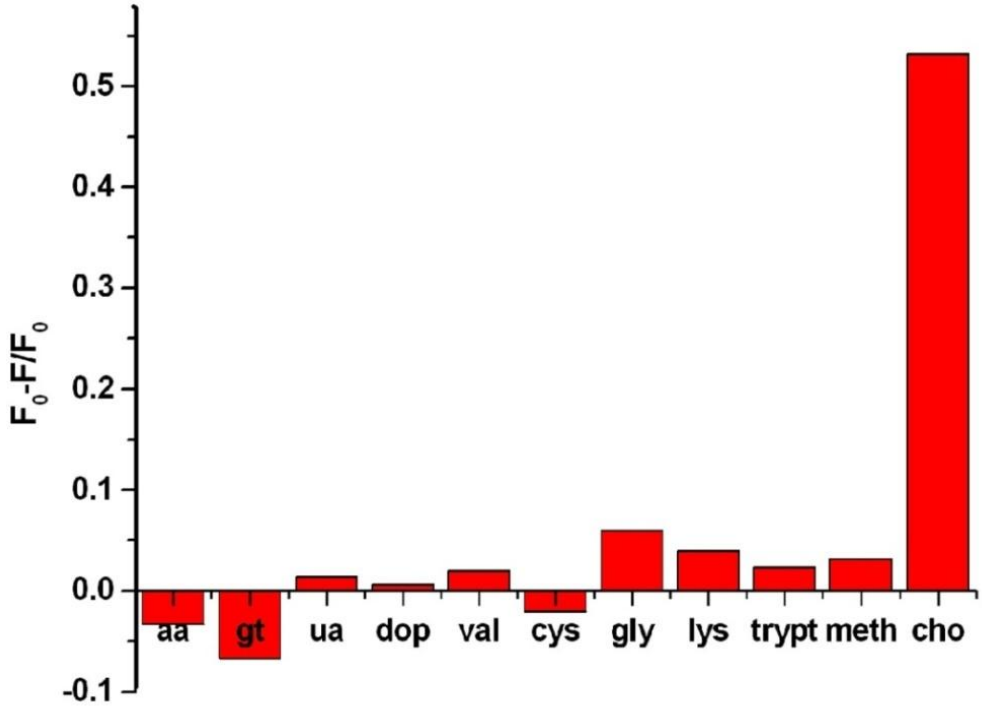

Figure 49: CDDG in presence of potential interfering biomolecules coexisting in serum. F0 and F are the fluorescent intensities of CDDG before and after adding the corresponding molecules respectively.

4.3.4 Preliminary experiments carried out to confirm the binding of CDDG to cholesterol

50 µL of 10 mM cholesterol solution was sprayed onto a glass cover slip, air dried and incubated with aqueous CDDG (0.06 mg/mL). After an hour, the surface was washed and viewed under a fluorescence microscope at 20X using various filters (Blue, green and red). It can be seen that in all the three images given in Figure 50

cholesterol rich areas on the glass slides are fluorescent and the empty areas are dark in colour confirming that the CDDG has high affinity towards cholesterol.

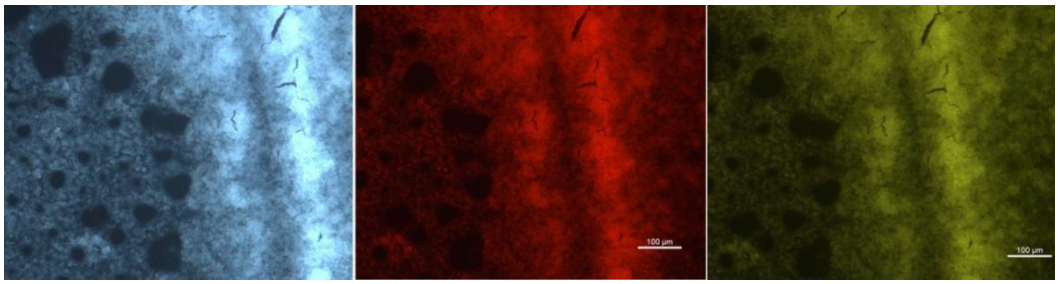

Figure 50: Fluorescence microscope images of cholesterol solution dried on a glass slide incubated with CDDG, at different excitations (using filters 350-380 nm, 450-490, 510-600 nm)

Further, the same experiment was carried out with PVA film doped with cholesterol. It can be seen in Figure 51 that the cholesterol doped area specifically fluoresce leaving the other part dark.

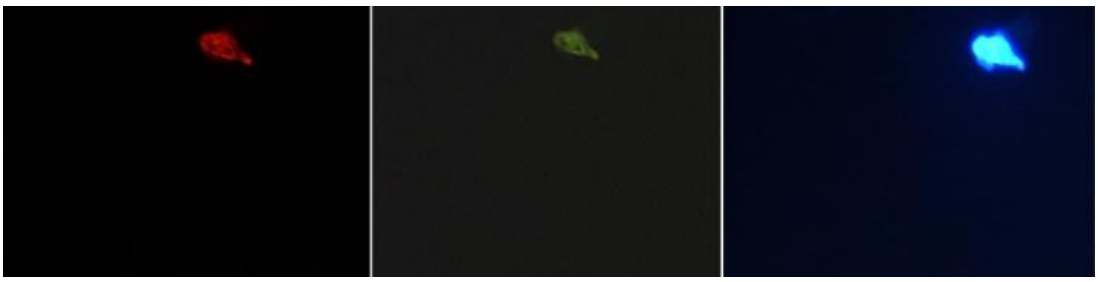

Figure 51: Fluorescence microscope images of cholesterol doped on PVA film, incubated with CDDG and viwed under different filters.

The fluorescence intensity of the residual solution after removing the PVA films was also measured (Figure 52) and found to be very less for the solution in which cholesterol doped PVA film was incubated. The intensity of the same was significantly high in which bare PVA film was immersed indicating the high affinity of CDDG towards cholesterol.

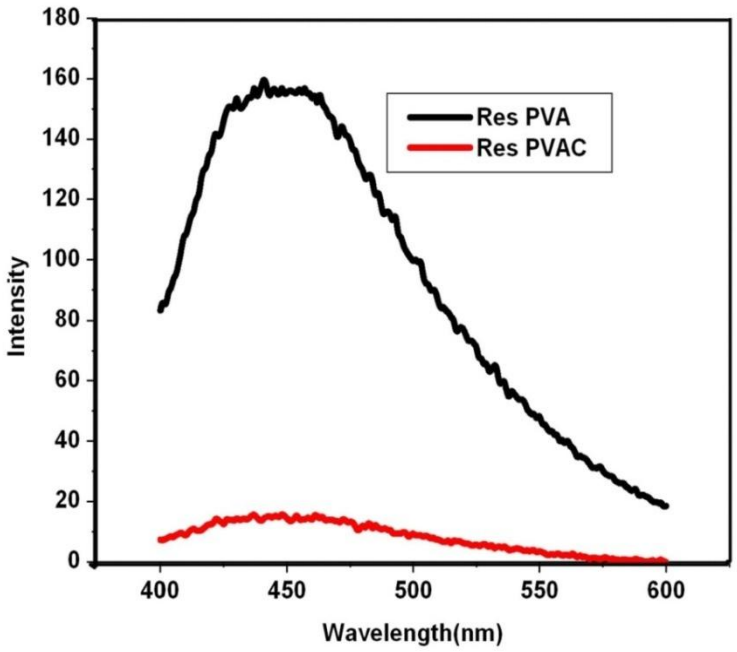

Figure 52: Fluorescent spectra of the residual solutions. (Res PVA- CDDG solution in which PVA film with no doped was incubated. Res PVAC- CDDG solution in which PVA film doped with cholesterol was incubated)

4.3.5 Haemolysis assay of CDDG

The percentage haemolysis for CDDG at two different concentrations, 0.06 mg/mL and 0.01 mg/mL were found to be 1.7% and 1.1 % respectively ensuring the material to be non-haemolytic. Concentration of 0.06 mg/mL was used throughout the study.

Table 5: Percentage haemolysis of CDDG

Concentration of CDDG (mg/mL)	Haemolysis %
0.01	1.1
0.06	1.7

4.3.6 Binding of CDDG onto the cholesterol deposited tissues

The experiment was carried out using a piece of tissue with heavy cholesterol deposit extracted from the blood vessels that surround the human heart. Modulated Differential Scanning Calorimetry (MDSC) analysis of the tissue with cholesterol deposit and the fat free tissue (muscle portion) was carried out to compare the phase transitions as depicted in Figure 53. The tissue with cholesterol deposit showed a prominent melting peak at 102 ^{o}C which is lower comparing to the melting point of pure cholesterol (148 ^{0}C). The lowering of the temperature may be due to the presence of other entities in the deposit. It is reasoned that the peak is a reflection on the presence of cholesterol in the tissue deposit.

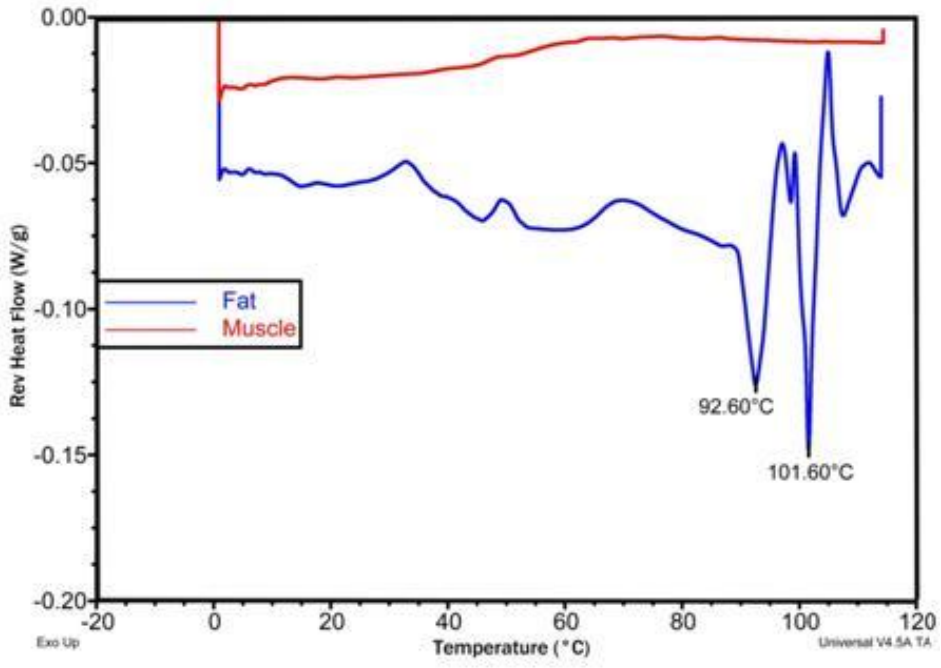

Figure 53: MDSC curve for the cholesterol deposited tissue and deposit free tissue

The tissue with cholesterol deposit was incubated with CDDG solution for various time intervals i.e. 5 min, 30 min, 1 h, 2 h and 24 h. Subsequently, they were taken out, washed with water and viewed under UV lamp at 365 nm. Images shown in Figure 54 demonstrate that even after 5 min the tissue shows fluorescence. On the other hand it can be seen in Figure 55 that the tissue with no cholesterol deposit did not fluoresce at all under the same conditions.

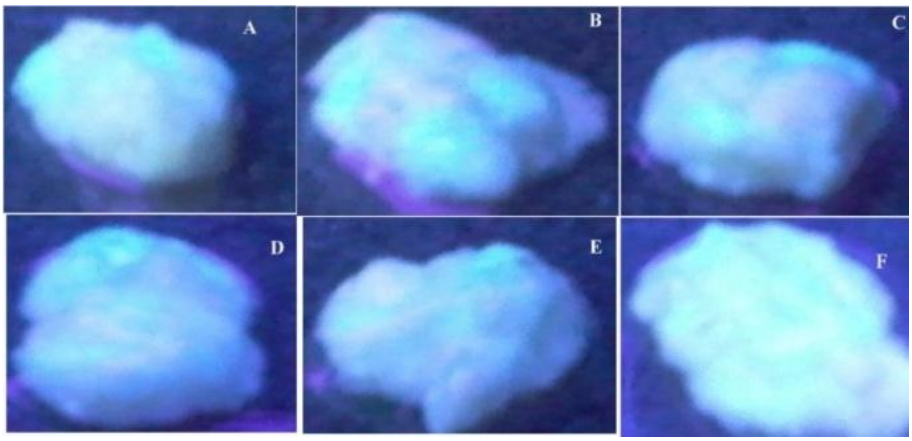

Figure 54: Photographic images of cholesterol deposited tissue incubated with CDDG for varied time intervals and viewed under UV lamp A) 5 min B) 15 min C) 30 min D) 1 h E) 2 h F) 24 h.

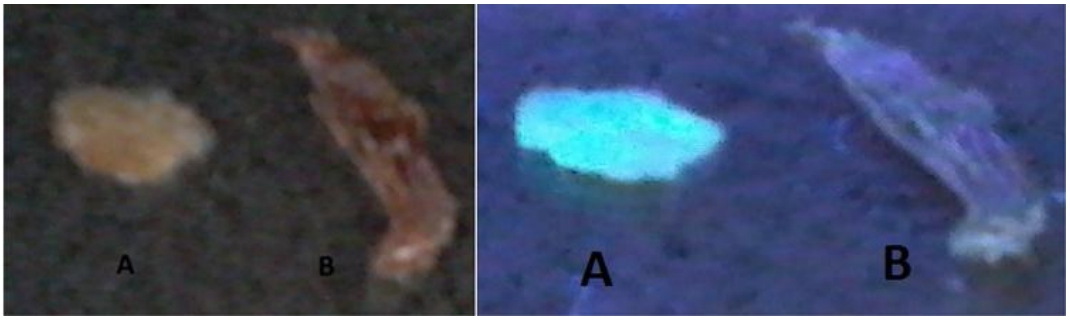

Figure 55: Photographic images of A) Tissue with cholesterol deposit B) Muscle tissue with no cholesterol deposit, incubated with CDDG for 24 h, when viewed in day light (left) and under UV lamp at 365 nm (right)

The tissues were then incubated with blood serum containing 230 mg/dL cholesterol and CDDG for 1h at 37ºC. The tissues were taken out, washed and viewed under UV lamp at 365 nm. From Figure 56 it is clear that the fat deposited tissue shows fluorescence while fat free tissue is non fluorescent confirming the probe could selectively bind cholesterol deposits in real conditions.

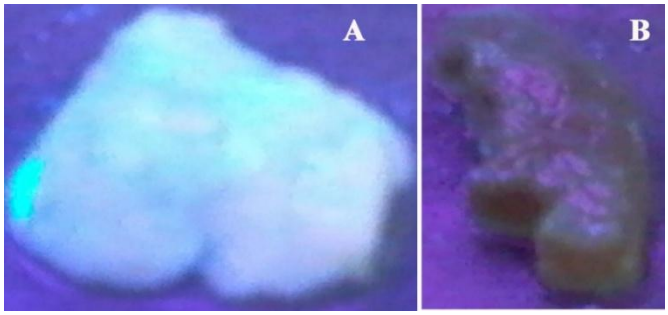

Figure 56: Photographic images of A) Fat tissue and B) Fat deposit free tissue incubated with CDDG in blood serum, under UV light at 365 nm. Only fat deposited tissue (A) shows fluorescence.

The tissues were then imaged with Xenogen (Caliper Life Sciences) IVIS Spectrum *in vivo* imaging system at an excitation wavelength of 430 nm (the starting wavelength available for the equipment). In Figure 57 it can be seen that the fat tissue (left) has maximum binding of the probe as evident from the color bar. This experiment further supports the ability of CDDG as an imaging probe for cholesterol deposits.

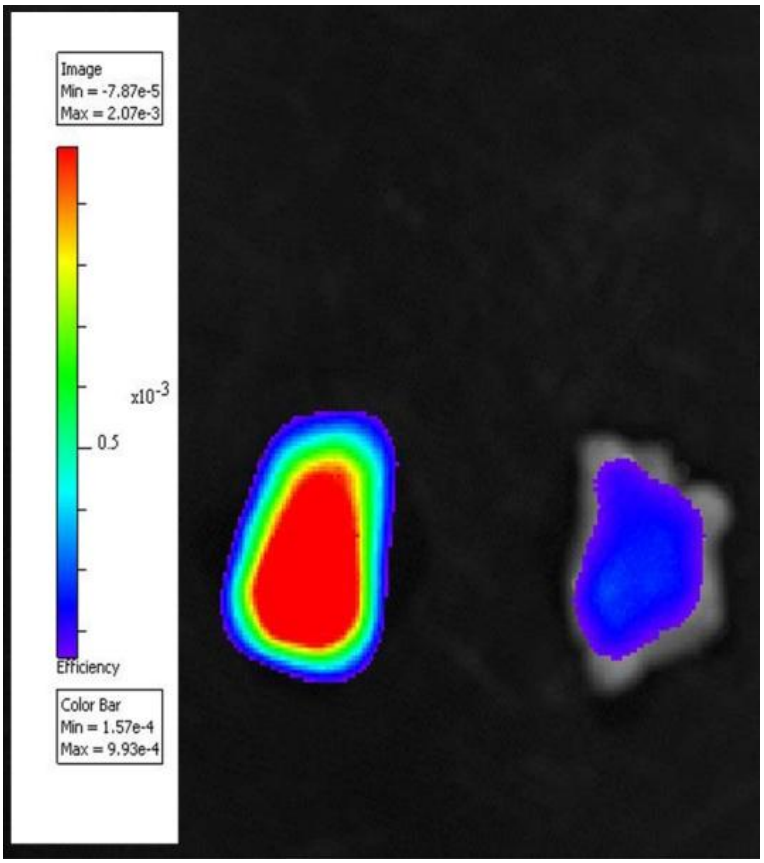

Figure 57: Fat Tissue (left) and muscle tissue (right) imaged with the IVIS system

4.4. Gold nano rod-carbon dot hybrid system for the simultaneous imaging and possible disruption of cholesterol plaques

4.4.1 Synthesis of the hybrid (CDNR) and their physicochemical characterization

NRs were prepared as detailed in the section (3.4.2) and further functionalized with carboxylic acid groups in presence of 30 mM MSA. CDDG were prepared as detailed in 3.3.2. The available NH_2 of CDs in CDDG was conjugated with COOH groups of NRMSA via EDC chemistry as detailed in 3.4.3.

Figure 58 displays FTIR spectra of NR, NRMSA and CDNR. For NR, peaks at 2915 cm^{-1} and 2847 cm^{-1} correspond to the symmetric C-H stretching and asymmetric C-H stretching respectively. The peak at 1462 cm^{-1} is due to the alkane CH_3 bend from the hydrophobic core of CTAB linked to NRs. Peaks at 960 $cm^{-1}$and 908 cm^{-1} are assigned to the C-N stretching bands and the peak at 724 cm^{-1} is due to the rocking mode of methylene chain. For NRMSA the peaks at 1731 cm^{-1} and 3474 cm^{-1} due to the C=O stretching and O-H stretching of carboxylic acid group clearly indicate the modification of NR with MSA. Symmetric stretching of COO^- is observed at 1349 cm^{-1}. Peak at 1099 cm^{-1} attributes to the C-O stretching of COOH group. CDNR (NRMSA and CDDG conjugated via EDC chemistry) was also analyzed by FTIR to confirm the conjugation. Peaks at 1650 cm^{-1} (-CO- stretching) and 1569 cm^{-1} (-N-H bending), the typical bands for amide bond can be observed in the FTIR spectrum of CDNR. In addition to these, peaks at 2925 cm^{-1} due to CDs and 1089 cm^{-1} due to digitonin are also present.

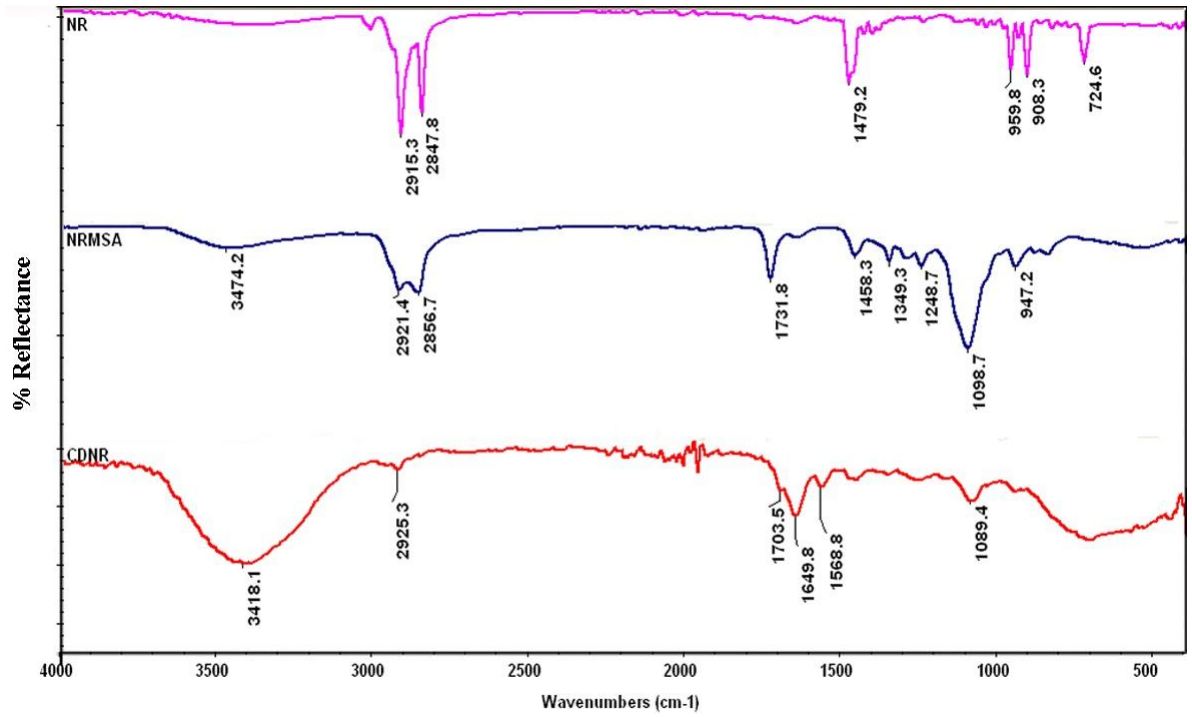

Figure 58: FTIR spectra of NR, NRMSA and CDNR

TEM micrographs of NRs formed are shown in Figures 59A. Figures 59B and 58C depict the TEM images of the conjugate, CDNR in which spherical particles along with the rod shaped structures are present (expanded view shown in the inset of figure 59B). As displayed in figure 59B, significant quantity of unmodified NRs are also present in the hybrid. By repeated centrifugation, hybrid structures were isolated (Figure 59C).

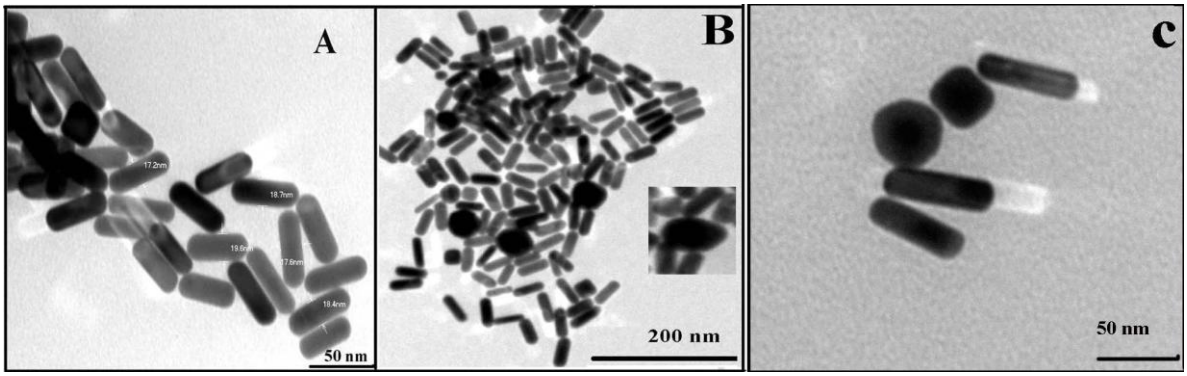

Figure 59: TEM images of NR (A) and CDNR (B & C)

Zeta potential values of NR and CDNR is given in Table 6. Zeta potential of NRs was found to be +24.00 mV due to the cationic surfactant, CTAB. On conjugation with CDDG, the zeta potential value drops to 0.60 mV.

Table 6: Zeta potential values measured by DLS

Sample	Zeta potential (mV)
NR	24.14
CDNR	0.603

UV-Visible absorption spectra of NRs and NRMSA are given in Figure 60. TSPR of NRs was observed at 534 nm and LSPR at 714 nm. On modification with MSA, a slight shift (red shift) was observed for TSPR which can be assigned to change in local polarity.

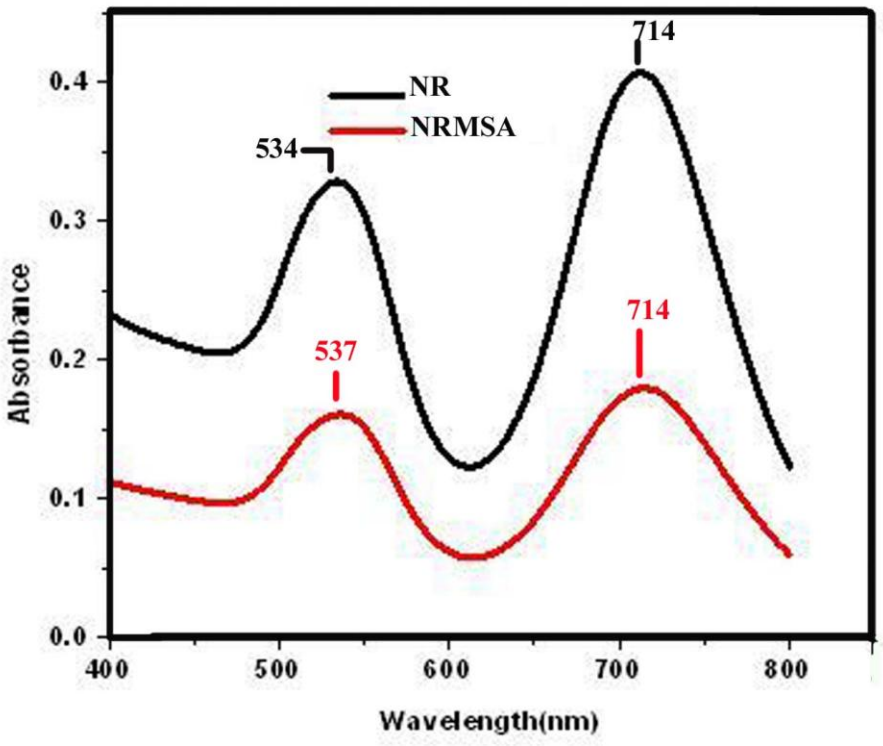

Figure 60: UV-visible absorption spectra of NR and NRMSA

UV-Visible absorption spectra of CDDG and CDNR are depicted in Figure 61. On conjugation of NRs with CDDG, the shoulder peak at 350 nm due to CDs is visible along with the characteristic peaks of NRs, TSPR at 540 nm and LSPR at 716 nm.

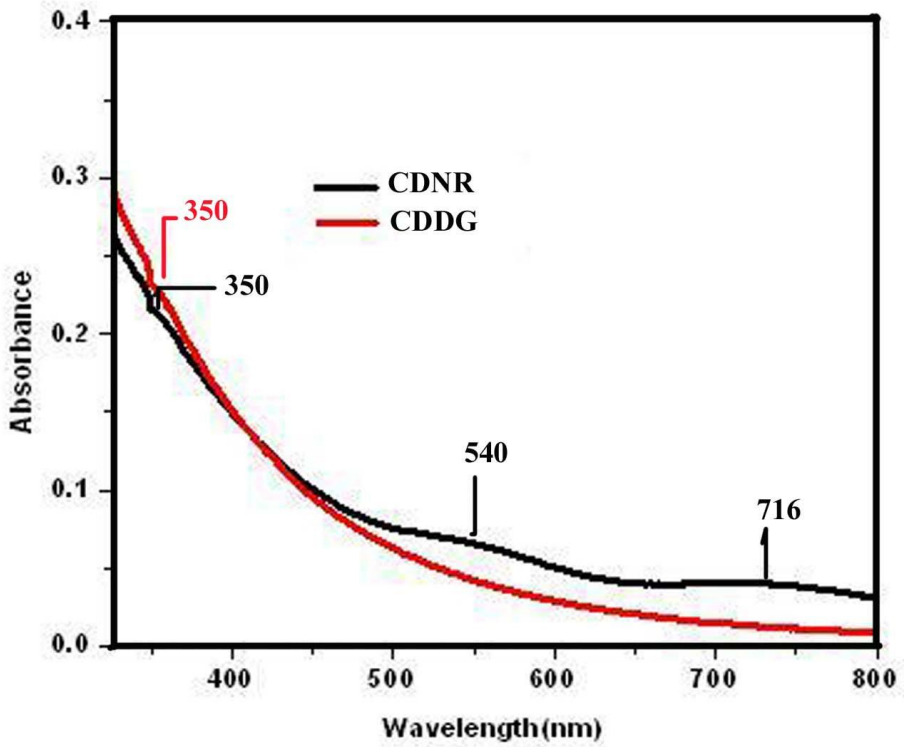

Figure 61: UV-Visible absorption spectra of CDDG and CDNR

The fluorescence emission spectrum of CDNR is given in Figure 62. Both CDDG and CDNR show emission at 455 nm when excited at 350 nm. The photographic images of CDDG (A) and CDNR (B) in day light (above) and UV light (below) are given in the inset of Figure 62.

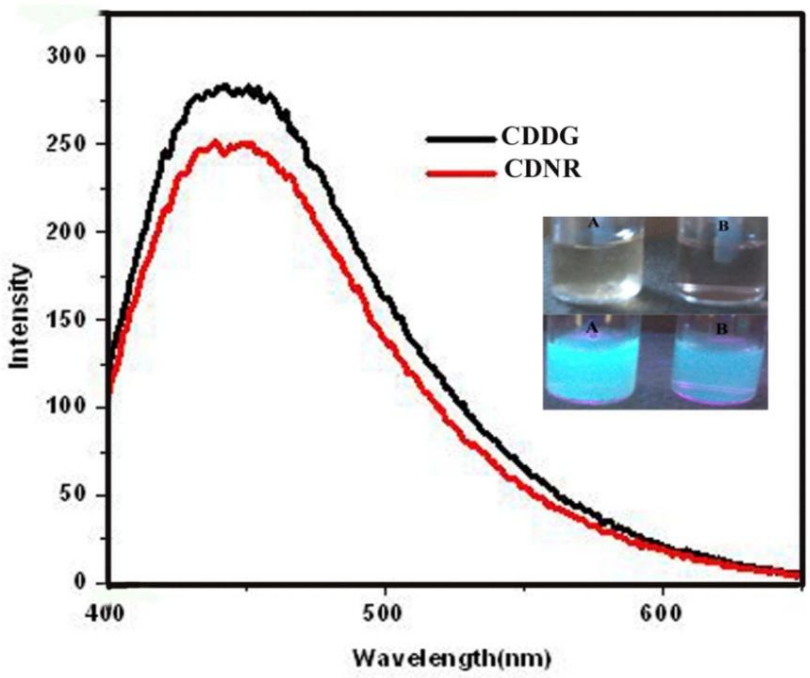

Figure 62: Fluorescence emission spectra of CDDG and CDNR

4.4.2 Binding of CDNR to the tissue with cholesterol deposit

Fat tissue with atherosclerotic deposit incubated in CDNR for 30 minutes was viewed under UV lamp at 365 nm and the photographic image is shown in Figure 63. The binding affinity of DG for cholesterol is well known. From Figure 63 it can be seen that the tissue is highly fluorescent confirming the binding of CDNR on to the tissue

Figure 63: Photographic image of cholesterol deposited tissue extracted from the arterial wall incubated with CDNR when viewed under the UV lamp at 365 nm

The incubated tissue was washed well and exposed to Laser light (808 nm and 1.5 W) for 5 minutes. Temperature was noted down at each time interval (Table 7). The temperature was measured using multimeter (Multiravi). This was compared with another piece of cholesterol rich tissue incubated with bare CDs. It was observed that for the tissue incubated with CDNR the temperature increased from 20.4 °C to 30.2 °C. The temperature almost remained the same even after 5 minutes for the tissue incubated with bare CDs.

Table 7: Temperature changes with time on Laser light exposure onto the tissues

Time in seconds	Temperature in °C for tissue incubated with CDNR	Temperature in °C for tissue incubated with CD
0	20.4	20.6
60	22.0	20.9
120	23.6	20.7
180	25.8	20.8
240	28.3	20.6
300	30.2	20.7

The morphology of the tissues incubated in CD and CDNR, after the exposure to Laser light was observed by ESEM analysis (Figure 64A and 64B respectively). The surface morphology of the tissue incubated with CD after Laser light exposure is smooth whereas the ESEM image of the tissue incubated with CDNR has got a ruptured surface morphology as evident from the Figure 64. The change in morphology is attributed to the increase in temperature affecting the architecture of the fatty deposit on the tissue.

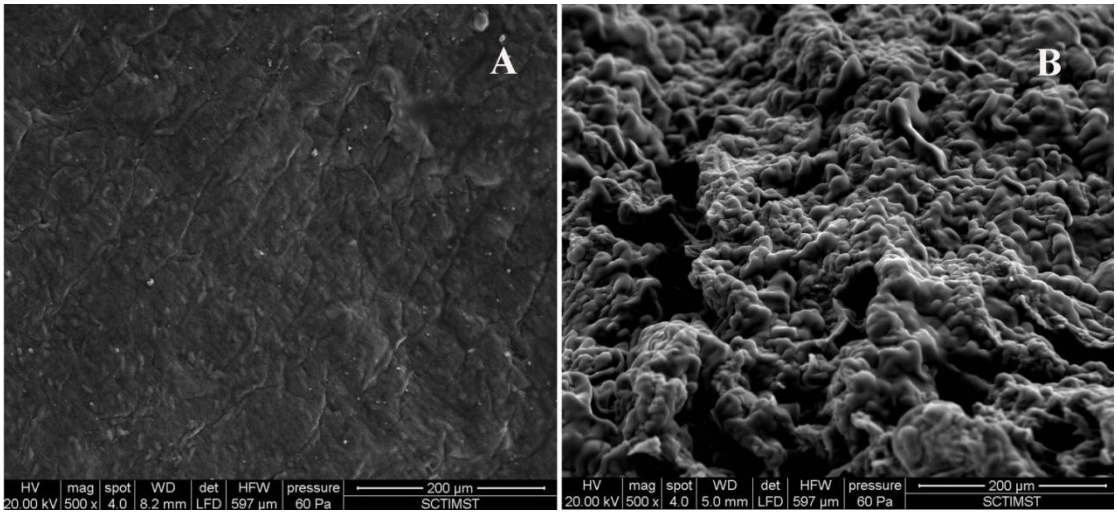

Figure 64: ESEM image of cholesterol rich tissues incubated with A) CD B) CDNR

4.4.3 *In vitro* cytotoxicity by MTT assay

Figure 65 shows the cytototoxic evaluation of NR and CDNR by MTT assay using C6 glioma cells. CDNR showed cytocompatibility at all chosen concentrations whereas NR showed cytotoxicity for all the concentrations.

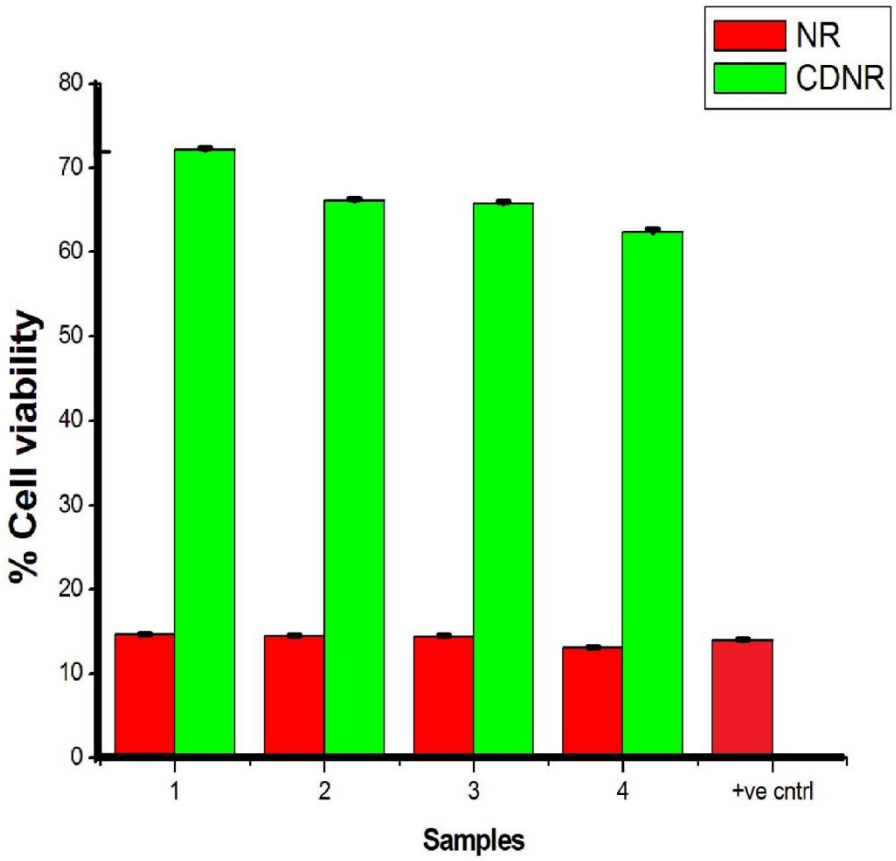

Figure 65: MTT assay (Samples: 1 (12.5 µg/mL) , 2 (25 µg/mL) , 3 (37.5 µg/mL), 4 (50 µg/mL), +ve control (Triton x 100)

4.4.4 Cellular uptake studies

The internalization was studied by incubating CDNR with C6 glioma cells for 3 h and the uptake was observed by confocal laser microscope, exploiting the fluorescence property of CDs. It can be observed from Figure 66 that CDNR is effectively internalized by the cancer cells.

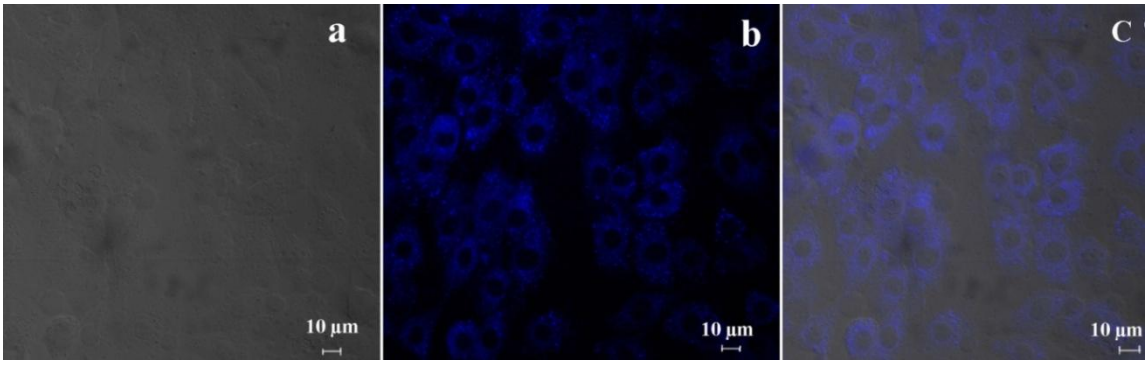

Figure 66: Confocal laser microscopic images of a) cells alone b) CDNR c) Merged images

4.5 Methotrexate anchored carbon dots as theranostic probes: Digitonin conjugation enhances cellular uptake and cytotoxicity

4.5.1 Synthesis and physicochemical characterisation of CDMX

The Synthetic strategy is shown in the scheme 2. The -OH groups present on CDDG react with the -COOH groups in MX via DCC/DMAP reaction resulting in the formation of the conjugate, CDMX. The formation of CDMX is confirmed from the FTIR spectrum and H^1NMR spectrum depicted in Figures 67 and 68 respectively.

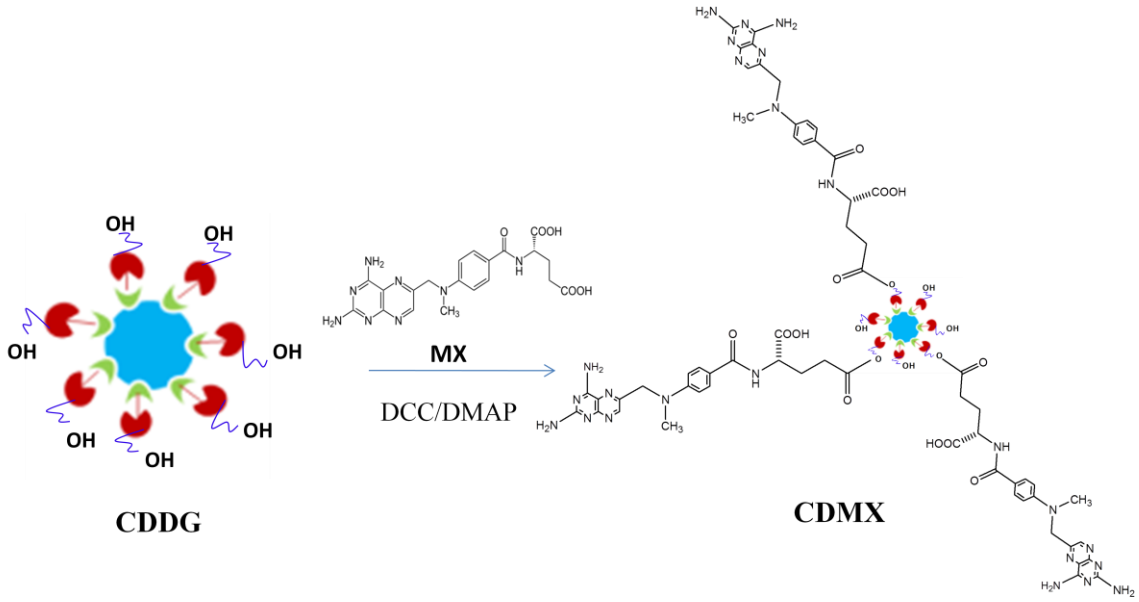

Scheme 2: Schematic representation for the conjugation of MX onto CDDG

In the FTIR spectrum of MX, the peak at 1687 cm^{-1} corresponds to the C=O stretching of the COOH group. The bands at 1641 cm^{-1} and 1598 cm^{-1} are assigned to the C=O stretching and N-H bending of the amide groups in MX . Thus in CDMX, the peak at 1700 cm^{-1} is due to the C=O stretching of COOH group and the peak at 1650 cm^{-1} attributes to the C=O stretching of the amide group in MX. The peak at 1735 cm^{-1} is assigned to the C=O stretching frequency of ester reflecting the conjugation of CDDG with MX via esterification. The sharp peak at 1104 cm^{-1}, the characterstic of C-O-C is observed due to the presence of DG in CDMX. The characterstic peaks of CDs at 2916 cm^{-1} and 2869 cm^{-1} due to CH stretching are also present in CDMX.

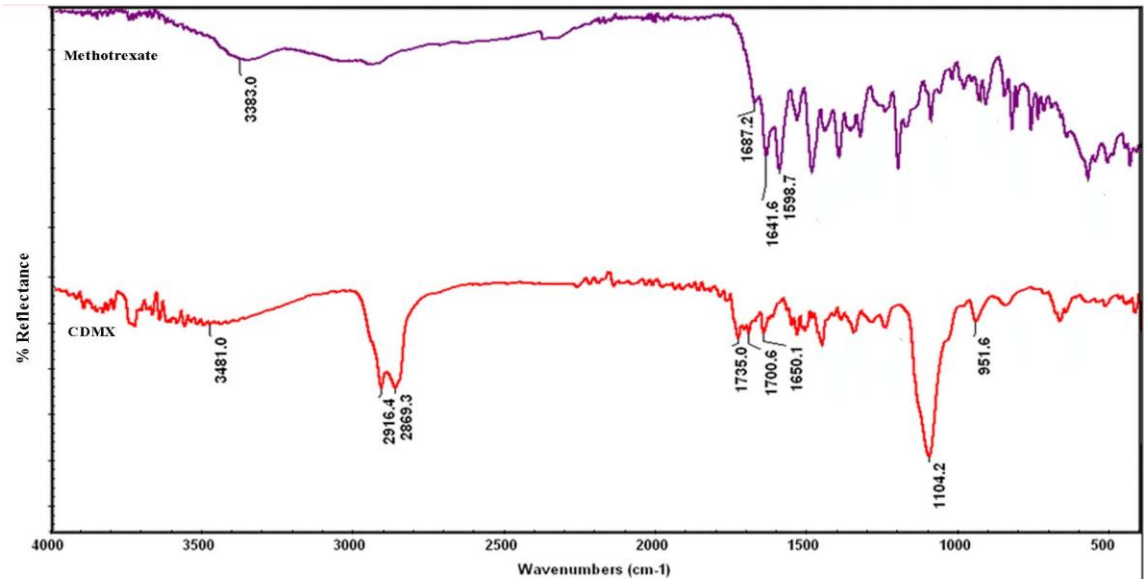

Figure 67: FTIR spectra of MX and CDMX

H^1NMR spectrum of CDMX (Figure 68) showed signals at 3.0-3.3 ppm assigned to the aliphatic protons of MX. The peak at 3.6 ppm corresponds to the methylene group of PEG diamine. Peaks at 6.8 ppm, 7.7 ppm and 8.6 ppm correspond to the benzoyl group and pteridine ring of MX. Peak at 2.6 ppm is due to the methylene groups and that at 1.2 ppm is attributed to the aliphatic hydrogen atoms of DG. Thus the above results clearly indicate the conjugation of DG and MX onto CDs.

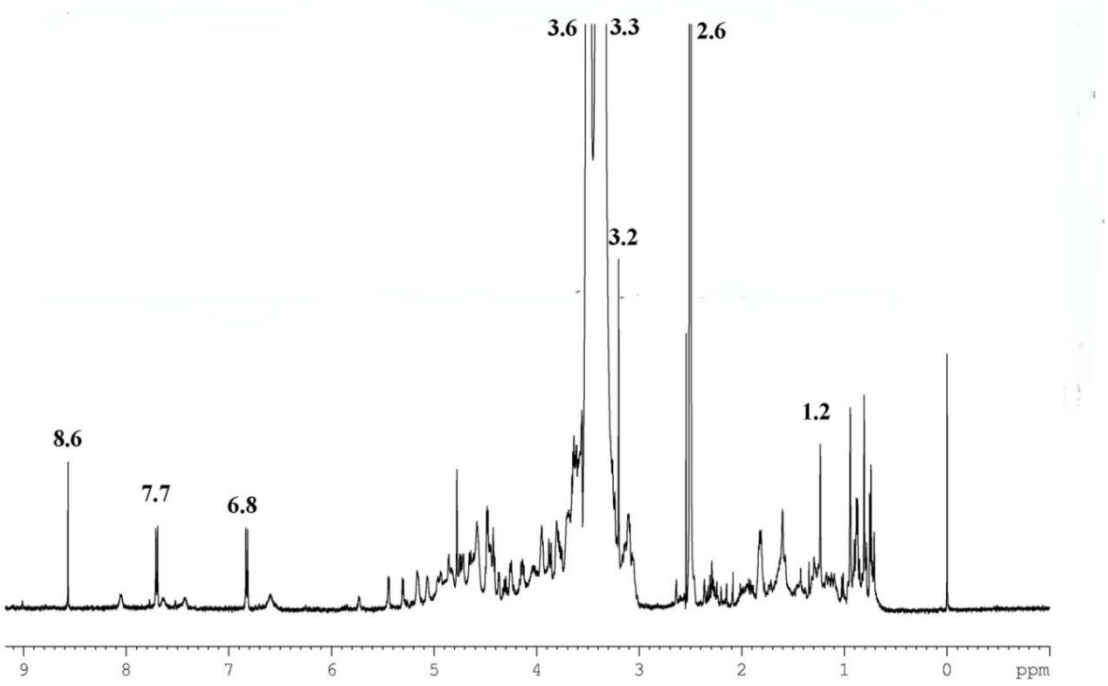

Figure 68: H^1NMR spectrum of CDMX

Table 8 displays the zeta potential measurements of CD, CDDG and CDMX. Change in the zeta potential value from -20.90 mV to -4.99 mV further assures the conjugation of DG onto CDs.

Table 8: Zeta potential by DLS

Sample	Zeta potential (mV)
CD	-20.90
CDDG	-4.99
CDMX	0.572

The UV-visible spectrum of CDMX further confirms the conjugation of MX onto CDDG (Figure 69). The peaks at 258 nm, 303 nm and a broad peak at 370 nm due to MX were observed apart from the absorbance peak at 360 nm due to CDs.

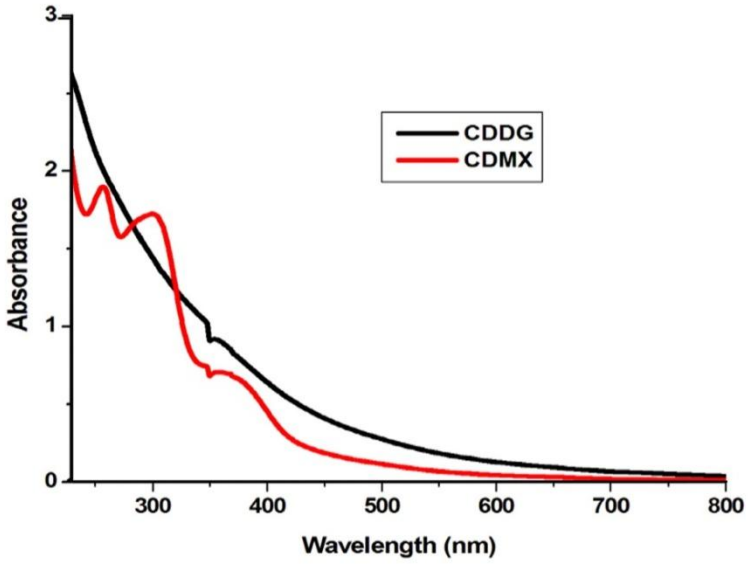

Figure 69: UV-Visible absorption spectra of CDDG and CDMX

CDMX showed emission at 455 nm when excited at 360 nm. Fluorescence spectrum of CDMX is given in Figure 70. The photographic images given in the inset of the Figure 70 affirm that the fluorescence of CD is intact after the conjugation of MX onto CDDG.

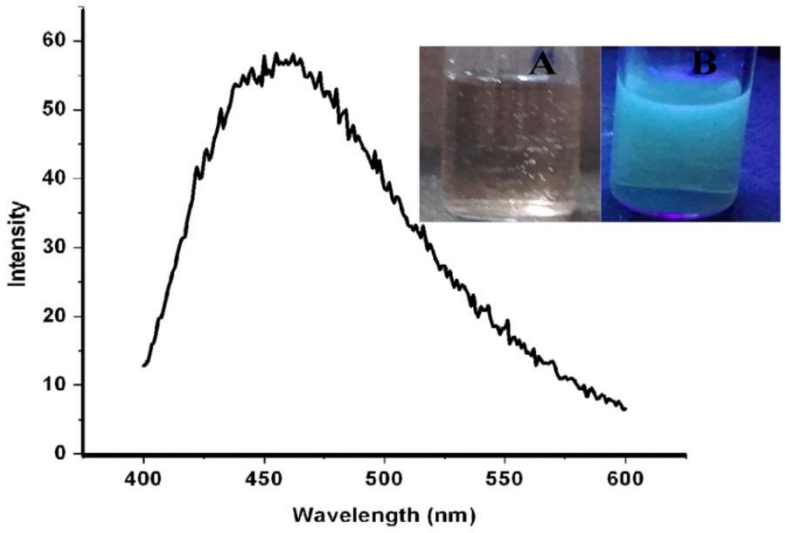

Figure 70: Fluorescence emission spectrum of CDMX [In the inset are the photographic images of CDMX A) in daylight B) under UV lamp at 365 nm]

4.5.2 *In vitro* drug release study

Drug release study was performed at pH 7.4 (physiological pH) and pH 5.0. The drug release profile in Figure 71 indicates that ~20 % of drug was released from CDMX at physiological pH (7.4) whereas 81% release was observed at pH 5.0 over a period of 6 h. The release study was carried out based on the OD of MX from the release medium.

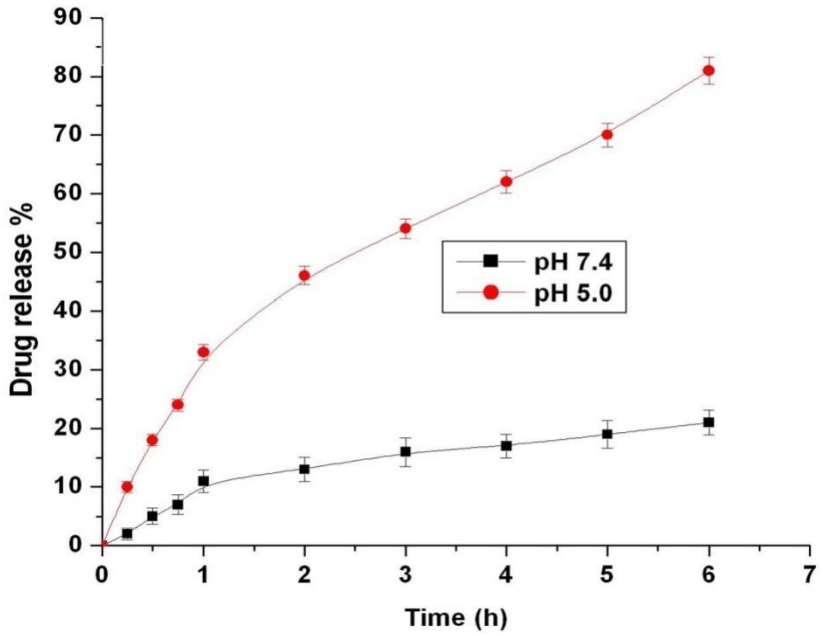

Figure 71: Drug release profile of MX from CDMX

4.5.3 Cytotoxicity studies

Cytotoxic evaluation was carried out by MTT assay against C6 glioma cells. The cytotoxic activity of CDMX, CDDG and MX conjugated to CDs without DG (CM) is given in Figure 72. CDDG was found to be cell friendly at all chosen concentrations (93.03 %, 90.67 %, 88.68 % and 81.99 % for 12.5 µg/mL, 25 µg/mL, 37.5 µg/mL and 50 µg/mL respectively). CDMX showed enhanced cytotoxic response when compared to CM. The lowest concentration of 12.5 µg/mL CM

showed cell viability of 92.01% whereas only 57.40 % cell viability was observed for the same concentration of CDMX. Quantitative assessment of the cytotoxicity to cells on contact with 12.5 µg/mL, 25 µg/mL, 37.5 µg/mL and 50 µg/mL of the free drug (MX) showed 81.43%, 78.64%, 77.01% and 71.63% metabolic activity respectively. Whereas for the same concentrations CDMX showed 57.40 %, 56.99 %, 56.67 % and 51.49 % cell viability respectively. Thus CDMX exhibited higher cytotoxicity when compared to the free drug.

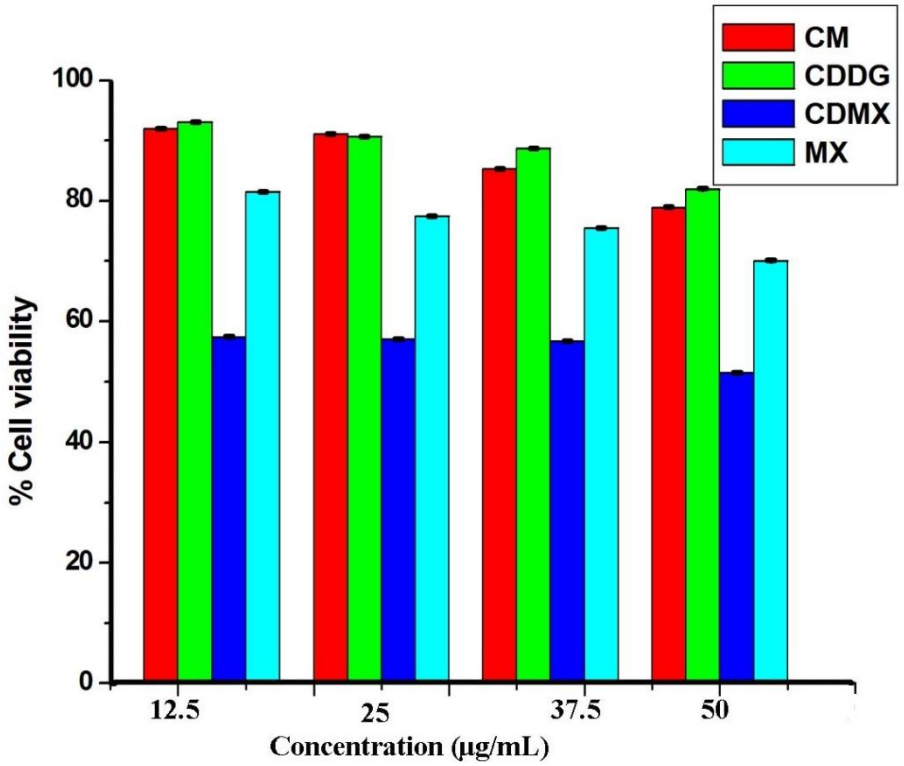

Figure 72: MTT assay of CDDG, CM, CDMX and free methotrexate

4.5.4 Cellular uptake studies

To further annotate MTT assay results, the internalisation of CDDG, CM and CDMX was studied by incubating C6 glioma cells for 3 h and the uptake was

visualized by confocal laser microscope. Fluorescent images in Figure 73A and Figure 73B indicate effective internalization of CDDG and CDMX by C6 glioma cells. The uptake of CM was also carried out and it is evident from Figure 73C that the fluorescence intensity of the cells is less when compared to those incubated with CDMX.

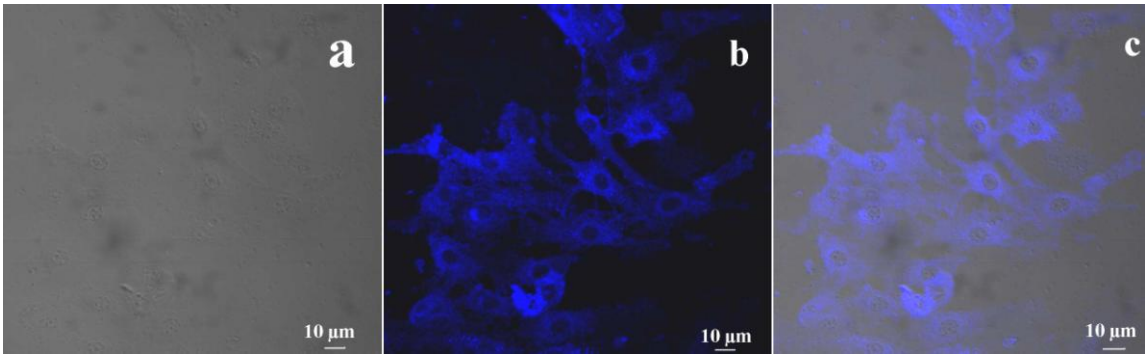

Figure 73A: Confocal laser microscopic images under bright field of a) cells alone b) CDDG c) merged images

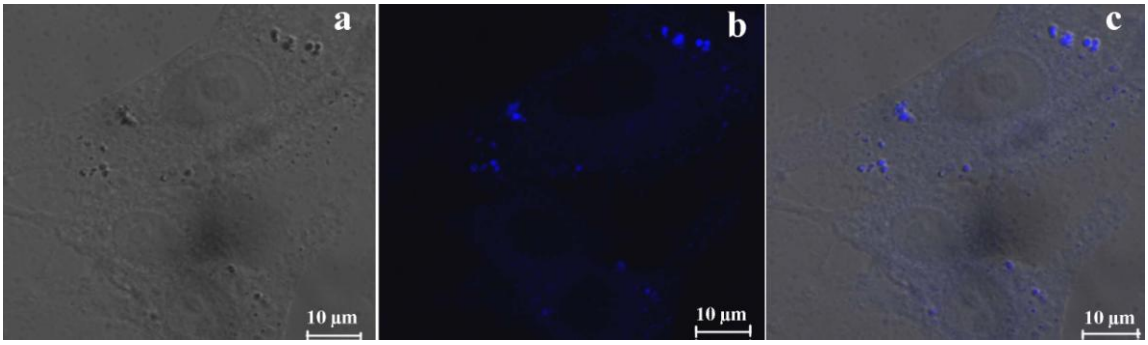

Figure 73B: Confocal laser microscopic images under bright field of a) cells alone b) CDMX c) merged images

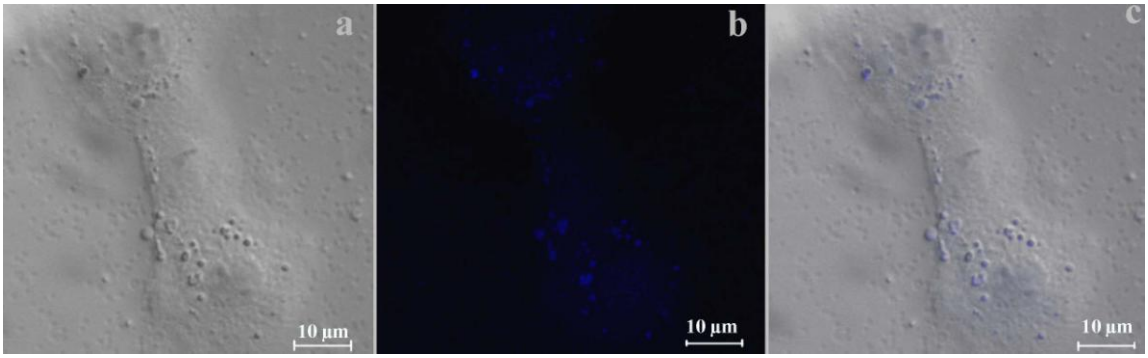

Figure 73C: Confocal laser microscopic images under bright field of a) cells alone b) CM c) merged images

5 DISCUSSION

5.1 In Vitro detection of calcium in bone by modified carbon dots

In this study we used functionalized CDs for the location of substrate containing Ca ions. GA, a naturally occurring amino acid with a proven affinity to Ca (Fujisawa et al., 1996) was conjugated onto CD. We intentionally chose HA considering its biocompatibility. HA is widely used for arthritis treatment, tissue engineering and drug delivery applications. As a carrier, HA is known to have several advantages such as ability to prevent protein adsorption and opsonisation stemmed from its hydrophilic and polyanionic features in physiological environment (Kim et al., 2010).

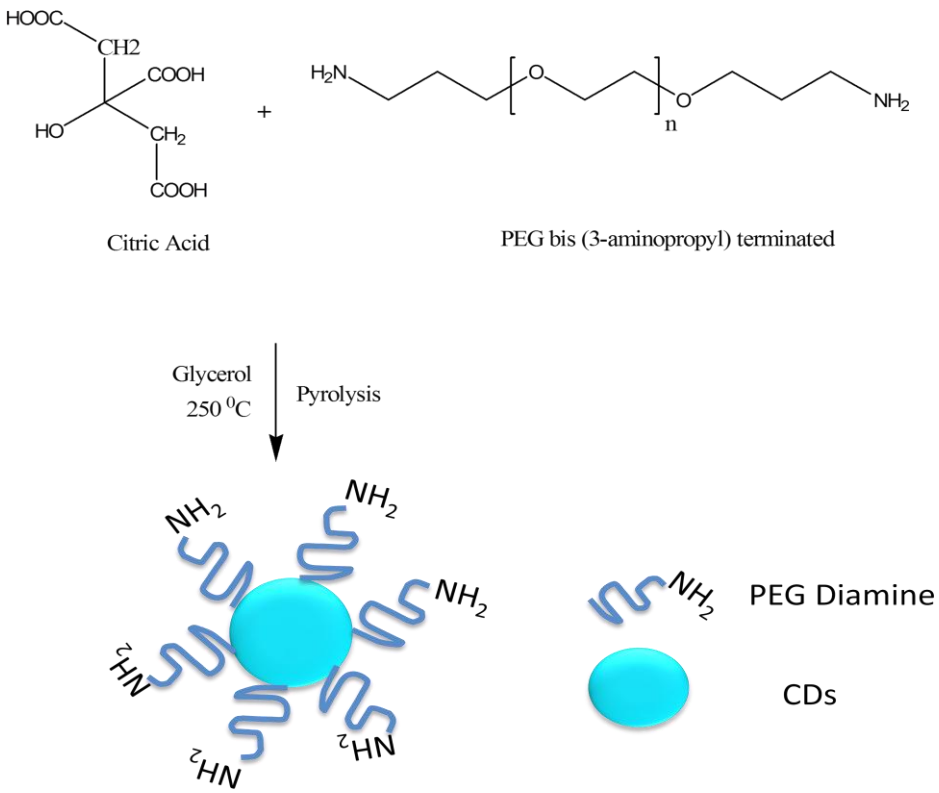

Scheme 3: Schematic representation for the formation of CDs

HA and GA was conjugated onto the amino functionalized CDs to form the probe (HAGACD) via EDC reaction as detailed in the experimental section and its physico chemical characterizations were carried out. FTIR spectra, thermograms and the decrease in zeta potential value confirm the formation of the conjugate.

HRTEM micrographs of CDs depicted in Figure 12A &12B showed a size 3-5 nm which is in par with the reported data and they possess spherical morphology (Wang et al., 2010). The size of HAGACD significantly increases to 95 nm-139 nm as can be seen in the TEM images, in Figure 12C &12D which can be due to the fact that several CD could be conjugated onto a single polymer chain and CD moieties can possibly form aggregates surrounded by the hydrophilic polymer chains. To support this view, we carried out DLS to determine the size of the HAGACD which showed higher values (i.e. ~ 500 nm). DLS measurement records higher values compared to TEM since the light is scattered by the core particle and the layers formed on the surface of the particles which have been already reported (Radhakumary and Sreenivasan, 2011) (Babic et al., 2009). Decrease in zeta potential of CD from -20.90 mV to -0.58 mV on conjugation (Table 1), further confirm the formation of HAGACD. The interaction of functional groups of CDs with HA and GA tilt zeta potential values to a less negative value. Despite low surface charge for HAGACD good colloidal stability is observed. Stabilization may be attributed to the presence of hydrophilic HA.

Photoluminescence of CDs is associated with core and surface related emissions (Miao et al., 2015). Strong visible emission attribute to the electronic transitions due to the recombination of electron hole pairs in the localised π and π^* levels of sp^2

sites (Lim et al., 2015). HAGACD shows photo luminescence intensity at 450 nm on 360 nm excitation as evident from Figure 16. There is no shift in the peak maximum of the conjugate reflecting that the conjugation didn't alter inherent emission features of CD. HAGACD shows excitation dependent emission (Figure 17) which may be attributed to the different sizes of CDs (Zhao et al., 2008) and due to the emissive sites which gets excited at certain excitation wavelength resulting in fluorescence (Baker and Baker, 2010).

Direct contact method confirms the non cytotoxic behavior of HAGACD. HAGACD does not cause any lysis, degeneration or loss of spindle shape morphology of the cells as evident from Figure 18A. As per ISO 10993-5 the achievement of numerical grade more than 2 is considered as cytotoxic effect. HAGACD achieved a numerical grade zero hence the material is considered to be non-cytotoxic. MTT assay also confirms the non cytotoxic nature of HAGACD (Figure 19).

In vitro haemolysis is a simple and reliable method for estimating the blood compatibility of materials. According to the E2524-08 protocol, if the assay result for a test-nanomaterial falls below 2 %, the material is considered non-haemolytic. HAGACD at two different concentrations, 1.0 mg/mL and 0.5 mg/ mL were found to be 0.62% and 0.30 % confirming their non-haemolytic behaviour. Concentration of 0.5 mg/ mL of HAGACD was used throughout the study.

The specificity of HAGACD was also proved. Figure 22 depicts that the fluorescence intensity of the HAGACD is not significantly affected on adding different cations (Na^+, K^+, Mg^{2+}, and Fe^{3+}) which are commonly present in blood. The addition of these ions did not quench the fluorescence intensity of the probe,

proving that these ions are not binding to the HAGACD. Zhou et al have shown that fluorescence of CDs are unaffected by cations except Hg^{2+} (Zhou et al., 2012). In our study, we excluded Hg^{2+} since these ions are not found in blood. Further, to investigate the interferences from other coexisting substances, the experiment was repeated with human blood serum and it was observed that the fluorescence intensity of the probe remained unaffected as demonstrated in Figure 23. These results ascertain the high selectivity of the probe.

PVA (Poly Vinyl Alcohol) doped with Ca^{2+} and fresh bones collected from slaughter house were used to demonstrate the binding of the probe at calcium containing sites. The probe was found to dock onto these substrates and the event of binding could be visualized when viewed through a fluorescent microscope or exposed to UV light (365nm). Images of the bones incubated with HACD and HAGACD are demonstrated in Figures 25B and 25C respectively. Binding of the probe is very low for the bone incubated with HACD as the probe does not contain GA. A notable observation was the enhanced fluorescence for the bone incubated with HAGACD indicative of more binding of the probes from the freshly cut portions of the bone which is known to be releasing Ca^{2+}. This observation, in fact, suggests that GA is necessary to lock the probe onto the bone.

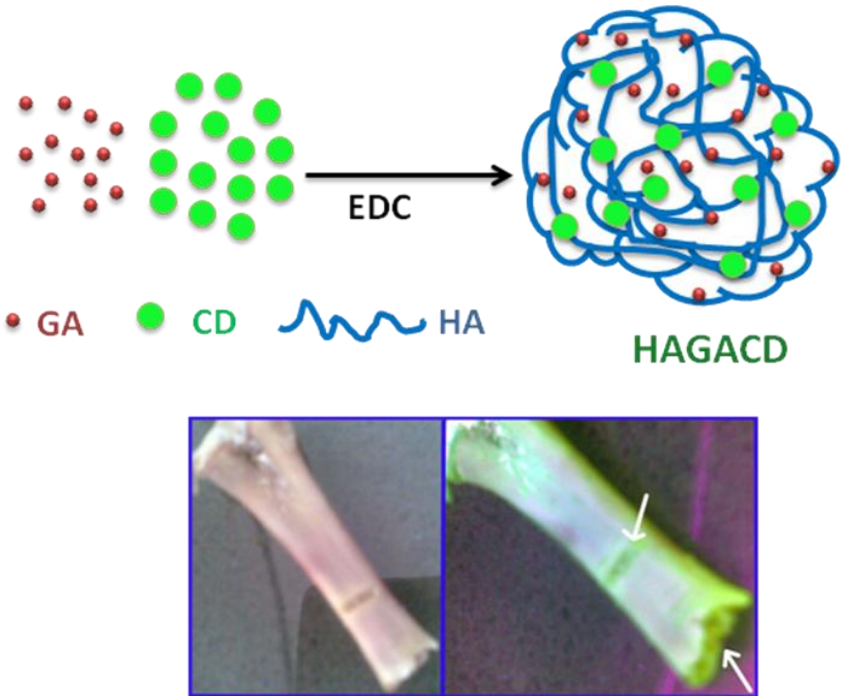

Scheme 4: Schematic representation of the formation of the probe, HAGACD and the targeting ability of the probe to lock onto the calcium rich sites

5.2 Simultaneous bone crack detection and drug deposition using modified carbon dots

New strategies to address bone diseases are currently focused on designing nanoparticles capable of docking onto cracks. Nanoparticles functionalized with bone targeting molecules are specific in nature. By this approach, simultaneous crack visualization and site specific drug delivery could be achieved. This study depicts the generation of a fluorescent nano probe using CDs for viewing bone cracks and simultaneous drug delivery to the cracked sites. GA, well known for its targeted labeling of calcium rich sites like bone cracks and calcified was used as calcium targeting ligand. Ciprofloxacin was chosen in this study as a model drug owing to its

antibacterial activity. It is the most commonly used antibiotic to treat infections of urinary tract, abdomen, bone and skin. PEGD passivated CDs were conjugated with GA and ciprofloxacin simultaneously via EDC chemistry to locate bone cracks and deliver appropriate drugs to facilitate rapid healing and check infection.

The formation of CDGAC was confirmed by FTIR and the H^1NMR spectra given in Figure 26 and Figure 27 respectively. The conjugation was again evident from the HRTEM results (Figure 28) due to which the size of CDs increased from 4-7 nm to 55-60 nm. CDs functionalized with GA and Ciprofloxacin may interact with one another via H-bonding among the functional groups. Such interaction facilitates the formation of small aggregates. The significant increase in the particle size on the onset of modification may be assigned to the formation of aggregated structures. The amount of ciprofloxacin and GA on 1 mg CDGAC was quantified as 96 μg and 58 μg respectively.

Thermogravimetric analysis was carried out and it was observed that CDGAC decomposed at a faster rate when compared to CD. This might be due to the presence of ciprofloxacin and GA in the conjugate. As per the literature decomposition of ciprofloxacin takes place around 135 ℃ (Refat et al., 2011) and that of GA occur in the range of 250 ℃ – 300 ℃.

XRD pattern of CD exhibit a strong peak at 2θ=19.24º with interlayer spacing (d value) 4.6 Aº Pan et al have shown that carbon nanoparticles possess a graphitic nature with interlayer spacing 4.2 Aº, larger than that of bulk graphite (3.3 Aº) (Goh et al., 2012). The sharp peak around 19.24º is assigned to PEG chains by conducting XRD analysis of PEG diamine (PEGD) used for the synthesis of CDs (Figure 30). This was confirmed by MDSC scan. MDSC trace showed a melting peak around

29 ºC (Figure 31) which was assigned to the melting of PEGD associated with CDs by running a separate MDSC analysis on PEGD though pure PEGD melted at higher temperature (51 ºC). CDs after modification with drug and GA also showed more or less similar thermal behavior.

UV visible absorption spectrum of CDGAC (Figure 32) shows a peak at 272 nm in addition to the characteristic absorption peak of CD around 360 nm, confirming the presence of ciprofloxacin in the conjugate. Both CD and CDGAC show emission peak maximum around 450 nm as depicted in Figure 33, when excited at a wavelength of 360 nm again showing that modification is not affecting the inherent fluorescence of CD. Excitation dependent emission is exhibited by CDGAC. As the excitation wavelength of CDGAC increases the peak emission shifts slightly to longer wavelengths causing a reduction in the fluorescence intensity, maximum emission is observed when CDGAC is excited at 360 nm as seen in Figure 34. CDs exhibit different emissions depending on excitation wavelengths and such varied optical features are due to the size distribution of CD or emission trap distribution on CD surfaces (Goh et al., 2012) (Zhu et al., 2009) .

In vitro cytotoxicity of CDGAC was evaluated with L929 mouse fibroblast cells. The material does not cause any lysis, degeneration or loss of spindle shape morphology of the cells further confirming their non cytotoxicity as evident from Figure 35A. As per ISO 10993-5 the achievement of numerical grade more than 2 is considered as cytotoxic effect. CDGAC achieved a numerical grade zero hence the material is considered to be non-cytotoxic.

MTT assay also confirms the non cytotoxic nature of CDGAC. According to the statistical analysis, % viability of the samples is significantly high when compared to the positive control as reflected in Figure 36.

In vitro haemolysis is a simple and reliable method for estimating the blood compatibility of materials. Haemolysis values between 2% and 5 % are interpreted as moderately haemolytic and those above 5% qualify the test-material as haemolytic (Dobrovolskaia and McNeil, 2013). From the results as observed in Figure 37 the haemolysis percentage is less than 1% reflecting the compatibility of CDGAC with blood.

Antibacterial study was carried out for CDGAC. Ciprofloxacin (C), CD and CDGAC were taken in the same petri dish as shown in Figure 38. It can be seen that CDs showed scanty bacterial growth for the first two cases, moderate growth in the third and heavy growth for the remaining concentrations. The scanty growth may be due to the nonspecific inhibition by the comparatively high concentration of CD. However, the bacterial growth (bacterial strain *E.coli*) is inhibited by the probe (CDGAC) at varying concentrations. The results prove that CDGAC itself is antibacterial and for checking bacterial infection, the drug need not be cleaved from the probe.

The studies done so far confirm that CDGAC is highly fluorescence and possesses excellent antibacterial property. Additionally, GA on the probe could guide it towards calcium rich sites like bone crack. The binding of CDGAC to the bone cracks was demonstrated using IVIS Spectrum in vivo imaging system with freshly collected bones from slaughter house. Excitation was given at 430 nm as it is the

starting wavelength for IVIS. It is evident from Figure 34 that the CDGAC can be excited at this wave length due to its excitation dependent emission. As per the colour bar, the red region indicates maximum fluorescence intensity and blue the minimum. It is clear from Figure 39 that the cracked portions gave maximum fluorescence intensity and the result apparently suggests the ability CDGAC to concentrate and thereby to locate even minor bone cracks.

5.3 Detection and imaging of fatty plaques on blood vessels using functionalized carbon dots

Visualization of cholesterol rich plaques using fluorescent nano probes may aid in diagnosis of atherosclerosis in the early stage. CDs were functionalized with DG so that the probes can selectively bind the cholesterol rich tissues owing to the strong affinity of digitonin towards cholesterol. The formation of CDDG is confirmed by FTIR and H^1NMR spectra. Modification of CDs with DG result in an increase in size due to the interaction among functional groups leading to the formation of aggregates as discussed in case of HAGACD and CDGAC. The negative value for the Zeta potential of CDs dropped from -20.90 mV to -4.99 mV on conjugation with DG. The overall reduction of negative charge could be attributed to the integration of DG which is relatively hydrophobic. The absorbance maximum for CDDG was found to be 360 nm. CDDG showed emission at 455 nm when excited at 360 nm. No shift in the peak maximum after conjugation but an increase in the fluorescence intensity of CDDG was observed comparing to CD which could be due to the enhanced hydrophobic environment resulted by incorporation of DG moieties.

The cholesterol concentration range 2 mM-20 mM was chosen to study the change in the fluorescence intensity of CDDG as the elevated individual plasma cholesterol levels exceeding 6.2 mM (240 mg/dL) are indications of poor cardiovascular conditions. The fluorescence intensity was found to decrease as the concentration of cholesterol increases (Figure 46). Decrease in fluorescence intensity may be due to the complexation of cholesterol with CDDG in the ground state. DG is well known for its cholesterol affinity as it binds with cholesterol forming complexes referred to as digitonides.. Linear relationship was observed between the relative fluorescence intensities of CDDG and various cholesterol concentrations with correlation coefficient of 0.987 (Figure 47). The detection limit was found to be 2 mM though the estimation or quantification of cholesterol is not the objective of our approach.

The interference of CDDG with other steroids (Figure 48) and also some potential coexisting substances in serum, including some amino acids [valine (val), Cystine (cys), Glycine (gly), Lysine (lys), Tryptophan (trypt) and Methionine (meth)] ascorbic acid (aa), dopamine (dop), glutathione (gt) and uric acid (ua) (Figure 49) were evaluated. No change in the fluorescence intensity of CDDG was observed in presence of these moeities confirming the selectivity of CDDG towards cholesterol. The binding of CDDG to cholesterol was proved by incubating CDDG with cholesterol solution sprayed onto the cover slip as well as PVA films doped with cholesterol confirming the binding as evident from Figure 50 and Figure 51. The blue, green and red fluorescence observed in both the figures using various filters [UV range (350-380 nm), blue (450-490 nm) and green (515-560 nm) respectively] show that CDDG exhibit excitation dependent fluorescence property similar to that

of bare CDs. Excitation dependent emission spectra for CDDG is shown in Figure 45. These types of varied optical features attribute to the size distribution of CD or emission trap distribution on CD surfaces (Mochalin and Gogotsi, 2009) (Tang et al., 2012) (Zhu et al., 2009). Excitation dependent photoluminescence exhibited by CDs when coated on paper, animal fur or skin have recently been reported (Qu et al., 2012).

Experiment was repeated with fat tissue extracted from the arterial walls of human heart and fat free tissue from the muscle portion. MDSC analysis was carried out using fat deposited tissue as well as fat free tissue (muscle) to compare the phase transitions. Melting point of pure cholesterol is 148 ºC as per literature. The fat tissue showed a prominent melting peak at 102 ºC. We presumed that this peak is associated with lipids predominantly cholesterol. The reduction in melting peak may be explained by the fact that the deposit contains apart from cholesterol, other entities like cholesterol esters and lipids in various proportions. No such transition is shown by the muscle tissue as evident from Figure 53.

The tissues were incubated with CDDG at different time intervals, thereafter washed, dried and viewed under UV lamp at 365 nm. Tissue with deposit showed fluorescence within 5 min pointing out that the method is an easy and efficient one for imaging cholesterol plaques. The muscle portion did not fluoresce at all confirming that the probe is selective to cholesterol rich sites.

The same was repeated mimicking the actual *in vivo* condition, the fat deposited tissue and the fat free tissue were incubated with blood serum containing 230 mg/dL.

This experiment was performed to get an insight into the probe's behaviour in a medium which already contains cholesterol in free and bound forms. Under such a situation, the probe need not bind onto the cholesterol deposit instead it can bind to the cholesterol present in the medium. It was found that the fat deposited tissue shows fluorescence while fat free tissue is non fluorescent confirming that the probe can recognize and dock onto the fat deposits in real situation (*in vivo*).

The same tissues were then imaged with *in vivo* imaging system at an excitation wavelength of 430 nm. The fat tissue has maximum binding of the probe as evident from the color bar in Figure 57. The red region indicates maximum fluorescence intensity and blue the minimum. The fat deposit free tissue is completely blue in color confirming that the probe has not bound to it at all. This experiment further supports the ability of CDDG as a cholesterol plaque imaging probe.

5.4 Gold nanorod-carbon dot hybrid system for the simultaneous imaging and possible disruption of cholesterol plaques

NRs were synthesized as reported by sayed et al (Nikoobakht and El-Sayed, 2003). Synthesized NRs display purple colour due the interaction between light and the particles (Henglein, 1993) (Stephan Link, 1999). FTIR spectrum of NRs (Figure 58A) confirm their formation which matches with the earlier reports (Gole et al., 2004) (Nikoobakht and El-Sayed, 2001). The formation of NRs is further confirmed from the UV Visible absorption spectrum which exhibit two peaks one at shorter wavelength i.e Transverse Surface Plasmon Resonance (TSPR) and the other, Longitudinal Surface Plasmon Resonance (LSPR) at higher wavelength.

NRs are surface functionalized with COOH groups in presence of MSA and further conjugated with CDDG via EDC reaction to get the hybrid CDNR. The formation of CDNR is confirmed from the FTIR spectrum due to the presence of bands at 1650 cm^{-1} (-CO- stretching) and 1569 cm^{-1} (-N-H bending), the typical bands for amide bond.

NRs are purified by centrifugation at 10000 rpm. Figure 59A shows the TEM image of NRs with length ~ 17 nm and width ~ 4 nm. The hybrid CDNR is purified by dialysis using dialysis membrane, MWCO 3500. Figure 59B shows the TEM image of CDNR in which rod shaped NRs and spherical shaped CDDG are present. Modified CDs typically register significantly higher size comparing to bare CDs which show normally <4 nm. We have already seen that the size of CDDG increases to 10 nm (Figure 42) and when conjugated to NRs their size further increase to 18 nm as observed in Figure 59B and 59C. Several unconjugated NRs are present as shown in Figure 59B. To isolate the conjugated entities, CDNR were further centrifuged and dialyzed. The isolated hybrid entities were subjected to TEM analysis and the corresponding image is shown in Figure 59C.

Zeta potential of NRs was found to be 24 mV due to the cationic surfactant, CTAB. On conjugation with CDDG, the zeta potential value dropped to 0.603 which might be due to the replacement of CTAB by CDDG.

Photoluminescent nature of CDDG is not affected by the Conjugation of NRs. Both CDDG and CDNR give emission at 455 nm when excited at 360 nm (Figure 62). Binding of CDNR to the cholesterol deposited tissue was checked. Due to the presence of DG in the hybrid it could bind onto the tissue as a result of which the

tissue fluoresce (Figure 63). The tissue incubated with CDNR was exposed to laser light for 5 min and temperature was measured. The elevation of temperature suggests that the property of NR is unaffected even after the conjugation of CDDG. The hybrid system designed here can thus be used for the localization of the cholesterol deposit and the possible rupture of the deposit by elevating the local temperature. The ruptured and loosened deposit may be removable by the flowing blood in real situation.

Cytotoxicity evaluation by MTT assay showed enhanced cytotoxicity for NR which might be due to CTAB, the surfactant used for the synthesis. It is evident from Figure 65 that the toxicity of NRs is highly reduced when conjugated with CDDG. That is the hybrid generated here is highly cytocompatible and can be used safely as theranostic probe for the dual applications of imaging and photo thermal therapy. The confocal laser microscopic image in Figure 66 confirms the effective internalization of CDNR by the cancer cells. As reflected, they are uniformly distributed in the cytoplasm. Thus the results provide an insight towards the potential of the hybrid system as a useful entity for theranostic applications.

5.5 Methotrexate anchored carbon dots as theranostic probes: Digitonin conjugation enhances cellular uptake and cytotoxicity

To explore CD based probes as carrier for anticancer drug, CD modified with DG (CDDG) was used since DG has been traditionally known as cell membrane permeabilizing agent. Hence we presumed that CDDG is a better nanocarrier when compared to bare CDs. MX is conjugated to CDDG via DCC/DMAP reaction. MX

is a widely used in cancer treatment. MX can enter cells via the similar transport system to folic acid (FA) as its structure being similar to FA (Rijnboutt et al., 1996) (Mizusawa et al., 2012). Conjugation of MX to CDDG was confirmed by FTIR, H^1NMR and UV-visible absorption spectrum. Change in the zeta potential value from -20.90 mV to -4.99 mV assures the conjugation of DG onto CDs. Though the zetapotential value is dropped, no aggregation was observed (as evident from the TEM image of CDDG in Figure 42), since there was enough repulsive force for preventing the same. On conjugation with MX change in zeta potential from -4.99 mV to 0.57 mV was observed which is assigned to the additional functional groups (e. g. amino) incurred by the incorporation of MX.

From the drug release profile (Figure 71) it is evident that significantly more amount of drug is released at pH 5.0 which is beneficial considering the lower pH inside cancer cells. The release profile apparently suggests that drug is retained in the matrix at physiological pH. The release of drug at acidic pH is due to the hydrolysis of ester bond facilitating the rapid release of MX from the nanocarrier, CDDG. One of the essential criteria of a drug delivery vehicle is its ability to minimize drug loss during circulation. In that sense, the matrix highlighted in the present study has the potential to carry the drug safely to the predetermined site.

Figure 72 shows the cytotoxic activity of CDMX, CDDG and MX conjugated to CDs without DG (CM). CDMX showed enhanced cytotoxic response when compared to CM. Improved cytotoxic response of CDMX might be due to the cell permeabilizing effect of DG in CDMX. This observation can be assigned to enhanced uptake of CDMX by the cells which in fact facilitates the transport of more drugs into the cells. CDMX exhibited higher cytotoxicity when compared to the free

drug thus confirming the efficiency of the carrier thereby interacting with the cells in a better manner when compared to the free drug. A similar observation has been made in an earlier study using MX loaded Chitosan nanoparticles (Chen et al., 2014). The action of the free drug at the site is based on the passive diffusion mechanism and may not be effective in inflicting instant cellular damage (Nogueira et al., 2013).

Confocal images in Figure 73A and Figure 73B indicate effective internalization of CDDG and CDMX by C6 glioma cells. The fluorescence was mainly observed in the cytoplasm area as it is a known fact that CDs get distributed in cytoplasm. The uptake of CM was also carried out and it is evident from Figure 73C that the fluorescence intensity of the cells is less when compared to those incubated with CDMX. The results apparently suggest that the enhanced cytotoxicity of CDMX comparing to CM as reflected in MTT assay is due to the improved internalization of CDMX facilitated by DG. The results emerged indicate that the new probe, CDMX, generated here has the versatility of potential agent for the imaging and destruction of killer cells.

6 SUMMARY AND CONCLUSION

CDs are one of the most attractive photoluminescent materials with tremendous potential in the field of nanomedicine. Our attempt was to use CDs modified with suitable moieties for meeting diverse applications. We succeeded in developing CD based probes for *in vitro* detection of cracks in bone, simultaneous bone crack detection and drug deposition, detection of cholesterol followed by imaging fatty deposits on arterial walls which may aid in diagnosis of atherosclerosis and modified CDs as a potential carrier in cancer therapy. CDs were conjugated with appropriate entities for each study.

Initially we designed CDs modified with GA for the *in vitro* detection of calcium. GA being calcium specific the modified CDs can be used to locate calcium rich sites especially bone cracks. PEG diamine capped CDs of size 3-5 nm were synthesized using citric acid as the carbon precursor. In our first study HA and GA were conjugated on to CDs simultaneously via EDC chemistry. The conjugate, HAGACD was characterized by FTIR, TEM, TGA and DLS. Fluorescence property of CDs was found to be unaffected by the conjugation. The fluorescence intensity of the probe remained unaffected in presence of ions present in blood serum. The interferences from other coexisting substances were also checked using human blood serum and the selectivity of the probe was confirmed**.** *In vitro* cytotoxicity evaluation confirmed that HAGACD is non toxic. The nanoprobe, HAGACD was used to map calcium rich areas. The fluorescence was not quenched in presence of Ca^{2+} rather strongly binds to the calcium rich sites as demonstrated with polymer (PVA film) doped with various concentrations of calcium and fresh bones. The bone is freshly cut and it is

well known that cut or cracked portions of the bone release Ca^{2+} towards which calcium-binding ligands are attracted more. The study conclusively indicated that CD based probes has potential to map Ca rich areas as well as Ca releasing points such as bone cracks.

Next we designed CD based probe for viewing the bone cracks as well as deliver appropriate drugs to facilitate rapid healing. Ciprofloxacin was chosen as an antibacterial model drug in our study. CDs were functionalized with GA and ciprofloxacin simultaneously via EDC chemistry. After the purification of the conjugate by dialysis, the amount of GA and ciprofloxacin conjugated onto CDGAC were estimated and found to be 58 µg and 96 µg respectively. Physicochemical characterizations confirmed the conjugation of GA and ciprofloxacin onto CDs. *In vitro* cytotoxicity studies were carried out by direct contact method and MTT assay which showed high cell viability confirming the non cytotoxicity of CDGAC. Haemolysis assay was also performed and the probe was found to be non-haemolytic with haemolysis values <1%. Microbial inhibition assay of CDGAC was done and the result assured that CDGAC is antibacterial in nature, hence no need for the cleavage of the drug from the conjugate. Docking of the probe onto the bone crack was demonstrated using freshly collected bone and the bound probe on the bone cracks were located by *in vivo* imaging system at an excitation wavelength of 430 nm. Thus CD based bone targeting drug delivery system non cytotoxic, non haemolytic and antibacterial in nature was successfully designed. The results indicated that there is scope of developing CD based probes as theranostic agents.

Next our attempt was to conjugate CDs with DG and use this probe for the early detection of cholesterol deposits in the arterial walls which may aid in diagnosis of

atherosclerosis. DG is well known for its affinity towards cholesterol. The risk of developing atherosclerosis is proportional to blood cholesterol level which in turn eventually leads to heart attack and hence early diagnosis is very essential. The conjugation of DG on to CDs was confirmed by FTIR, H^1NMR, TEM and zeta potential values. Non cytotoxic and non haemolytic behavior of CDDG was ascertained. Response of the probe to cholesterol was determined fluorimetrically and the detection limit was found to be 2 mM. The selectivity of the probe towards cholesterol was also confirmed. The probes could bind onto the cholesterol rich areas as evident from fluorescent microscope and IVIS Spectrum images. Hence the probe can be used for the early detection of plaque formation, saving the lives of many asymptomatic atherosclerotic patients. The methodology portrayed here has significant promise for *in vivo* imaging.

Next we designed a hybrid (CDNR) containing NR and CDDG, for the simultaneous detection and possible disruption of cholesterol deposits in the artery walls through photo thermal therapy. NRs were successfully synthesized and characterized. The formation of the hybrid was confirmed by using FTIR, TEM and UV-Visible absorption UV-Visible absorption spectrometer. Tissue with atherosclerotic deposit incubated in CDNR was highly fluorescent confirming the binding of the conjugate on to the tissue. 10^0C rise in temperature was observed for the tissue incubated with CDNR followed by laser exposure. ESEM analysis of the tissues after laser light exposure showed altered morphology of the tissue incubated in CDNR reflecting the loosening of fatty plaques probably by melting of the constituents in the plaques. Non cytoxicity and the cellular internalization of CDNR further indicate that it may be an efficient system for in vivo applications. The hybrid probe seems to have

potential to carve as a therapeutic approach for simultaneous detection and possible removal of cholesterol deposits.

CDs were modified with DG as a nanocarrier for loading the anticancer drug, MX. FTIR, H^1NMR and UV-Visible spectra confirms the conjugation of MX onto CDDG. *In vitro* drug release profile of MX from the system ensured the safe delivery of the drug under physiological conditions thereby meeting the criteria of an efficient drug delivery carrier. Nearly 80 % of the drug was released at pH 5.0 which is beneficial considering the lower pH of the cancer cells. The probe CDDG showed negligible cytotoxicity to C6 glioma cells but CDMX showed enhanced cytoxicity when compared to the free drug. The confocal images of the cells incubated with CDDG and CDMX confirmed that they are efficiently taken up by the cells. Our results suggest that DG can assist in better internalization of drug carriers and thus significantly can increase the therapeutic potential of the drug. Additionally it seems that potential theranostic probes can be created from CD by less complex chemical approaches.

Thus the study indicates that novel theranostic probes with improved features can be generated from CDs by a judicious modification. Future studies will be focused to assess the suitability of the probes for the *in vivo* applications. To achieve these goals, *in vivo* studies using appropriate animals will be carried out.

REFERENCES

Agnihotri N, Chowdhury AD, De A (2015) Non-enzymatic electrochemical detection of cholesterol using β-cyclodextrin functionalized graphene. *Biosens. Bioelectron*. 63: 212–217.

Anderson DG, Burdick JA, Langer R (2004) Materials science. Smart biomaterials. *Science* 305: 1923–1924.

Babic M, Horák D, Jendelová P, Glogarová K, Herynek V, Trchova M, Likavanová K, Lesný P, Pollert E, Hájek M, Syková E (2009) Poly(N,N-dimethylacrylamide)-coated maghemite nanoparticles for stem cell labeling. *Bioconjug. Chem*. 20: 283–294.

Bai W, Zheng H, Long Y, Mao X, Gao M, Zhang L (2011) A carbon dots-based fluorescence turn-on method for DNA determination. *Anal. Sci. Int. J. Jpn. Soc. Anal. Chem*. 27: 243–246.

Baker SN, Baker GA (2010) Luminescent Carbon Nanodots: Emergent Nanolights. *Angew. Chem. Int. Ed*. 49: 6726–6744.

Barua S, Yoo JW, Kolhar P, Wakankar A, Gokarn YR, Mitragotri S (2013) Particle shape enhances specificity of antibody-displaying nanoparticles. *Proc. Natl. Acad. Sci.* 110: 3270–3275.

Basu A, Suryawanshi A, Kumawat B, Dandia A, Guin D, Ogale SB (2015) Starch (Tapioca) to carbon dots: an efficient green approach to an on-off-on photoluminescence probe for fluoride ion sensing. *The Analyst* 140: 1837–1841.

Bourlinos AB, Stassinopoulos A, Anglos D, Zboril R, Karakassides M, Giannelis EP (2008) Surface functionalized carbogenic quantum dots. *Small* 4: 455–458.

Cao L, Meziani MJ, Sahu S, Sun YP (2013) Photoluminescence properties of graphene versus other carbon nanomaterials. *Acc. Chem. Res*. 46: 171–180.

Cao L, Wang X, Meziani MJ, Lu F, Wang H, Luo PG, Lin Y, Harruff BA, Veca LM, Murray D, Xie SY, Sun YP (2007) Carbon dots for multiphoton bioimaging. *J. Am. Chem. Soc.* 129: 11318–11319.

Chen B, Li F, Li S, Weng W, Guo H, Guo T, Zhang X, Chen Y, Huang T, Hong X, You S, Lin Y, Zeng K, Chen S (2013) Large scale synthesis of photoluminescent carbon nanodots and their application for bioimaging. *Nanoscale* 5: 1967–1971.

Chen CW, Robertson J (1998) Nature of disorder and localization in amorphous carbon. *J. Non-Cryst. Solids.* 227–230, Part 1, 602–606.

Chen J, Huang L, Lai H, Lu C, Fang M, Zhang Q, Luo X (2014) Methotrexate-loaded PEGylated chitosan nanoparticles: synthesis, characterization, and in vitro and in vivo antitumoral activity. *Mol. Pharm*. 11: 2213–2223.

De M, Ghosh PS, Rotello VM (2008) Applications of Nanoparticles in Biology. *Adv. Mater*. 20: 4225–4241.

Demchenko AP, Dekaliuk MO (2013) Novel fluorescent carbonic nanomaterials for sensing and imaging. *Methods Appl. Fluoresc*. 1: 042001.

Deng J, Lu Q, Mi N, Li H, Liu M, Xu M, Tan L, Xie Q, Zhang Y, Yao S (2014) Electrochemical synthesis of carbon nanodots directly from alcohols. *Chemistry* 20: 4993–4999.

Deng Y, Zhao D, Chen X, Wang F, Song H, Shen D (2013) Long lifetime pure organic phosphorescence based on water soluble carbon dots. *Chem. Commun*. 49: 5751–5753.

Ding C, Zhu A, Tian Y (2014) Functional surface engineering of C-dots for fluorescent biosensing and *in vivo* bioimaging. *Acc. Chem. Res*. 47: 20–30.

Dobrovolskaia MA, McNeil SE (2013) Understanding the correlation between in vitro and in vivo immunotoxicity tests for nanomedicines. *J. Control. Release Soc*. 172: 456–466.

Eda G, Lin YY, Mattevi C, Yamaguchi H, Chen HA, Chen IS, Chen, CW, Chhowalla M (2010) Blue photoluminescence from chemically derived graphene oxide. *Adv. Mater*. 22: 505–509.

Esteves da Silva JCG, Gonçalves HMR (2011) Analytical and bioanalytical applications of carbon dots. *Trends Anal. Chem*. 30: 1327–1336.

Ferlay J, Soerjomataram I, Dikshit R, Eser S, Mathers C, Rebelo M, Parkin DM, Forman D, Bray F (2015) Cancer incidence and mortality worldwide: sources, methods and major patterns in GLOBOCAN 2012. *Int. J. Cancer* 136: E359–386.

Fujisawa R, Wada Y, Nodasaka Y, Kuboki Y (1996) Acidic amino acid-rich sequences as binding sites of osteonectin to hydroxyapatite crystals. *Biochim. Biophys. Acta* 1292: 53–60.

Gindy ME, Prud'homme RK (2009) Multifunctional nanoparticles for imaging, delivery and targeting in cancer therapy. *Expert Opin. Drug Deliv*. 6: 865–878.

Goh EJ, Kim KS, Kim YR, Jung HS, Beack S, Kong WH, Scarcelli G, Yun SH, Hahn SK (2012) Bioimaging of Hyaluronic Acid Derivatives Using Nanosized Carbon Dots. *Biomacromolecules* 13: 2554–2561.

Gole A, Orendorff CJ, Murphy CJ (2004) Immobilization of gold nanorods onto acid-terminated self-assembled monolayers via electrostatic interactions. *Langmuir* 20: 7117–7122.

Gong J, Lu X, An X (2015) Carbon dots as fluorescent off–on nanosensors for ascorbic acid detection. *RSC Adv* 5: 8533–8536.

Gu, Wu, Chen, Xiao Y (2013) Nanotechnology in the targeted drug delivery for bone diseases and bone regeneration. *Int. J. Nanomedicine* 2305.

Henglein A (1993) Physicochemical properties of small metal particles in solution: "microelectrode" reactions, chemisorption, composite metal particles, and the atom-to-metal transition. *J. Phys. Chem*. 97: 5457–5471.

Hsu PC, Chen PC, Ou CM, Chang HY, Chang HT (2013) Extremely high inhibition activity of photoluminescent carbon nanodots toward cancer cells. *J. Mater. Chem. B* 1: 1774–1781.

Hu L, Sun Y, Li S, Wang X, Hu K, Wang L, Liang X, Wu Y (2014) Multifunctional carbon dots with high quantum yield for imaging and gene delivery. *Carbon* 67: 508–513.

Hu SL, Niu KY, Sun J, Yang J, Zhao NQ, Du XW (2009) One-step synthesis of fluorescent carbon nanoparticles by laser irradiation. *J. Mater. Chem.* 19: 484–488.

Hummers WS, Offeman RE (1958) Preparation of Graphitic Oxide. *J. Am. Chem. Soc*. 80: 1339–1339.

Janib SM, Moses AS, MacKay JA (2010) Imaging and drug delivery using theranostic nanoparticles. *Adv. Drug Deliv. Rev*. 62: 1052–1063.

Jun ME, Roy B, Ahn KH (2011) "Turn-on" fluorescent sensing with "reactive" probes. *Chem. Commun*. 47: 7583–7601.

Kang YF, Li Y, Fang YW, Xu Y, Wei XM, Yin XB (2015) Carbon Quantum Dots for Zebrafish Fluorescence Imaging. *Sci. Rep*. 5: 11835.

Kim J, Park J, Kim H, Singha K, Kim WJ (2013) Transfection and intracellular trafficking properties of carbon dot-gold nanoparticle molecular assembly conjugated with PEI-pDNA. *Biomaterials* 34: 7168–7180.

Kim KS, Hur W, Park SJ, Hong SW, Choi JE, Goh EJ, Yoon SK, Hahn SK (2010) Bioimaging for targeted delivery of hyaluronic Acid derivatives to the livers in cirrhotic mice using quantum dots. *ACS Nano* 4: 3005–3014.

Lai CW, Hsiao YH, Peng YK, Chou PT (2012) Facile synthesis of highly emissive carbon dots from pyrolysis of glycerol; gram scale production of carbon dots/mSiO2 for cell imaging and drug release. *J. Mater. Chem*. 22: 14403.

Lee YJ, Park JY (2010) Nonenzymatic free-cholesterol detection via a modified highly sensitive macroporous gold electrode with platinum nanoparticles. *Biosens. Bioelectron.* 26: 1353–1358.

Li H, He X, Liu Y, Huang H, Lian S, Lee ST, Kang Z (2011) One-step ultrasonic synthesis of water-soluble carbon nanoparticles with excellent photoluminescent properties. *Carbon* 49: 605–609.

Li H, Liu, J, Yang M, Kong W, Huang H, Liu Y (2014) Highly sensitive, stable, and precise detection of dopamine with carbon dots/tyrosinase hybrid as fluorescent probe. *RSC Adv*. 4: 46437–46443.

Li X, Wang H, Shimizu Y, Pyatenko A, Kawaguchi K, Koshizaki N (2011) Preparation of carbon quantum dots with tunable photoluminescence by rapid laser passivation in ordinary organic solvents. *Chem. Commun*. 47: 932–934.

Li Y, Bai H, Liu Q, Bao J, Han M, Dai Z (2010) A nonenzymatic cholesterol sensor constructed by using porous tubular silver nanoparticles. *Biosens. Bioelectron*. 25: 2356–2360.

Li Z, Sun Q, Zhu Y, Tan B, Xu ZP, Dou SX (2014) Ultra-small fluorescent inorganic nanoparticles for bioimaging. *J. Mater. Chem. B* 2: 2793–2818.

Lim SY, Shen W, Gao Z (2015) Carbon quantum dots and their applications. *Chem Soc Rev* 44: 362–381.

Lin Z, Xue W, Chen H, Lin JM (2012) Classical oxidant induced chemiluminescence of fluorescent carbon dots. *Chem. Commun.* 48: 1051–1053.

Link S, El-Sayed MA (1999) Size and temperature dependence of the plasmon absorption of colloidal gold nanoparticles. *J. Phys. Chem. B* 103: 4212-4217.

Liu C, Zhang P, Zhai X, Tian F, Li W, Yang J, Liu Y, Wang H, Wang W, Liu W (2012) Nano-carrier for gene delivery and bioimaging based on carbon dots with PEI-passivation enhanced fluorescence. *Biomaterials* 33: 3604–3613.

Liu Y, Xiao N, Gong N, Wang H, Shi X, Gu W, Ye L (2014) One-step microwave-assisted polyol synthesis of green luminescent carbon dots as optical nanoprobes. *Carbon* 68: 258–264.

Luhmann T, Germershaus O, Groll J, Meinel L (2012) Bone targeting for the treatment of osteoporosis. *J. Control. Release Soc*. 161: 198–213.

Luo PG, Sahu S, Yang, ST, Sonkar SK, Wang J, Wang H, LeCroy GE, Cao L, Sun YP, (2013) Carbon “quantum” dots for optical bioimaging. *J. Mater. Chem. B* 1: 2116–2127.

Mensah F, Seyoum H, Misra P (2015) Nanomaterials in Nanomedicine. In: Misra, P. (eds.), *Applied Spectroscopy and the Science of Nanomaterials*, Progress in Optical Science and Photonics, Springer, Berlin, pp. 253–277.

Mewada A, Pandey S, Thakur M, Jadhav D, Sharon M (2014) Swarming carbon dots for folic acid mediated delivery of doxorubicin and biological imaging. *J Mater Chem B* 2: 698–705.

Meyer H (1957) The ninhydrin reaction and its analytical applications. *Biochem. J.* 67: 333–340.

Miao P, Han K, Tang Y, Wang B, Lin T, Cheng W (2015) Recent advances in carbon nanodots: synthesis, properties and biomedical applications. *Nanoscale* 7: 1586–1595.

Mizusawa K, Takaoka Y, Hamachi I (2012) Specific cell surface protein imaging by extended self-assembling fluorescent turn-on nanoprobes. *J. Am. Chem. Soc.* 134: 13386–13395.

Mochalin VN, Gogotsi Y (2009) Wet chemistry route to hydrophobic blue fluorescent nanodiamond. *J. Am. Chem. Soc.* 131: 4594–4595.

Mondal A, Jana NR (2012) Fluorescent detection of cholesterol using β-cyclodextrin functionalized graphene. *Chem. Commun.* 48: 7316–7318.

Nauck M, März W, Wieland H (2000) Is Lipoprotein(a) Cholesterol a Significant Indicator of Cardiovascular Risk? *Clin. Chem*. 46: 436–437.

Nikoobakht B, El-Sayed MA (2001) Evidence for Bilayer Assembly of Cationic Surfactants on the Surface of Gold Nanorods. *Langmuir* 17: 6368–6374.

Nikoobakht B, El-Sayed MA (2003) Preparation and Growth Mechanism of Gold Nanorods (NRs) Using Seed-Mediated Growth Method. *Chem. Mater*. 15: 1957–1962.

Nogueira DR, Tavano L, Mitjans M, Pérez L, Infante MR, Vinardell MP (2013) In vitro antitumor activity of methotrexate via pH-sensitive chitosan nanoparticles. *Biomaterials* 34: 2758–2772.

Pandey S, Mewada A (2013) Cysteamine hydrochloride protected Carbon dots as a vehicle for efficient release of Anti-Schizophrenic drug haloperidol. *RSC Adv*. 3: 26290 – 26296.

Pandey S, Thakur M, Mewada A, Anjarlekar D, Mishra N, Sharon M (2013) Carbon dots functionalized gold nanorod mediated delivery of doxorubicin: tri-functional nano-worms for drug delivery, photothermal therapy and bioimaging. J. *Mater. Chem. B* 1: 4972.

Pareta RA, Taylor E, Webster TJ (2008) Increased osteoblast density in the presence of novel calcium phosphate coated magnetic nanoparticles. *Nanotechnology* 19:265101.

Park SY, Lee HU, Park ES, Lee SC, Lee JW, Jeong SW, Kim CH, Lee YC, Huh YS, Lee J(2014) Photoluminescent green carbon nanodots from food-waste-derived sources: large-scale synthesis, properties, and biomedical applications. *ACS Appl. Mater. Interfaces* 6: 3365–3370.

Peng H, Travas-Sejdic J (2009) Simple Aqueous Solution Route to Luminescent Carbogenic Dots from Carbohydrates. *Chem. Mater.* 21: 5563–5565.

Qiao ZA, Wang Y, Gao Y, Li H, Dai T, Liu Y, Huo Q (2010) Commercially activated carbon as the source for producing multicolor photoluminescent carbon dots by chemical oxidation. *Chem. Commun*. 46: 8812–8814.

Qu K, Wang J, Ren J, Qu X (2013) Carbon dots prepared by hydrothermal treatment of dopamine as an effective fluorescent sensing platform for the label-free detection of iron(III) ions and dopamine. *Chemistry* 19: 7243–7249.

Qu S, Wang X, Lu Q, Liu X, Wang L (2012) A biocompatible fluorescent ink based on water-soluble luminescent carbon nanodots. *Angew. Chem. Int. EdEngl.* 51: 12215–12218.

Radhakumary C, Sreenivasan K (2011) Naked Eye Detection of Glucose in Urine Using Glucose Oxidase Immobilized Gold Nanoparticles. *Anal. Chem*. 83: 2829–2833.

Raj V, Jaime R, Astruc D, Sreenivasan K (2011) Detection of cholesterol by digitonin conjugated gold nanoparticles. *Biosens. Bioelectron*. 27: 197–200.

Raj V, Johnson T, Joseph K (2014) Cholesterol aided etching of tomatine gold nanoparticles: A non-enzymatic blood cholesterol monitor. *Biosens. Bioelectron*. 60: 191–194.

Ray SC, Saha A, Jana NR, Sarkar R (2009) Fluorescent Carbon Nanoparticles: Synthesis, Characterization, and Bioimaging Application. *J. Phys. Chem. C* 113: 18546–18551.

Rijnboutt S, Jansen G, Posthuma G, Hynes JB, Schornagel JH, Strous GJ (1996) Endocytosis of GPI-linked membrane folate receptor-alpha. *J. Cell Biol*. 132: 35–47.

Ross RD, Cole LE, Roeder RK (2012) Relative binding affinity of carboxylate-, phosphonate-, and bisphosphonate-functionalized gold nanoparticles targeted to damaged bone tissue. *J. Nanoparticle Res.*14: 1175

Ross RD, Roeder RK (2011) Binding affinity of surface functionalized gold nanoparticles to hydroxyapatite. *J. Biomed. Mater. Res. A* 99: 58–66.

Sahu S, Behera B, Maiti TK, Mohapatra S (2012) Simple one-step synthesis of highly luminescent carbon dots from orange juice: application as excellent bio-imaging agents. *Chem. Commun*. 48: 8835–8837.

Shen P, Xia Y (2014) Synthesis-modification integration: one-step fabrication of boronic acid functionalized carbon dots for fluorescent blood sugar sensing. *Anal. Chem*. 86: 5323–5329.

Shinde KN, Dhoble SJ, Swart HC, Park K (2012) Phosphate Phosphors for Solid-State Lighting, Springer Series in Materials Science. Springer Berlin Heidelberg.

Siegel RL, Miller KD, Jemal A (2015) Cancer statistics (2015) CA. *Cancer J. Clin*. 65: 5–29.

Sk MP, Jaiswal A, Paul A, Ghosh SS, Chattopadhyay A (2012) Presence of amorphous carbon nanoparticles in food caramels. *Sci. Rep*. 2: 383.

Song Y, Feng D, Shi W, Li X, Ma H (2013) Parallel comparative studies on the toxic effects of unmodified CdTe quantum dots, gold nanoparticles, and carbon nanodots on live cells as well as green gram sprouts. *Talanta* 116: 237–244.

Song Y, Zhu S, Yang, B (2014) Bioimaging based on fluorescent carbon dots. *RSC Adv*. 4: 27184–27200.

Stone J, Jackson S, Wright D (2011) Biological applications of gold nanorods. *Wiley Interdiscip. Rev. Nanomed. Nanobiotechnol*. 3: 100–109.

Suhalim JL, Chung CY, Lilledahl, MB, Lim RS, Levi M, Tromberg BJ, Potma EO (2012) Characterization of cholesterol crystals in atherosclerotic plaques using stimulated Raman scattering and second-harmonic generation microscopy. *Biophys. J.* 102: 1988–1995.

Sun YP, Zhou B, Lin Y, Wang W, Fernando KAS, Pathak P, Meziani MJ, Harruff BA, Wang X, Wang H, Luo PG, Yang H, Kose ME, Chen B, Veca LM, Xie SY (2006) Quantum-Sized Carbon Dots for Bright and Colorful Photoluminescence. *J. Am. Chem. Soc.* 128: 7756–7757.

Tang L, Ji R, Cao X, Lin J, Jiang H, Li X, Teng KS, Luk CM, Zeng, S, Hao J, Lau SP(2012)Deep ultraviolet photoluminescence of water-soluble self-passivated graphene quantum dots. *ACS Nano* 6: 5102–5110.

Tao H, Yang K, Ma Z, Wan J, Zhang Y, Kang Z, Liu Z (2012) In Vivo NIR Fluorescence Imaging, Biodistribution, and Toxicology of Photoluminescent Carbon Dots Produced from Carbon Nanotubes and Graphite. *Small* 8: 281–290.

Teng P, Xie J, Long Y, Huang X, Zhu R, Wang X, Liang L, Huang Y, Zheng H (2014) Chemiluminescence behavior of the carbon dots and the reduced state carbon dots. *J. Lumin.* 146: 464–469.

Wang F, Pang S, Wang L, Li Q, Kreiter M, Liu C (2010) One-Step Synthesis of Highly Luminescent Carbon Dots in Noncoordinating Solvents. *Chem. Mater*. 22: 4528–4530.

Wang F, Xie Z, Zhang H, Liu C, Zhang Y (2011) Highly Luminescent Organosilane-Functionalized Carbon Dots. *Adv. Funct. Mater*. 21: 1027–1031.

Wang H, Shen J, Li Y, Wei Z, Cao G, Gai Z, Hong K, Banerjee P, Zhou S (2014) Magnetic iron oxide–fluorescent carbon dots integrated nanoparticles for dual-modal imaging, near-infrared light-responsive drug carrier and photothermal therapy. *Biomater. Sci*. 2: 915.

Wang P, Zhao L, Liu J, Weir MD, Zhou X, Xu HHK (2014) Bone tissue engineering via nanostructured calcium phosphate biomaterials and stem cells. *Bone Res*. 2: 14017.

Wang Q, Liu X, Zhang L, Lv Y (2012) Microwave-assisted synthesis of carbon nanodots through an eggshell membrane and their fluorescent application. *The Analyst* 137: 5392–5397.

Wang Y, Hu A (2014) Carbon quantum dots: synthesis, properties and applications. *J. Mater. Chem. C* 2: 6921–6939.

Wang Z, Liao H, Wu H, Wang B, Zhao H, Tan M (2015) Fluorescent carbon dots from beer for breast cancer cell imaging and drug delivery. *Anal Methods* 7: 8911–8917.

Wen J, Xu Y, Li H, Lu A, Sun S (2015) Recent applications of carbon nanomaterials in fluorescence biosensing and bioimaging. *Chem. Commun*. 51: 11346–11358.

Wicki A, Witzigmann D, Balasubramanian V, Huwyler J (2015) Nanomedicine in cancer therapy: challenges, opportunities, and clinical applications. *J. Control. Release Soc*. 200: 138–157.

Wu W, Zhou T, Berliner A, Banerjee P, Zhou S (2010) Glucose-mediated assembly of phenylboronic acid modified CdTe/ZnTe/ZnS quantum dots for intracellular glucose probing. *Angew. Chem. Int. Ed*. 49: 6554–6558.

Xie J, Lee S, Chen X (2010) Nanoparticle-based theranostic agents. *Adv. Drug Deliv. Rev*. 62: 1064–1079.

Xu B, Zhao C, Wei W, Ren J, Miyoshi D, Sugimoto N, Qu X (2012). Aptamer carbon nanodot sandwich used for fluorescent detection of protein. *The Analyst* 137: 5483–5486.

Xu X, Ray R, Gu Y, Ploehn HJ, Gearhear L, Raker, K, Scrivens, WA (2004) Electrophoretic analysis and purification of fluorescent single-walled carbon nanotube fragments. *J. Am. Chem. Soc*. 126: 12736–12737.

Xu X, Zhao Y, Xue X, Huo S, Chen F, Zou G, Liang XJ (2014) Seedless synthesis of high aspect ratio gold nanorods with high yield. *J. Mater. Chem. A* 2: 3528–3535.

Yadav V, Freedman JD, Grinstaff M, Sen A (2013) Bone-Crack Detection, Targeting, and Repair Using Ion Gradients. *Angew. Chem. Int. Ed Engl*. 52: 10997–11001.

Yang C, Thomsen RP, Ogaki R, Kjems J, Teo BM (2015) Ultrastable green fluorescence carbon dots with a high quantum yield for bioimaging and use as theranostic carriers. *J Mater Chem B* 3: 4577–4584.

Yang L, Zhao H, Fan S, Zhao G, Ran X, Li CP (2015) Electrochemical detection of cholesterol based on competitive host–guest recognition using a β-cyclodextrin/poly(N-acetylaniline)/graphene-modified electrode. *RSC Adv*. 5: 64146–64155.

Yang ST, Wang X, Wang H, Lu F, Luo P.G, Cao L, Meziani MJ, Liu JH, Liu Y, Chen M, Huang Y, Sun YP (2009) Carbon Dots as Nontoxic and High-Performance Fluorescence Imaging Agents. *J. Phys. Chem. C*. 113: 18110–18114.

Yang ZC, Wang M, Yong AM, Wong SY, Zhang XH, Tan H, Chang AY, Li X, Wang J (2011) Intrinsically fluorescent carbon dots with tunable emission derived from hydrothermal treatment of glucose in the presence of monopotassium phosphate. *Chem. Commun*. 47: 11615–11617.

Yuan C, Liu B, Liu F, Han MY, Zhang Z (2014) Fluorescence "turn on" detection of mercuric ion based on bis(dithiocarbamato)copper(II) complex functionalized carbon nanodots. *Anal. Chem*. 86: 1123–1130.

Zhai X, Zhang P, Liu C, Bai T, Li W, Dai L, Liu W (2012) Highly luminescent carbon nanodots by microwave-assisted pyrolysis. *Chem. Commun. Camb*. 48: 7955–7957.

Zhang Z, Ross RD, Roeder RK (2010) Preparation of functionalized gold nanoparticles as a targeted X-ray contrast agent for damaged bone tissue. *Nanoscale* 2: 582.

Zhao L, Di F, Wang D, Guo LH, Yang Y, Wan B, Zhang H (2013) Chemiluminescence of carbon dots under strong alkaline solutions: a novel insight into carbon dot optical properties. *Nanoscale* 5: 2655–2658.

Zhao QL, Zhang ZL, Huang BH, Peng J, Zhang M, Pang DW (2008) Facile preparation of low cytotoxicity fluorescent carbon nanocrystals by electrooxidation of graphite. *Chem. Commun*. DOI:10.1039/B812420E: 5116–5118.

Zheng H, Wang Q, Long Y, Zhang H, Huang X, Zhu R (2011) Enhancing the luminescence of carbon dots with a reduction pathway. *Chem. Commun*. 47: 10650–10652.

Zheng M, Liu S, Li J, Qu D, Zhao H, Guan X, Hu X, Xie Z, Jing X, Sun Z(2014) Integrating Oxaliplatin with Highly Luminescent Carbon Dots: An Unprecedented Theranostic Agent for Personalized Medicine. *Adv. Mater*. 26: 3554–3560.

Zheng M, Ruan S, Liu S, Sun T, Qu D, Zhao H, Xie Z, Gao H, Jing X, Sun Z (2015) Self-Targeting Fluorescent Carbon Dots for Diagnosis of Brain Cancer Cells. *ACS Nano* 9: 11455–11461.

Zhong W (2009) Nanomaterials in fluorescence-based biosensing. *Anal. Bioanal. Chem*. 394: 47–59.

Zhou J, Booker C, Li R, Zhou X, Sham TK, Sun X, Ding Z (2007) An electrochemical avenue to blue luminescent nanocrystals from multiwalled carbon nanotubes (MWCNTs). *J. Am. Chem. Soc*. 129: 744–745.

Zhou L, Lin Y, Huang Z, Ren J, Qu X (2012) Carbon nanodots as fluorescence probes for rapid, sensitive, and label-free detection of Hg2+ and biothiols in complex matrices. *Chem. Commun*. 48: 1147–1149.

Zhu A, Qu Q, Shao X, Kon, B, Tian Y (2012) Carbon-Dot-Based Dual-Emission Nanohybrid Produces a Ratiometric Fluorescent Sensor for In Vivo Imaging of Cellular Copper Ions. *Angew. Chem. Int. Ed*. 51: 7185–7189.

Zhu H, Wang X, Li Y, Wang Z, Yang F, Yang X (2009) Microwave synthesis of fluorescent carbon nanoparticles with electrochemiluminescence properties. *Chem. Commun*. DOI:10.1039/B907612C: 5118–5120.

Zhu X, Wang H, Jiao Q, Xiao X, Zuo X, Liang Y, Nan J, Wang J, Wang L (2014) Preparation and Characterization of the Fluorescent Carbon Dots Derived from the Lithium-Intercalated Graphite used for Cell Imaging. *Part. Syst. Charact*. 31: 771–77

List of Publications

Publications from the thesis

1. **A. Shanti Krishna**, C. Radhakumary and K. Sreenivasan. *In vitro* detection of calcium in bone by modified carbon dots, Analyst, 2013, 138, 7107.
2. **A. Shanti Krishna**, C. Radhakumary, Molly Antony and K. Sreenivasan. Functionalized carbon dots enable simultaneous bone crack detection and drug deposition, J. Mater. Chem. B, 2014, 2, 8626.
3. **A. Shanti Krishna**, C. Radhakumary and K. Sreenivasan. Detection and imaging of fatty plaques in blood vessels using functionalized carbon dots, Anal. Methods, 2015,7, 9482-9488
4. **A. Shanti Krishna**, C. Radhakumary, M.R. Rekha, Priya. S and K. Sreenivasan. Methotrexate anchored carbon dots as theranostic probes: Digitonin conjugation enhances cellular uptake and cytotoxicity RSC Adv**,** 2016, 6, 56313
5. **A. Shanti Krishna**, C. Radhakumary, M.R. Rekha, Priya. S and K. Sreenivasan. Gold nano rod-Carbon dot hybrids for simultaneous imaging and disruption of Cholesterol plaques (Communicated).

Other Publications

1. **A. Shanti Krishna**, C. Radhakumary and K. Sreenivasan, Calcium ion modulates protein release from Chitosan-Hyaluronic Acid Poly Electrolyte Gel, Polymer engineering and science 2015,55, 2089–2097
2. **A. Shanti Krishna**, Priya A. Nair, C. Radhakumary and K. Sreenivasan Carbon dot based non enzymatic approach for the detection and estimation of glucose in blood serum. Materials Research Express, 2016, 3, 055001
3. C. L. Gopu, **A. Shanti Krishna**, K. Sreenivasan, Fluorimetric detection of hypochlorite using albumin stabilized gold nanoclusters, Sensors and Actuators B, 2015, 209, 798–802.

4. C. L. Gopu, **A. Shanti Krishna**, C. Radhakumary, K. Sreenivasan, Fluorescence off-on probe for drug sensing based on graphene oxide's inherent fluorescence, Biomed. Phys. Eng. Express, 2015,1, 045013

Conference presentations

1. **A. Shanti Krishna**, C. Radhakumary and K. Sreenivasan, "Mapping of Ca^{2+} rich sites by polymer conjugated carbon quantum dots, FAPS-MACRO 2013, May 2013 **(**Poster presentation).

2. **A. Shanti Krishna**, C. Radhakumary and K. Sreenivasan, "Chitosan-Hyaluronic Acid Poly Electrolyte Gel as a Ca^{2+} responsive release system International Conference On Membranes", ICM 2013, Oct 3-6,2013 (Poster presentation).

3. **A. Shanti Krishna**, C. Radhakumary and K. Sreenivasan, "Multifunctionalized carbon dots enable simultaneous bone crack detection and drug delivery", Kerala Science congress, Jan 28-31, 2014 (Oral presentation).

4. **A. Shanti Krishna**, C. Radhakumary and K. Sreenivasan, Novel fluorescent probe to detect and visualize cholesterol deposit in tissue National Conference on Materials Science and Technology, NCMST 2014, July 28-30, 2014 (Poster presentation).

Curriculum Vitae

Education

05/2012 till date **Research Scholar** at Sree Chitra Tirunal Institute for Medical Sciences and Technology, Trivandrum, Kerala, India.
Advisor: Dr. K. Sreenivasan.

07/2007 – 07/2009 **Master of Science in Chemistry (Polymer Science),** (CGPA – 7.87 and third rank).School of Chemical Sciences, Mahatma Gandhi University, Kottayam, Kerala, India

07/2004 – 03/2009 **Bachelor of Science in Chemistry,** (89.5%, First class) Kannur University.

Professional Experience

02/2011– 03/2012 Project fellow at Sree Chitra Tirunal Institute for Medical Sciences and Technology, Trivandrum, Kerala, India.
Project Advisor: Dr. P. Ramesh

01/2009 – 06/2009 M Sc project at Vikram Sarabhai Space Centre, Trivandrum under the joined guidance of Sri Surej. S and Sri Ranajit Pal

National Exam and awards

Qualified UGC-JRF 2011(Chemical sciences)
Qualified GATE 2010 in chemistry with All India Rank 45 (99.94 percentile)

Permanent address

Parvathee Puram (H)

Nettur (P.O)

Thalassery-5

Kannur 670105

Phone no: 09847627380

Email id: shanthikrishna01@gmail.com